THE MECHANICS OF ABRASION ON CONCRETE CROSSTIE RAIL SEATS

BY

RYAN G. KERNES

THESIS

Submitted in partial fulfillment of the requirements
for the degree of Master of Science in Civil Engineering
in the Graduate College of the
University of Illinois at Urbana-Champaign, 2013

Urbana, Illinois

Advisers:

Research Scientist and Senior Lecturer J. Riley Edwards
Professor David A. Lange
Professor Christopher P.L. Barkan

ABSTRACT

A sustained increase in gross rail loads and cumulative freight tonnages on heavy haul railways, as well as increased interest in high and higher-speed passenger rail development, is placing an increasing demand on railway infrastructure and its components. Several failure mechanisms are limiting the service life of track components as this demand increases. Rail seat deterioration (RSD) continues to be identified as one of the primary factors limiting concrete crosstie service life, particularly in heavy-haul freight operations. RSD refers to the degradation of the material at the contact interface between the concrete crosstie rail seat and the rail pad assembly that protects the bearing area of the crosstie from the rail base. Abrasion is widely considered to be a viable mechanism leading to RSD. The factors that control the abrasion mechanism (i.e. relative slip at the rail seat, normal and shear stresses, presence of abrasive fines, and moisture) are frequently encountered on primary heavy-haul corridors in North America. This thesis includes results from several laboratory experiments using test setups and protocols that were designed to isolate the abrasion mechanism and facilitate the acquisition of quantitative and qualitative data related to the severity of deterioration and the frictional properties of rail pad assembly materials sliding on concrete surfaces. The results of these experiments have shown that abrasion is a feasible RSD mechanism. Frictional characteristics at the contact interface between a rail pad assembly and concrete rail seat vary, and influence the transfer of forces and relative slip. Concrete rail seats and pad assemblies should be designed based on the considerations for mitigating the abrasion mechanism. The most feasible way of mitigating abrasion may be to reduce the amount of relative slip at the rail seat.

to Jesus,

for pursuing me,

using this project to break me down,

and showing me that your strength is the only way that I can stand

Psalm 73:26

ACKNOWLEDGMENTS

I would like to express sincere gratitude to the Association of American Railroads (AAR) Technology Scanning Committee and the NEXTRANS Region V Transportation Center for sponsoring this research. Additionally, I am very thankful to the Eisenhower Graduate Fellowship for funding my second year as a MS student.

There are not enough words to express my thanks to Riley Edwards. I want to thank Riley for being extremely intentional in mentoring me, for investing his life into mine such that I could do the same for others, and for devoting so much energy into building me up as a leader. Thank you for challenging me on a regular basis from the day we met in Southern Illinois in 2009.

Many thanks are due to Chris Barkan for challenging me to apply rigorous scientific thinking to this problem. I appreciate Chris' questions and advice that have changed the way I think and equipped me to tackle any problem as an engineer. I appreciate the advice and encouragement from David Lange, who challenged me to see the big picture and appreciate the value of unexpected results.

Thanks are due to Mauricio Gutierrez for inviting me to join the RailTEC family and becoming a brother to me as we worked alongside each other for a year. I appreciate the encouragement and assistance from Marcus Dersch, whose positive energy and loving personality helped drive me to finish this work. I appreciate the encouragement and detailed notes from John Zeman who set the stage for me to succeed.

Additionally, I would like to thank Amsted RPS and Amsted Rail, for providing me with critical resources for the laboratory experiments. Special thanks go to Dave Bowman, Jose Mediavilla, and Dave Davis for providing direction, advice, and encouragement. Many thanks to the members of AREMA Committee 30 (Ties) and the rail infrastructure community, including

John Bosshart, Tom Brueske, Steve Mattson, Jim Parsley, Michael Steidl, Winfried Boesterling, Greg Grissom, Eric Gehringer, Dwight Clark, Kevin Hicks, Steve Ashmore, Scott Tripple, Bob Coats, Tim Johns, Fabian Webber, and Pelle Duong.

This work would not have been possible without contributions from Tim Prunkard, Darold Marrow, Chester Riggins, Chuck Cook, Don Marrow, Jamar Brown, and Brian Renoylds, all of the UIUC CEE Machine Shop. Thank you for your patience with me and taking the time to teach an engineer what it takes to make an idea come to life. Thanks to Calvin Nutt, Ryan Feeney, Brad Jones, Michael Wnek, Emily Van Dam, Josh Brickman, Steven Jastrzebski, Andrew Kimmle, Xiang Liu, Rapik Saat, Brandon Van Dyk, Chris Rapp, all of UIUC at the time when this work was completed.

Finally, thank you to my amazing family. I deeply appreciate my dad, Tim, and mom, Patty for always supporting me in every challenge that I have undertaken. Thanks to my brother Andrew for being a role model my entire life, and for believing in me when I did not. I would have given up on this project if not for the love they expressed toward me and the work ethic these three people instilled in me. Thank you to Tina Venghaus for loving me unconditionally, showing me how to find joy in this work, and for becoming my wife.

TABLE OF CONTENTS

CHAPTER 1: INTRODUCTION

1.1 Background

Railroad track is a system of components and materials that function together to support and guide the movement of trains while dispersing the wheel loads to the subgrade (Kerr 2003). Within the system, the crosstie maintains the gauge, or distance between the rails of the track, is part of the system for distributing loads to acceptable levels for the track substructure layers, and provides support and restraint for the rail in the vertical, lateral, and longitudinal directions (Kerr 2003). Rail seats are the locations on the crosstie that provide the bearing surface for the rails. Crossties are made of several materials, including wood, concrete, plastic composites, and steel. In North America, concrete crossties are typically prestressed, precast beam elements that are used in some of the most demanding track conditions in terms of tonnage, gradient, and curvature.

For concrete crossties, the rail seat is protected by a rail pad assembly, which is located between the rail base and the rail seat of the crosstie. The rail pad assembly, or rail pad, is a part of the system that fastens the rail to the crosstie. On heavy-haul freight corridors in North America, the rail pad assembly typically consists of two or three layers, which often include a rail pad and an abrasion frame. The terms rail pad assembly, rail pad, and tie pad are often used interchangeably. In addition to the rail pad assembly, the fastening system typically includes cast-in steel shoulder inserts or dowels, spring clips or clamps attached to the shoulder inserts or dowels, and plastic insulators between the clips/shoulders and the rail. The fastening system functions to restrain rail movement, electrically isolate the concrete crosstie from the rail (if track circuits are used), and distribute the pressure from the rails.

Rail seat deterioration (RSD) is the term used to describe the degradation of material directly beneath the rail pad on the bearing surface of concrete crossties. The loss of material at the rail seat reduces the fastening system's clamping force on the rail and can lead to track geometry problems such as gauge widening and loss of cant (inclination of rail seat surface). These types of track defects increase the risk of derailment by altering the ratio of lateral to vertical (L/V) forces, consequently reducing the stability of the rail. As a result of the problems associated with RSD, the service life of many concrete crossties on demanding railway lines has been reduced.

In order to avoid the premature replacement of concrete crossties well before the design life has expired, several Class I railways include production-level rail seat repairs in the capital maintenance plan to prevent track geometry problems. Rail seat maintenance is relatively expensive because RSD is difficult to accurately detect and impossible to repair without removing the fastening system and lifting the rail. If the durability of the materials that compose the rail seat is not sufficient to last as long as rail steel in severe service conditions, then interim repairs of the rail seat may be necessary. Thus, increasing the performance and durability of the rail seat materials for concrete crossties serves the future requirements of increasing freight tonnages and high-speed rail development.

First identified in the 1980's, RSD continues to be a notable problem on North American freight railways as axle loads and rail life cycles increase (Zeman et al. 2010b). A survey conducted at the University of Illinois at Urbana-Champaign (UIUC) in 2012 indicated that RSD is the most critical failure mode related to concrete crossties and fastening systems (Edwards 2012). Few data exist related to occurrence of RSD, and most of the information that is known today is based on experience and is shared anecdotally. On freight railways in North America,

RSD tends to occur on tracks with high annual tonnages, sharp curves, steep grades, and wet climates (Zeman 2010b). The location and severity of RSD is inconsistent even on the same line. For example, RSD may be severe for concrete crossties in one curve, while little or no RSD may occur on the crossties in another curve of the same degree on the same line with identical traffic and tonnage. Furthermore, crossties in the same curve may have different levels of RSD. Anecdotal evidence of ties with severe RSD has been reported directly adjacent to ties with little to no RSD in the same curve.

Although RSD was previously reported as only occurring in North America, evidence of RSD has been observed in several countries around the world, including India, Austria, and South Africa. The terminology associated with this particular problem varies around the world. More international collaboration related to concrete crossties and fasteners will lead to more information and anecdotes related to RSD in other countries that operate with heavy axle loads. Also, RSD may be reaching a level of severity in other countries such that railway engineers are beginning to recognize it as a problem. Nevertheless, RSD is still most prevalent in North America, where the track, operating, and environmental characteristics result in extreme demands on concrete rail seats.

1.2 Previous Research

Previous research at the UIUC and other organizations focused on an investigation of the complex physical processes, or mechanisms, that contribute to RSD (Bakharev 1994, Choros et al. 2007, Zeman et al. 2010a). Five mechanisms were identified that have the potential to deteriorate materials at the rail seat: abrasion, crushing, freeze-thaw cracking, hydraulic-pressure cracking, and hydro-abrasive erosion. Each of these is briefly introduced below.

Abrasion is defined as the wear of particles on the rail seat surface as frictional forces act between the rail pad and the concrete rail seat, which move relative to one another. The abrasion mechanism will be described in detail in Chapter 2. Another RSD mechanism, crushing, occurs when concentrated stresses on the rail seat exceed the strength or fatigue limits of the rail seat materials, resulting in localized damage of the rail seat surface (Zeman et al. 2010b).

The three remaining RSD mechanisms are referred to as moisture-driven mechanisms because the physical process that damages the concrete at the rail seat is only possible when moisture is present in the concrete pore structure. Freeze-thaw cracking initiates when the tensile strength of concrete is exceeded by stresses due to volumetric changes of water in the concrete pore structure with variations in temperature (Bakharev 1994). Hydraulic pressure cracking occurs when rail seat loads and surface water create pore pressures in the concrete (Zeman et al. 2010a). Based on experimental laboratory testing performed at the UIUC, pore pressures have the potential to exceed the concrete's tensile strength, resulting in micro-cracking and subsequent spalling (Zeman et al. 2010c). Hydro-abrasive erosion, also called abrasive erosion or suspended particle erosion, refers to concrete wear through the action of flowing water (Zeman et al. 2010c). In Table 1.1, the five mechanisms are related to the causes of RSD that have been identified.

In North America, the design and manufacture of various track components including concrete crossties is primarily guided by Part 4 of Chapter 30 of the American Railway Engineering and Maintenance-of-Way Association (AREMA) Manual for Railway Engineering (AREMA 2012). Familiar with the challenges associated with the durability of concrete crossties, members of the AREMA committee on ties (Committee 30) have formed working groups charged with identifying the primary causes and factors that contribute to RSD. The

working groups are composed of industry experts that represent various organizations including freight and passenger railways, suppliers, and research institutions. Table 1.2 summarizes the current industry understanding of RSD. factors and causes (Zeman et al. 2010b).

Table 1.1 Relevance of the causes of RSD related to potential concrete deterioration mechanisms (adapted from Zeman 2010b)

Causes	Concrete Deterioration Mechanisms				
	Abrasion	Crushing	Freeze-Thaw	Hydraulic Pressure	Hydro-Abrasive
High stresses at rail seat	✓	✓		✓	✓
Relative motion at rail seat	✓	✓		✓	✓
Presence of moisture	✓		✓	✓	✓
Presence of abrasive fines	✓				✓

The primary causes of RSD – high stresses, relative motion, moisture, and abrasive fines – are related to internal and external factors that affect the primary causes (Table 1.2). Internal factors refer to aspects of concrete crosstie and fastening system design. Alternatively, external factors are directly related to track geometry, track maintenance, railway operations, climate, and environmental characteristics (Zeman et al. 2010b). Table 1.2 illustrates the challenges associated with designing a concrete crosstie and fastening system to mitigate RSD. There are a variety of factors and causes that interact in complex processes that are difficult to analyze simultaneously.

Table 1.2 Summary of internal and external factors related to the causes of RSD

(adapted from Zeman 2010b)

	High Stresses at the Rail Seat	**Relative Motion at the Rail Seat**	**Presence of Moisture**	**Presence of Abrasive Fines**
Internal Factors	*Loss of proper rail cant* • Loss of material at rail seat • Loss of material at shoulder • Loss of clamping force *Contact area of pad* • Material properties and surface geometry of rail pad	*Looseness of fastening system (loss of clamping force)* • Gaps in fastening system due to manufacturing tolerances • Loss of material at rail seat • Loss of material at shoulder • Yielded or fractured clips • Worn insulators *Scrubbing action* • Poisson's ratio of rail pad • Pad geometry • Confinement of pad	*Rail pad seal* • Material properties and surface geometry of rail pad • Looseness of fastening system • Wear of rail seat and rail pad *Concrete saturation* • Permeability of concrete and rail seat surface	*Rail pad seal* • Material properties and surface geometry of rail pad • Looseness of fastening system • Wear of rail seat and rail pad *Fines from wear of rail seat components*
External Factors	*High vertical loads* • Impact loads • Degraded track geometry *High L/V ratio* • Truck hunting • Over-/under-balanced speeds on curves • Sharp curves • Degraded track geometry *High longitudinal loads* • Steep grades • Thermal stresses in rail • Train braking and locomotive traction *Poor load distribution among adjacent* rail • Non-uniform track substructure • Non-uniform crosstie spacing • Degraded track geometry	*Uplift action* • Low stiffness of track substructure, higher deflections *Lateral action* • Truck hunting • Truck steering around curves (push and pull) • Over-/under-balanced speeds on curves • Sharp curves *Longitudinal action* • Steep grades • Thermal stresses in the rail • Train braking and locomotive traction	*Climate* • Average annual rainfall, days with precipitation, humidity, etc. • Average evaporation rate, etc. • Extreme daily or annual temperatures • Number of annual freeze/thaw cycles	*Environment* • Wind-blown sand or dust • Moisture to transport the abrasive fines under the rail pad *Track maintenance* • Ground ballast • Metal shavings from rail grinding or rail/wheel wear *Train operations* • Application of locomotive sand (especially on grades) • Coal dust and other abrasive commodities

1.3 Scope of Thesis

Abrasion was selected for detailed investigation in this study because the influence of abrasion as an RSD mechanism is unknown. Though abrasion is widely considered to be a viable mechanism that leads to RSD, a lack of understanding of the complex parameters that cause abrasion has resulted in a highly iterative process of concrete crosstie and fastening system design. When combined with abrasive fines and water that penetrate into the rail seat, the frictional forces and relative movement of the concrete crosstie and fastening system likely lead to abrasive wear. The mechanics of abrasion were analyzed in order to better understand its influence as an RSD mechanism and to quantify the critical parameters and causes. The service life of concrete crossties and fastening systems may be extended if the causes of RSD are considered in the design process.

1.4 Thesis Organization

Chapter 2 is a review of the mechanics of abrasion as described in the literature and an analysis of the characteristics needed for abrasion to occur. A small laboratory experiment investigating the hardness of rail seat materials is also described. Chapter 3 examines the characteristics of interactions between the rail pad assembly and the concrete rail seat. By focusing on the movement of the pad assembly and friction at the rail seat interface, the mechanics of abrasion are analyzed. A fundamental experiment related to the coefficient of friction between the pad and rail seat is explained. Chapter 4 summarizes the motivation, design, and results of a large-scale abrasion experiment. Chapter 5 describes an experiment that was performed in order to understand the coefficient of friction between pad materials and mock concrete rail seats. Chapter 6 is a discussion of the conclusions drawn from this work and proposes future work relating to RSD**.**

CHAPTER 2: MECHANICS OF ABRASION

2.1 Fundamentals of Abrasive Wear

Wear is defined as the progressive damage or loss of material from a surface that is a result of relative motion at its contact interface with another surface (Bayer 2004, Czichos 1986, Yamaguchi 1990). Wear can also be described as the change in a surface over time that negatively affects the functionality of the component (Bayer 2004). Scientists and engineers recognize several types of wear that are affected by the materials, environmental conditions, mechanical interaction, and the geometry at the contact interface (Bayer 2004, Yamaguchi 1990). Adhesion, oxidation, thermal wear, tribofilm-based wear, atomic wear, and abrasion are types of wear found in recent literature, classified by the mechanism that causes damage (Bayer 2004).

Adhesion, the propensity of dissimilar particles to be attracted to one another, occurs at local contact points, called asperities, where material from one surface is bonded to the surface it is contacting (Bayer 2004, Czichos 1986, Yamaguchi 1990). When the surfaces move relative to one another, material from one surface pulls material off of the surface it is contacting, resulting in adhesive wear (Bayer 2004). Evidence of adhesion has been observed on concrete rail seats in the field and after laboratory tests where asperities made up of pad materials have been lost from the pad surface and bonded to the concrete rail seat. Additional types of wear may occur at the rail seat, but abrasion is typically considered the dominant wear mechanism of concrete crossties. Therefore, the rest of this chapter will focus on abrasion.

Abrasion occurs as frictional forces act between two surfaces that move relative to one another. The harder surface cuts or ploughs into the softer surface, resulting in the removal of some of the softer material (Bayer 2004, Williams 1997, Halling 1978). Typically, abrasion is

classified as two-body abrasion or three-body abrasion. Two-body abrasion occurs when the contact points, often referred to as protuberances (asperities), on one surface are harder than the other surface. Three-body abrasion occurs when hard particles that are not part of either surface penetrate the contact interface and slide and roll between the two surfaces (Bayer 2004, Williams 1997). Abrasive particles that are introduced to a frictional interface typically result in greater volumes of material loss due to wear at that interface (Godet 1984).

Other distinctions within the mechanism of abrasive wear include single-cycle deformation, repeated-cycle deformation, and fretting. Single-cycle deformation is characterized by the removal or plastic deformation of the material due to one interaction (Bayer 2004). Repeated-cycle deformation is different because multiple load cycles are required to cause the fatigue-like processes (Bayer 2004). For example, fatigue load cycles can cause microcracking and networks of cracks below the surface of a material, resulting in damage (Bayer 2004). Another classification of abrasion is fretting wear, which is distinguished by the type of motion that causes the loss of material. When the relative displacement of two surfaces that are sliding reciprocally is less than a few millimeters, the abrasion on the surface is classified as fretting (Bayer 2004).

Hokkirigawa and Kato (1988) found that normal load, shear strength, hardness, and the shape of the abrasive asperity determine the abrasion mechanism. Additionally, the amount of abrasive wear a surface undergoes is typically proportional to the normal force between the two surfaces and the amount of movement (Halling 1978). Bayer reported that the distance of sliding, number of cycles, time, load, roughness, speed, and hardness are some of the parameters that influence abrasive wear. The relationship between these parameters and wear vary based on

the materials involved in the interaction. Therefore, the effect of these parameters on the abrasion of concrete materials must be analyzed.

2.2 Abrasion of Concrete

Abrasion of concrete has been described as surface damage due to scraping, rubbing, cutting, grinding, gouging, sliding action, frictional processes, attrition, and impact (Atis 2002, Bakke 2006, Mindess 2003). Traditionally, concrete abrasion is defined as "wear due to hard particles or hard protuberances forced against and moving along a solid surface" (Bakke 2006). According to the American Concrete Institute (ACI) Repair Manual, concrete will be abraded only if the abrading material is harder than the concrete (The Concrete Society 2000). However, this definition should be revised in order to include fatigue-like processes such as those characterized as repeated-cycle deformation. Many terms are used to describe the detailed process of concrete abrasion because of the large number of complex interactions that can cause abrasion. The key factors that lead to the occurrence of concrete abrasion include a normal force, shear force, friction, and relative shear displacement.

The hardness of the material in contact with the concrete is typically included in the definition because single-cycle deformation, where the concrete surface is damaged by very few interactions, is not possible without a harder contact surface. If the counterface is not harder than the concrete surface, single cycle deformation can occur by the presence of abrasive particles, which is referred to as three-body abrasion. Concrete abrasion is accelerated by the infiltration of hard particles, such as sand or metal shavings (Bakke 2006). Although hardness is an important factor, it should not be considered requisite for abrasion. Repeated-cycle deformation can occur where the concrete will undergo fatigue damage due to many loading cycles. Fatigue

load cycles can cause damage, even without a harder countersurface or abrasive particles. The hardness of materials at the rail seat interface will be discussed further in Section 2.4.

Regardless of the specific process that causes abrasion, abrasion resistance is a term used to describe a material's ability to withstand frictional contact forces and relative movement that have the potential to produce abrasive wear. The abrasion resistance of concrete is typically analyzed by small-scale deterioration tests where the amount of concrete material lost is quantified. Abrasion testing is discussed in more detail in Section 2.5. Previous studies have illustrated that the abrasion resistance of concrete depends on the quality of materials used, manufacturing and construction practices, and mechanical properties of the finished concrete (Bakke 2006).

The most common relationship reported in the literature is a strong positive correlation between compressive strength and abrasion resistance. In general, the abrasion resistance of concrete increases with compressive strength (Ghafoori and Tays 2010, Bakke 2006, Siddique et al. 2009, Sonebi and Khayat 2001, Naik et al. 1995, Smith 1958). It follows that compressive strength can be used to estimate the abrasion resistance of a concrete surface. However, for a given concrete mixture design, some parameters have a larger effect on the abrasion resistance than they do on the compressive strength.

Ghafoori and Tays (2010) found that moisture in the concrete, cement content, introduction of accelerating admixture, and curing age had a larger effect on the abrasion resistance of the concrete than on the compressive strength. Shurpali et al. (2013) reported that the abrasion resistance of concrete mixtures with fly ash and silica fume increased even though the compressive strength decreased. Parameters that affect the porosity of the concrete typically have an impact on the compressive strength, but the significance of the impact on abrasion

resistance is greater. The microstructure of concrete, and more specifically, the pore structure of the cement on the surface of the concrete, governs the abrasion resistance (Zeman 2010b, Bakharev 1994).

Several studies have shown that the abrasion resistance of concrete is reduced as the water-to-cement ratio (w/c) increases. Similarly, increased concrete absorption has a negative effect on abrasion resistance (Dhir et al. 1994). Increases in w/c and absorption indicate that the concrete has a greater volume of micropores, thus reducing the strength of the concrete microstructure and resulting in reduced abrasion resistance. The effect of air-entraining admixture, which is used to increase the freeze-thaw durability of the concrete, does not appear to have a significant influence on the abrasion resistance of concrete (Shurpali et al. 2013).

The surface pore structure is also affected by the technique used to finish the concrete. Finishing techniques that compact the local concrete matrix and remove capillary channels improve the hardness of the concrete surface (Bakharev 1994). One study reported that power finishing led to an increased abrasion resistance over hand finishing due to additional surface compaction and a lower w/c on the surface (Kettle and Sadegzadeh 1987). Concrete crossties are cast upside down such that the rail seat is formed against steel molds. The microstructure of the rail seat is affected by the manner in which the concrete is consolidated against the steel forms. The method of consolidation likely affects the abrasion resistance of concrete rail seats.

Curing techniques also affect the microstructure of the concrete surface. The abrasion resistance of the concrete is highest when moisture is readily available throughout curing. Nanni (1989) found that the abrasion resistance of concrete specimens tested at 28 days increased as the number of days spent curing in a moist room increased. A similar result was found by Shurpali

et al. (2013) where concrete specimens cured in ambient air or in the oven abraded faster than specimens cured in a moist room or submerged in water.

Mineral admixtures are finely ground materials that are used to increase the durability of concrete (Mindess 2003). Mineral admixtures have been shown to effectively increase the abrasion resistance of concrete in several studies. The replacement of sand with fly ash significantly increased the abrasion resistance of concrete (Siddique and Khatib 2010). The replacement of cement with fly ash increased the abrasion resistance as long as the percentage was less than 50% (Siddique and Khatib 2010). Atis (2002) found that large volumes of fly ash significantly improved the abrasion resistance of concrete, while the curing conditions and superplastizer had no significant effect. Silica fume can increase the abrasion resistance of concrete, but is typically optimal at less than 10% replacement of fine aggregate (Ghafoori and Diawara 2007) and 10% replacement of cement (Shurpali et al. 2013). Yazici and Inan (1996) found that 30% replacement of cement with silica fume increased the abrasion resistance of concrete. Replacement of cement with steel slag powder and blast furnace slag increased abrasion resistance by 20% (Yunfeng et al. 2009). A few studies have shown that the abrasion resistance of concrete can be negatively influenced by the addition of fly ash or silica fume (Naik et al. 1997).

After the cement paste layer is worn away from the concrete surface, the quality of the aggregate becomes critical to the abrasion resistance. For lower strength concrete, the abrasion resistance is largely affected by the hardness of the aggregates (Mindess et al. 2003). Exposed aggregate surfaces have greater abrasion resistance than the cement paste surfaces because the exposed course aggregate is harder than the cement paste (Sonebi and Khayat 2001). One early study found that aggregate has a minimal effect on abrasion resistance at concrete strengths

greater than 8,000 psi (Smith 1958). Therefore, it is likely that the quality of aggregates becomes more important as the depth of abrasion increases, and the coarse aggregate becomes part of the wear surface. Relatively hard course aggregates like chert, traprock, granite, or metallic aggregates yielded concrete that was up to two times more abrasion resistant than concrete with softer coarse aggregate, such as limestone (Sonebi and Khayat 2001, Bakke 2006).

Previous studies have also shown that concrete surfaces experience significantly more abrasive wear when they are wet, possibly due to the weakening of mortar paste as it is exposed to moisture (Bakke 2006, Fwa 1990). Similarly, the presence of fine materials (e.g. contaminants) in standard abrasion resistance tests accelerated the rate of abrasion (Atis 2002, Turk 2011).

2.3 Mechanics of Abrasion at the Rail Seat Interface

Abrasion at the rail seat surface occurs when 1) forces imposed on the rail induce shear forces at the interface between the bottom of the rail pad assembly and the concrete rail seat, 2) the shear forces overcome static friction, 3) the rail pad assembly slips relative to concrete, and 4) strain is imparted on the concrete matrix. Over time, this strain exceeds the fatigue limit of the concrete material and a brittle failure occurs, dislodging individual particles of mortar paste. Alternatively, a harder surface (e.g. abrasive fines) can cut or plough into the softer surface (e.g. concrete rail seat). Initially, microscopic particles are worn away, resulting in a surface that appears polished or burnished (Johns 2010). After many loading cycles, enough particles can be degraded so that a noticeable depth of material is lost, yielding a rough, uneven rail seat.

The rail seat is initially composed of concrete mortar paste and air voids. The concrete mortar paste surface is composed of a matrix of cement grains that bond to one another as the cement is hydrated (Mindess 2003). As RSD initiates and the cement paste is worn away, coarse

and fine aggregate is exposed. Regardless of the ratio of cement paste to coarse aggregate, the concrete provides a brittle bearing surface that exhibits a limited amount of elastic behavior.

Surface coatings of epoxies and urethanes are currently used to restore the rail seat surface in maintenance applications after the rail seat surface is deteriorated. Furthermore, at least one North American railway company is applying a surface coating to new concrete crossties as part of the production process in order to increase the durability of the rail seat. Fundamentally, epoxy and urethane materials are expected to exhibit behavior that is different than concrete in the rail seat environment. The rail pad assembly plays a critical role in movement at the rail seat and will be discussed further in Chapter 3. External materials or contaminants in the form of dust, dirt, locomotive sand, steel shavings, etc. can penetrate into the rail seat interface. In order to understand the potential for abrasion by the cutting or ploughing of abrasive fine particles, the relative hardness values of materials at the rail seat were investigated.

2.4 Hardness of Rail Seat Materials

The relative hardness of interacting materials affects the rate of abrasive wear and is typically considered the most important property related to abrasion (Hokkirigawa and Kato 1988, Halling 1978). Hardness is a property that is used to describe the capacity of a surface to resist plastic deformation under point loads, simulating localized stresses at contact asperities. As the abrasion mechanism initiates due to stresses at local contact points, it is hypothesized that a harder surface would provide greater resistance to abrasive wear. Since the materials used in rail pad assemblies are not harder than concrete, abrasive fines from locomotive sand, ground ballast material, coal dust, steel shavings from rail grinding, etc. are expected to play a major role in abrasion at the rail seat.

2.4.1 Comparing Relative Hardness Values

Several scales are used to measure hardness including the: Mohs, Rockwell, Brinell, Knoop, Vickers, and Shore. Each scale uses different testing procedures to characterize the hardness of materials. In order to compare the relative hardness of materials at the rail seat, the hardness of each relevant material was converted to the Vickers Scale (Granta Design 2013). Although the conversions are estimated, the relative differences in hardness of materials at the rail seat are large, thus making the comparison meaningful (Table 2.1).

Table 2.1 Comparison of hardness values of materials at the concrete rail seat

Material	Hardness (scale)	Estimated Equivalent Vickers Hardness (HV)
Rail Steel	200 - 440 (HB)	200 - 440
Concrete	110 (HR)	250
Cement Paste	75 (HR)	130
Polyurethane Pad	<50 (HR)	N/A
Nylon 6/6 abrasion frame	<50 (HR)	N/A
Sand particles	1000 - 1800 (HV)	1000 - 1800

Silica particles that make up sand are harder than the hardest rail pad assembly materials, the concrete rail seat, and premium rail steel (Williams 2005). Siliceous materials (e.g. quartz, clays, sandstones), which are very common in the Earth's crust, have hardness numbers in excess of 1,800 on the Vickers Hardness (HV) scale (Williams 1997). Sand particles measured with a nano-indenter had a hardness of 10.7 gigapascals (GPa), which equates to 1,000 HV (Daphalapurkar et al. 2011). Rail steel typically ranges from 200 to 440 Brinell Hardness (HB), which is roughly the same value of 200 to 440 HV (Pointer et al. 2006). Rail pad assembly materials such as polyurethane and nylon 6/6 have hardness values less than 50 Rockwell Hardness (HR). These materials are not hard enough to be recognized on the Vickers scale. Wang and Chung (1998) measured the hardness of Portland cement mortar on the Rockwell H scale to be around 75 HR, which equates to about 130 HV. Cong et al. (2006) tested concrete

samples on the same scale, Rockwell H, and found values near 110 HR, equating to nearly 250 HV. Based on this comparison, abrasive particles are much harder than the concrete rail seat.

2.4.2 Estimating Rail Seat Surface Hardness with a Rebound Hammer

In addition to the review of the relevant literature, the hardness of the rail seat surface was investigated experimentally at the UIUC. The surface hardness of two concrete rail seat samples was evaluated with a rebound hammer to determine the feasibility of comparing the hardness of rail seat materials. Two different sections of a full-scale concrete crosstie manufactured in North America were prepared and tested as separate experiments to compare the cement paste surface of a concrete crosstie with two alternative surface treatments. Specimen A had six distinct regions prepared by precision grinding wheels to expose the coarse aggregate and one region that remained as cast, composed of cement paste. Specimen B had two distinct regions: half was coated with a high-viscosity repair epoxy and the other half remained as cast.

A rebound hammer, Schmidt type N-6 manufactured by Forney Testing Machines, was used to calculate the dynamic rebound numbers for each distinct surface. The Schmidt hammer measures the final height of the hammer mass after an impact with the testing surface. A softer material will experience more plastic deformation upon impact. Thus, less initial kinetic energy from the mass will be transferred to the rebound of the mass after impact, resulting in a lower rebound number (Popovics 1992). The hardness values measured by impact (e.g. Schmidt hammer) have different results than hardness values measured by indentation (e.g. Vickers, Rockwell). The relative comparison made in this experiment cannot be compared to the hardness values reported in Section 2.4.1. The average rebound numbers were calculated according to American Society of Testing Methods (ASTM) C805. Table 2.2 compares the average rebound values of the cement paste surface, ground surface, and epoxy-coated surface.

Table 2.2 Experimental rebound data for rail seat surfaces A and B

Specimen A		Specimen B	
Cement Paste	33	Cement Paste	48
Exposed Aggregate	43	Epoxy Coating	50

For Specimen A, the average rebound number for the cement paste surface was lower than the average value for the exposed aggregate surface. No significant difference was found between the average rebound number for the cement paste surface compared to the average for the epoxy-coated surface on Specimen B. It should be noted that the two specimens were not supported in the same way and had different thicknesses, which is likely the reason that Specimen B had higher rebound numbers than Specimen A. Further testing is needed to validate the effectiveness of using the rebound hammer to measure rail seat surface hardness, and to determine if a correlation exists between hardness and abrasion resistance.

2.5 Testing Methods for Abrasion Resistance

In addition to understanding relative hardness at the concrete rail seat, increasing the abrasion resistance of the rail seat should be strongly considered as a way of improving the durability and performance of concrete crossties. A number of test methods have been used in North America to compare the relative abrasion resistance of rail seat materials. Previously, the tests have been specified by railways for quality control purposes and employed by crosstie manufacturers for research and development purposes. The testing method that is employed depends on the objectives of the test and typically can be divided into two categories; system tests and materials tests.

Currently in North America, the AREMA Test 6: Wear/Deterioration is the recommended method of determining if a rail seat and fastening system have the ability to resist

RSD under repeated loads (AREMA 2012). As a qualification test for new crosstie and fastening system designs, AREMA Test 6 was designed to represent severe service conditions when concrete ties are subjected to high lateral forces on a high-degree curve with moisture and abrasive sand present. Test 6 is currently the most desirable test for studying the abrasion mechanism because it most closely represents the process that occurs on railway tracks in revenue service. Unfortunately, this system test is expensive for prototyping because a full-scale crosstie and fastening system is required for each new design or material improvement. Additionally, the test takes between 10 and 15 days to complete, resulting in the collection of few data.

Due to the time and cost of AREMA Test 6, several existing materials tests, standardized by the ASTM, have been used in the concrete crosstie industry to evaluate the abrasion resistance of rail seats. The Revolving Disks Test (ASTM C 779 A), Dressing Wheels Test (ASTM 779 B), Ball Bearings Test (ASTM C 779 C), and a modified version of the Robinson Test (ASTM C 627) successfully produced mechanical wear on concrete surfaces and provided some relative abrasion resistance data. However, these tests are not representative of the abrasion mechanism at the rail seat interface because they were designed to represent abrasion due to foot traffic, steel wheels, or studded tires on industrial slabs or pavements. In general, these tests use some type of steel contact surface that is constantly rotating or rolling to cause abrasion on a horizontal surface. Although some of the tests offer the ability to add an abrasive slurry of fine particles and water, the primary parameters of the tests are fundamentally different from the abrasion mechanism. For example, the continuous motion of the ASTM tests result in rolling friction or kinetic friction that is expected to produce frictional coefficients that remain at relatively static levels throughout the tests. In contrast, the frictional coefficient at the rail seat appears to be

dynamic because of the wheel loading cycles and elasticity in the system that accelerate (move) the rail pad assembly and then restore it to its original position. Combined with the natural variability in the tests, the standard abrasion resistance tests fail to facilitate the collection of qualitative data by means of a representative process.

A better test is needed to understand the abrasion process and link the existing body of abrasion research to the problem of abrasion on concrete rail seats. Numerous parameters that affect concrete abrasion resistance (Section 2.2) must be combined with parameters that affect the abrasion process (Section 2.1) to facilitate a more detailed understanding of abrasion. An experiment was designed to isolate the parameters that affect abrasion on concrete rail seats to lead to a more basic understanding of the abrasion process and help guide future experiments to evaluate innovative rail seat materials (Chapter 4).

CHAPTER 3: RAIL SEAT INTERACTIONS

3.1 Rail Seat Force Transfer

Vertical, lateral, and longitudinal forces on the rail must be resisted by the track components to maintain the geometry of the track within acceptable tolerances (Kerr 2003). The forces must be attenuated in each direction so that elements of the track structure are not loaded beyond their strength limits. Some elastic deformation or relative movement of track components must occur in order for the forces to be dissipated in the vertical, lateral, and longitudinal directions. Based on the mechanics of abrasive wear discussed in Chapter 2, relative movement of components drives deterioration. The interactions between the rail pad assembly and concrete rail seat must be understood in greater detail as abrasion is examined as a potential RSD mechanism.

The large normal and shear forces that produce relative slip between the bottom of the rail pad assembly and the rail seat initiate and drive the abrasion process. Although fastening systems are typically optimized to attenuate vertical forces (including dynamic and impact loads), shear forces that exist on heavy-haul rail lines in the lateral and longitudinal direction are critical to the occurrence of RSD. The fact the RSD is more common in sharp curves and on steep grades indicates the importance of shear forces on RSD (Zeman 2010b). Just as vertical forces are dissipated, shear forces in the lateral and longitudinal direction must be dissipated in order to avoid component wear and failure.

Lateral and longitudinal loads also affect the pressure distribution at the rail seat such that the normal forces on the rail pad assembly are not uniformly distributed (Rapp 2013). In both field and laboratory studies, the pressure on the rail seat surface became concentrated on the field side as the L/V ratio increased, resulting in higher peak pressures (Rapp 2013). Also, a large

amount of variability was observed in the pressure distributions that were measured in rail seats in the field due to inconsistent ballast support, manufacturing variation, etc.

For decades, many railroad owners and operators have resisted the idea of selecting concrete crosstie and fastening system designs that allow for increased load attenuation (Rhodes 1988). Fastening components that allow for additional load attenuation are thought to be more susceptible to wear and fatigue if the movement of the rail relative to the rail seat increases (Rhodes 1988). However, the scenario whereby the stiffer rail pad assemblies and increased clamping forces (less load attenuation within the fastening system) restrains the rail such that no slip occurs relative to the rail seat has been refuted by evidence of abrasion in both field and laboratory evaluations. Based on the principle that some form of slip must occur for the forces in the rail to be dissipated to acceptable stress levels, an increased understanding of the relative motion among track components remains a worthy endeavor.

The design of the fastening system, namely the rail pad assembly, governs the force versus slip relationship at each contact interface of the fastening assembly, including the rail seat surface (Kerr 2003, Rhodes 1988). Based on the current understanding of rail movement and the mechanics of materials that make up the pad assembly, three types of rail pad assembly movement at the rail seat have been identified and are discussed below. In the following discussion, "rail pad assembly" will be referred to as "pad" for simplicity.

3.2 Pad Motion at the Rail Seat

3.2.1 Compressive Slip

Three types of relative motion have been observed at the rail seat interface. First, compression of the pad due to a normal force leads to radial expansion of the pad. In other words, when the pad is loaded in a direction perpendicular to its surface, the thickness of the pad

is reduced, resulting in an increase in the length and width of the pad. This type of motion is referred to as compressive slip, and is also known as "Poisson's effect". The amount of slip in this type of motion is dependent on the magnitude of the normal force, pad stiffness, the Poisson's ratio of the pad material, and the pad thickness.

The stiffness of the pad material refers to the vertical deformation of the pad for a given normal force. The stiffer the pad, the less it deforms under a given normal force. Pads that are less stiff deform more under the same load. The Poisson's ratio of rail pads is a material property that is correlated to the ability of the pad material to resist internal shear forces under axial compression, and Poisson's ratio describes the relationship between transverse (shear) strain to axial (compressive) strain. Materials with a higher Poisson's ratio tend to expand more under a normal load. The shear strain is multiplied by the thickness of the pad to determine the deformation. Thus, thicker pads have the ability to experience larger magnitudes of deformation. Theoretically, a thin, stiff pad with a low Poisson's ratio would mitigate abrasion that is driven by compressive motion.

Compressive slip may cause local contact points to slip relative to particles on the concrete surface, driving abrasion as individual particles are worn away. Compressive motion could possibly explain RSD on tangent track, where lateral forces are lower. Since deterioration typically initiates along the perimeter of the pad, it follows that the outward expansion of the pad may be enough movement to drive the concrete deterioration (Bahkarev 1994). Also, an imprint of the geometry of the pad is common in the deterioration pattern of the concrete, suggesting that small, local displacements are occurring (Johns 2010).

3.2.2 Gross Slip

Second, gross slip occurs when shear forces cause the entire pad to translate relative to the rail seat. Shear forces capable of producing gross slip are caused by large lateral and longitudinal loads. High lateral to vertical (L/V) load ratios, such as those experienced on sharp curves, can result in shear forces that will cause the pad to translate laterally. Alternatively, high tractive forces during train acceleration and braking can create large shear forces causing the pad to translate longitudinally (Rhodes 2013).

The propensity for gross slip of the pad to occur depends on the magnitude of the normal and shear forces and the shear modulus of the pad material. The shear modulus is defined as the ratio of shear stress to shear strain. Pads with a higher shear modulus deform less under an applied shear force. Since less deformation occurs within a pad with a higher shear modulus, gross slip is more likely to occur. Because gross slip has the potential for larger displacements relative to compressive slip, it likely has the potential to generate more severe abrasion.

3.2.3 Elastic Shear

Third, elastic shear is a type of pad motion where the top surface of the pad displaces in the direction of an applied shear force, deforming relative to the bottom surface of the pad. If the entire shear force is expressed as elastic shear, the bottom of the pad will not slip relative to the concrete rail seat. Alternatively, if the frictional force at the rail seat is less than the shear strength of the pad, the shear force will be expressed as gross slip instead of elastic shear. Elastic shear motion is commonly referred to as elastic slip, or elastic displacement (Rhodes, 2013). Here, I will use the term elastic shear because the rail seat is the reference frame for slip.

Elastic shear motion depends on the magnitude of the shear force, the shear modulus of the pad material, and the frictional force at the bottom of the pad. Abrasion is least likely to

occur during this type of motion since the pad does not move relative to the concrete rail seat during elastic shear motion.

3.2.4 Resistance to Pad Motion

Mechanical interlock with other components of the fastening system such as insulators and shoulders, where the components bear against one another at several interfaces, opposes all three types of pad motion. However, gaps at fastening system interfaces limit the effectiveness of mechanical interlock in resisting motion. Gaps are caused by manufacturing tolerances, changes in part geometry due to environmental effects, and component wear. Without gaps, the fastening system would be impossible to install in the field. Some portions of the edge of the pad are not confined, or interlocked, with another component. The two edges of the pad that are parallel to the rail interlock with the cast in shoulders for most fastening system designs. The edges of the pad that are perpendicular to the rail are typically unconfined, and motion is not restrained along those edges.

In addition to mechanical interlock, compressive slip and gross slip are also opposed by friction at the rail seat that acts against the direction of motion. Friction must be present for elastic shear to occur. All three types of pad motion are affected by friction, which will be the subject of the remainder of this chapter.

3.3 Friction at the Rail Seat

3.3.1 Friction Theory

Friction is the force tangential to the contact interface between two bodies that resists the relative motion between the bodies due to an applied load (Gao 2004, Czichos 1986). The most fundamental relationships related to friction, known as the Amontons-Coulomb laws, have been observed experimentally for over 500 years and still guide the current understanding of friction

(Gao 2004, Czichos 1986). The magnitude of the frictional force is directly related to the normal force between the two bodies by the coefficient of friction (COF).

$$F = \mu N$$

In this equation, F stands for the frictional force, N stands for the normal force, and μ represents the COF. Based on this fundamental law, the COF describes the ratio between the tangential force and the normal force. In other words, a rail pad assembly with a higher COF would require a larger shear force to cause slip for a given normal force.

Through significant amounts of research on this topic, researchers have identified many critical parameters that govern friction at the molecular level (Srinath 2005, Gao 2004, Czichos 1986). Due to the highly variable nature of the railroad environment, most of the parameters at the molecular level are overly theoretical. For example, the real area of contact affects the frictional force at the molecular level. Calculating the area of contact at the macroscopic level is highly uncertain due to imperfections of the concrete at the rail seat, abrasive fine particles, and the variability of normal force distribution. Thus, attempting to calculate the real area of contact at the molecular level does not appear to be feasible. At the macroscopic level, the Amontons-Coulomb laws effectively describe the frictional relationship of most sliding bodies (Gao 2004).

3.3.2 Typical Frictional Coefficient Values for Rail Seat Materials

A variety of values have been published in the literature related to the COF for the types of materials that are present at the rail seat. Many types of nylon 6/6 and polyurethane materials are available, and COF values reported in this section represent materials that have properties similar to common rail pad assemblies. For example, rail pads are commonly made of polyurethane that has a durometer hardness value of 95A on the Shore scale. All of the

polyurethane values reported in this section have durometer hardness values within about 10% of 95A.

Most standard tests for coefficient of friction use a steel counter surface, or counter face. Therefore, researchers who investigate the COF for nylon 6/6 are measuring the frictional force that exists as the nylon 6/6 surface moves relative to steel. Researchers have found experimental COF values for nylon 6/6 sliding against steel that range from 0.12 to 1.20, with an average of approximately 0.35 (Shin 2011, Srinath 2005, Thorpe 1986). For polyurethane sliding against steel, published COF values range from 0.40 to 1.50 with an average of approximately 0.50 (Gallagher 2012, Kaltzakorta 2012, Thorpe 1986). Thorpe used abrasive paper to replace the steel counter face, and the results of his study give us the most insight into friction at the concrete rail seat. Initially, nylon 6/6 had an average COF value of 0.63 when sliding against the abrasive paper (Thorpe 1986). After a run-in phase of ten minutes, the final COF value for nylon 6/6 and abrasive paper was 0.26 (Thorpe 1986). Using the same procedure, polyurethane sliding against abrasive paper had an average initial COF value of 0.85 and a final average COF value of 0.66 (Thorpe 1986). Thorpe attributes the reduction of COF to the formation of a transfer film. A transfer film is a layer of softened or fractured material that forms between the two contacting surfaces and acts as a lubricant.

Other relevant COF values such as rubber sliding on wet concrete yielded COF values that ranged from 0.46 to 0.70 (Gunaratne 2000). The range of COF values for rubber on dry concrete was higher, from 0.95 to 1.60 (Gunaratne 2000). The static COF value of nylon 6 sliding against polyethylene was measured to be 0.41 (Yamaguchi 1990). This pair of materials is similar to those that compose the interface between the abrasion frame (nylon 6/6) and rail pad (polyurethane). For purposes of comparison, Polytetrafluoroethylene (PTFE), commonly known

by the trade name Teflon and used to reduce the friction of moving parts, has a COF value of 0.04 when in contact with itself (Cardarelli 2008). The broad range of published COF values (summarized in Table 3.1) provides limited insight into the frictional forces that exist at the concrete rail seat. As a result, I developed a fundamental experiment to examine the COF of rail pads.

Table 3.1 Summary of relevant COF values in literature

Material	Counter Face	COF Range	Average COF
Nylon 66	Steel	0.12 - 1.20	0.35
Polyurethane	Steel	0.40 - 1.50	0.5
Nylon 66	Abrasive paper	0.26 - 0.63	N/A
Polyurethane	Abrasive paper	0.66 - 0.85	N/A
Rubber	Wet concrete	0.46 - 0.70	N/A
Rubber	Dry concrete	0.95 - 1.60	N/A
Nylon 6	Polyethylene	N/A	0.41
PTFE	PTEF	N/A	0.04

3.3.3 Fundamental laboratory experiment to measure friction

A fundamental laboratory experiment was executed to estimate the static coefficient of friction between the rail pad and a concrete surface. A rail pad was loaded with a known mass of 8.5 pounds and placed on a relatively smooth concrete surface. A lateral force was applied to the pad by tying one end of string to the pad and the other end to a hanging mass. By mounting a pulley to the edge of the elevated concrete surface, the direction of the load provided by the hanging mass was transferred so that gravity could be used to provide the lateral load on the pad (Figure 3.1).

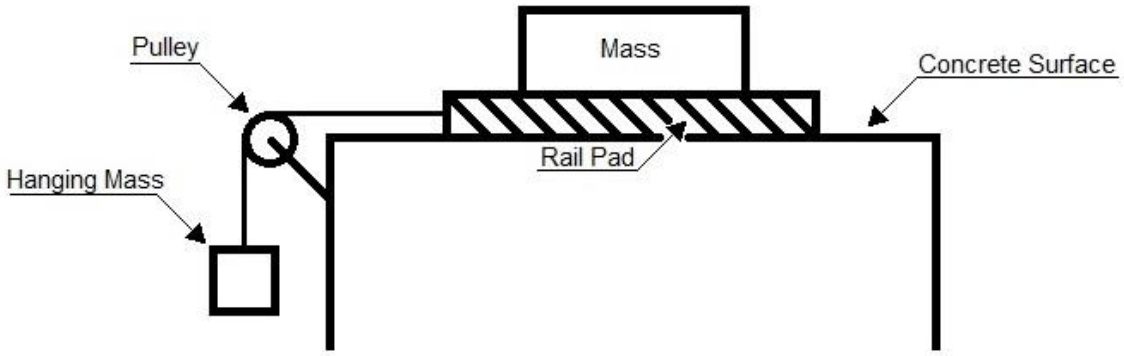

Figure 3.1 Schematic drawing of fundamental COF experimental setup

Three different rail pads were tested with four common conditions where contaminants from the environment infiltrate the rail seat. The first pad was a 2-part polyurethane pad assembly with a flat bottom (Figure 3.2). In contrast, the second and third polyurethane pads had studded (Figure 3.3) and dimpled (Figure 3.4) geometry, respectively. The conditions simulated were (i) dry contact interface (control), (ii) sand added, (iii) water added, and (iv) water and sand added. Sand and water were added manually to the contact interface in this experiment.

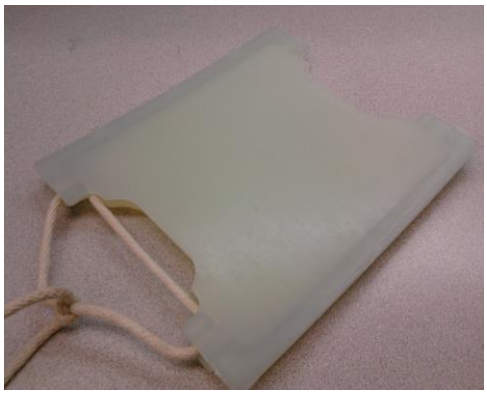

Figure 3.2 Bottom of two-part pad assembly (flat)

Figure 3.3 Bottom of studded pad

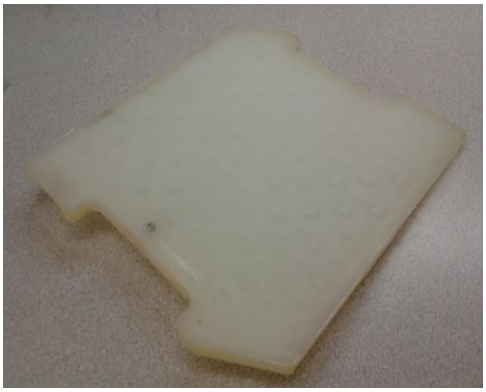

Figure 3.4 Bottom of dimpled pad

Weight was added to the hanging mass until the pad moved. The weight of the hanging mass required to move the pad was divided by the weight of the loaded pad, resulting in the experimental static coefficient of friction. For each pad geometry and rail seat contaminate condition, three repetitions were conducted and the mean COF values are reported in Table 3.2. The introduction of sand and water to the interface between the pad and the concrete surface reduced the average static COF values for each trial, regardless of the pad geometry. Sand at the interface reduced the static COF values by an average of 36% while water reduced the static COF values by 14%, as compared to the control surface condition. The average static COF of

the pad with a flat bottom was reduced at a greater rate than the pads manufactured with various geometries.

Table 3.2 Average experimental static COF values for rail pads on a concrete surface

Geometry of Pad Bottom	Surface Condition			
	Control	Sand	Water	Sand and Water
Flat	0.83	0.46	0.64	0.45
Studded	0.77	0.50	0.66	0.42
Dimpled	0.65	0.47	0.63	0.54

Overall, the COF values measured in this fundamental experimental are within the range of COF values published in previous studies of similar materials (Section 3.3.2). This experiment is limited by the applied normal load, which is many orders of magnitude smaller than normal loads on rail pads in the field. The static COF values observed in this study will be compared to those measured in the large-scale abrasion test (Chapter 5).

3.4 Relationship Between Friction and Abrasion

Some relative movement between the rail pad assembly and the rail seat is unavoidable due to the magnitude of normal and shear forces at the rail seat and gaps at fastening system interfaces. The three types of pad movement at the rail seat identified in this chapter are resisted by friction. One potential method of mitigating abrasion at the rail seat may be to limit the relative slip at the rail seat by increasing the frictional forces. The relationship between pad movement, friction, and abrasive wear is unknown. The need for an experiment to investigate these relationships was additional motivation for the large-scale abrasion test setup (Chapter 4).

CHAPTER 4: DETERIORATION EXPERIMENT

4.1 Motivation

The study of abrasion, which is a progressive failure mechanism, requires observation of wear surfaces after hundreds of thousands of loading cycles so that the amount of deterioration can be assessed. A laboratory test that is more representative of the rail seat abrasion mechanism than the ASTM standard tests described in Chapter 2 is necessary to determine the best approaches to mitigate abrasion of concrete rail seats. A novel laboratory test called the Large-Scale Abrasion Test (LSAT) was developed at the UIUC to produce measurable abrasive wear on mock concrete rail seat surfaces in a reasonable number of loading cycles. The LSAT was designed to isolate the parameters that are believed to affect the abrasion mechanism and facilitate the acquisition of quantitative and qualitative data related to each parameter.

Several hypotheses were formulated in order to systematically investigate the mechanics of abrasion of the concrete rail seat. It was hypothesized that (a) after 32,000 cycles, more than 0.01 inches of concrete could be worn away from the concrete surface. Additionally, it was hypothesized that increases in the severity of concrete abrasion results from (b) increases in the magnitude of pad displacement, (c) increases in the magnitude of the normal force, (d) the addition of water to the contact interface, and (e) the addition of sand to the contact interface.

Based on these hypotheses, the parameters included in the deterioration tests were the amount of horizontal displacement of the abrading surface relative to the concrete specimen, the magnitude of the normal vertical load, the presence of moisture on the surface of the concrete specimen, and the presence of abrasive fines at the beginning of the test. Response variables that were measured included the maximum and average depth of material lost. The testing protocol described in the next section was implemented to test these hypotheses, develop a tool for

evaluating the abrasion resistance of innovative rail seat materials, and improve the current understanding of the mechanics of abrasion of concrete surfaces.

4.2 Experimental Design

4.2.1 Test Equipment

A servo-hydraulic system was used to produce displacements of a pad relative to a concrete specimen while a static normal force was applied (Figure 4.1).

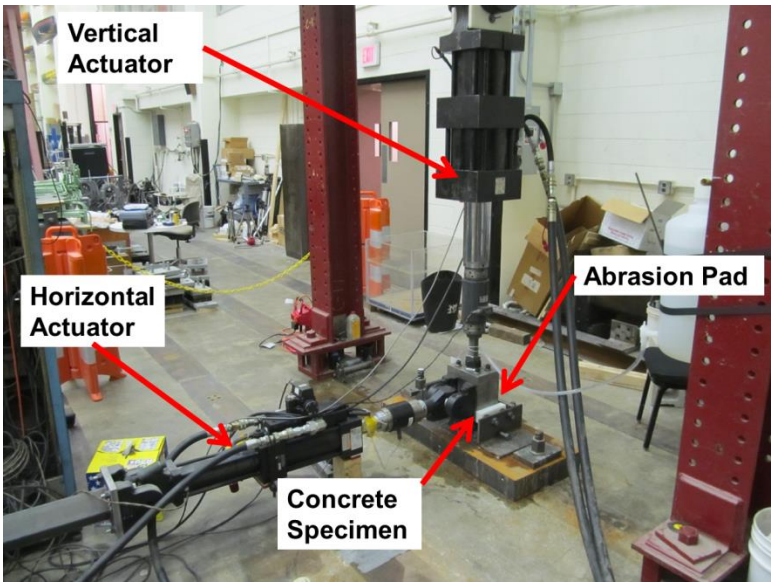

Figure 4.1 Photograph of Large-Scale Abrasion Test (LSAT) setup

A servo-hydraulic actuator with a force capacity of 35 kilopounds (kips) was used in displacement control to provide the force needed to accelerate the pad tangentially along the concrete surface (perpendicular to the normal load) and return the pad to its original position. Simultaneously, an additional servo-hydraulic actuator with a force capacity of 110 kips in force control provided a static normal force on the pad so that representative contact pressures could be maintained. An existing hydraulic power supply (pump) and hydraulic manifold (line tamer) were used to supply the actuators with hydraulic fluid.

The swivel base assemblies on the actuators were bolted to an existing structural frame in the Newmark Structural Engineering Laboratory (NSEL) at the UIUC. Based on previous testing experience with the frame, it was determined to be safe for the requirements of this test setup (Zeman 2010b). The hydraulic equipment was controlled with an MTS analog control system that consisted of a MTS 406/436 controller and a function generator.

The actuators were bolted to a steel loading head that housed the 3 x 4 x ¾-inch pad in a recessed cavity. The swivel base of the horizontally mounted actuator was bolted to the loading head. Alternatively, the vertically mounted actuator was rigidly attached to the loading head using a threaded rod and 1-inch thick steel plate. The loading head was 9 x 6 x 8 inches with a 3 x 4-inch cavity that was cut ½-inch deep into the solid steel loading head (Figure 4.2). The cavity was designed so that two thirds of the pads thickness was confined in the cavity. One third of the pad thickness protruded from the loading head and was unconfined. The unconfined portion of the pad was designed to be representative of the thickness of common rail pads.

Figure 4.2 Loading head and bottom view of pad housed in cavity

The bottom of the pad was designed to be in flush contact with the concrete specimen located directly beneath the loading head. Four 3 x 2½ x 6-inch long steel angles were used to

secure concrete specimens to a rigid base plate. To ensure that the angles were held flush with the concrete specimens, a threaded rod was used to press two adjacent angles against the concrete specimen. The rods were threaded through 1-inch thick steel plates that were welded or bolted to the base plate. The 42 x 18 x 4¼-inch thick base plate was made of steel and bolted to the NSEL strong floor. The design intent of this test setup was to rigidly secure all equipment and framework in order to restrict the movement of all components such that the slip of the system was isolated at the interface between the bottom of the pad and the top of the concrete specimen.

4.2.2 Testing Materials

The concrete mixture design used in this experiment was modeled after a mixture that is representative of current concrete crosstie technology in North America and was previously used for the UIUC concrete crosstie research (Bakharev 1994, Zeman 2010b). The constituents of the target concrete mixture design and the properties of the concrete are listed below (Table 4.1 and Table 4.2).

For each batch, fresh concrete was placed into forms to make twenty 6 x 6 x 3-inch specimens. The forms were made of plastic side panels for twenty individual molds that bolted to a steel base. The concrete in each mold was consolidated in two lifts with a rod and a shake table. Ten impacts with the rod and ten seconds of vibration with the shake table for each lift resulted in good consolidation. The top surface of the specimens was hand finished with a trowel. To simulate the surface finish of the concrete rail seat, the bottom of each specimen was cured against the steel base. Concrete crossties are constructed upside down such that the rail

Table 4.1 Mix design for concrete specimens

Material	SSD Weights	Stock Batch Weights (lb)	Moisture Content (%)
Coarse aggregate	1809 (lb/yd^3)	134.0	-1.78
Fine aggregate	1218 (lb/yd^3)	90.2	-2.00
Cement (Type I)	640 (lb/yd^3)	47.4	
Water	205 (lb/yd^3)	19.27	
Target air content	5%		
Target water-to-cement (W/C) ratio	0.32		
Target slump	3.0 in		
Target batch volume	1.0 ft^3		

Table 4.2 Properties of concrete specimens by batch

	Batch A	Batch B	Batch C	Batch D	Batch E*
Air entrainment (mL)	5.0	5.0	5.0	5.0	5.0
Super plasticizer (mL)	110.0	110.0	110.0	110.0	120.0
Air content %	5.0	6.6	4.8	4.9	7.0
Slump (in)	1.50	2.25	1.25	0.75	1.00
Unit weight (pcf)	144.4	144.8	145.6	146.0	144.8
28-day stength (psi)	5719	6757	N/A	8178	9275
	7291	7628	N/A	7628	9529
	6204	7126	N/A	7063	8674
Average strength (psi)	6405	7170	N/A	7623	9159

*Batch E was tested for strength at 96 days

seat is formed against steel molds. The forms in this experiment were designed with the intent that the bottom surface of the concrete specimens was in contact with the pad and abraded during deterioration tests.

The pad materials that were used in this study, nylon 6/6 and polyurethane, were selected based on their material properties and available thicknesses. Because of the ½-inch depth of the loading head cavity, pads for this test were cut from a ¾-inch thick sheet that was purchased from a general material supplier. The nylon 6/6 and polyurethane exhibited material properties similar to those used in rail pad assemblies that are currently in track on North American heavy-axle-load freight railways (Tripple 2011). The cross section of the pad was designed to reduce the normal force required to achieve contact pressures that are representative of those in the field. The cross-sectional areas of common rail pad assemblies are between 34 and 48 square inches (in^2). Nominal field pressures – pressures calculated assuming a perfectly uniform pressure distribution – are estimated to be 400 to 1,800 pounds per square inch (psi). The bearing area of the pad was scaled by a factor of four, resulting in 3 x 4-inch pads that have a cross-sectional area of 12 in^2. By scaling the experiment at a 1:4 ratio, wheel loads ranging from 0 to 40 kips, which make up most of the wheel loads occurring in the field, were replicated using actuators applying 0 to 10 kips (Zeman 2010b).

Water was added to the contact interface via a water tank and a channel cut into the loading head that allowed for water to drip at the four edges of the pad. This method proved to be an effective means for adding water to the interface between the pad and concrete. Approximately 80 grams of sand was measured with a measuring cup and added to the contact interface manually before starting each deterioration test. Sand could not be carried through the channel in the loading head because the sand clogged the channel and material could not be

deposited at the contact interface. Initially the same pit run sand (IDOT FA-02 gradation) that was the fine aggregate constituent of the concrete specimens was applied to the concrete surface. To add more control to the experiment, manufactured sand (Ottawa 20-30 gradation) was selected for the deterioration tests reported in Section 4.5.

4.2.3 Loading Regime

In an effort to cause measurable abrasion to the concrete specimens, the LSAT simulated the demands on the rail pad and concrete rail seat materials when high lateral loads and/or fastener component wear result in cyclic, lateral translation of the pad. During the deterioration tests, normal forces ranging from 0 to 10 kips were applied to the pad with the vertical actuator. The normal force on the pad remained relatively static (within approximately 15% of the target vertical force) throughout the tests, as the pad was moving laterally.

The cyclic lateral displacements of the pad were caused by the lateral actuator. The function generator specified a sine waveform for the input of the lateral displacements that ranged in frequency from 3 to 6 Hertz (Hz). A SoMat 2100 data collection system collected the force and displacement data from both actuators.

Because the concrete specimen was continuously loaded, the loading cycles in this abrasion resistance test should not be correlated to loading cycles on rail seats in the field. Field loading cycles are less damaging because the normal load is relaxed between wheel loads.

4.2.4 Methodology for Measuring Severity of Concrete Deterioration

The severity of concrete abrasion was the key response variable, or measured output, in the deterioration experiment. A three-dimensional imaging system, which uses laser triangulation to map the physical position of points in space, measured the amount and position of abrasive wear that occurred on the concrete specimens. Each deteriorated specimen was

systematically scanned with an arrangement of lasers and cameras (MicroScan) mounted to the arm of a contact scanning device (MicroScribe MLX). Each deteriorated specimen was scanned a total of five times using this equipment that was loaned by the BNSF Railway. Each scan lasted about 2 minutes and included approximately 20 passes, or sweeps, in multiple directions over the surface of the specimen. The concrete specimens were 3-inches wider and 2-inches longer than the abrasion pad. Therefore, any point less than ¾-inch from the edge of the specimen surface was estimated as the portion of each concrete specimen that was not deteriorated (Region O). Any points inside of Region O were called Region N. Although some small portions of Region N were not deteriorated, this classification system allowed nearly all of the deteriorated portions of the concrete surface to be systematically separated from the concrete that was undamaged.

The wear depth was calculated by subtracting the mean depth (z-coordinate) of every point contained in Region N from the mean depth of every point in Region O for each of the five scans. After the wear depth was calculated for each scan individually, the average of the five calculated wear depths was reported as the average wear depth, D_{avg}. Similarly, the maximum wear depth, D_{max} was found as the average difference between the mean z-coordinate of Region O and the minimum z-coordinate of Region N. This method of quantifying the severity of abrasion on concrete specimens proved to be accurate within approximately 0.006 inches based on two standard errors (approximately 95% confidence interval).

4.3 Experimental Test Problems

4.3.1 Test Setup Problems

Beyond the challenge of measuring the deterioration of the concrete, many valuable concepts were learned by addressing several problems with the setup and execution of the LSAT.

First, the load cells and linear variable differential transformers (LVDT) contained within both actuators were calibrated manually. In this way, I was able to reliably control and monitor the force and displacement continuously with the analog controller. Calibrating the load cells and LVDT's was necessary because a certifiable calibration was not available for any of the equipment that was assembled for the LSAT setup. The force calibration was performed by placing a previously-calibrated load cell between the load cell of the actuator and a fixed surface. This calibration occurred while the actuators were mounted in their final testing position, and a variety of forces were applied to the system. Then, the voltage of the calibrated load cell was used to calculate the force on the actuator load cell. Next, the known force was plotted relative to the voltages read from the actuator's load cell. The equation of this calibration curve was used to resolve the voltage of the load cell into force units throughout experimental testing with LSAT. The calibration of the horizontal actuator was difficult because a special steel fixture had to be fabricated to react against the lateral actuator.

Next, the LVDT in each actuator was calibrated using a dial gauge to measure the actual displacement of the actuator. Similar to the load cell calibration, the known displacements measured from the dial gauge were plotted relative to the voltages read in the actuator's LVDT. The equation of this calibration curve was used to resolve the voltage of the LVDT into displacement units throughout experimental testing with the LSAT.

Once the load cells and LVDT's were calibrated, shakedown tests were initiated to understand the behavior of the experimental test setup. A problem was observed immediately with the design of the connection of the vertical actuator to the loading head. I originally designed this connection to be a roller connection. During the first shakedown test, the loading head rotated relative to the vertical actuator. The LSAT was designed with the intention that the

loading head would translate in the lateral direction so the movement of the lateral actuator could occur as slip between the abrasion pad and the concrete specimen. Since the loading head was rotating, the pad did not appear to be slipping relative to the concrete surface. In order to resolve this challenge, the connection between the vertical actuator and loading head was redesigned to be a fixed connection. A threaded rod screwed into the actuator ram on one end and a steel plate bolted to the loading held on the other provided a connection that resisted rotation. Spanner nuts locked the threaded rod in place.

In addition to the connection challenge, the structural frame appeared to be vibrating in the direction of the motion (perpendicular to the orientation of the frame). Supplementary lateral bracing was considered to limit the displacement of the frame. However, adding steel shims under the base plate connections of the columns that made up the structural frame mitigated the vibration of the frame and resulted in negligible displacements.

Next, the propensity for large elastic deformations in the structural connections of the test setup had to be minimized in order to ensure that a repeatable structural response was achievable. By loading the test frame with vertical and horizontal actuators at forces that were near the capacity of each cylinder, the connections were stretched beyond their elastic limit to minimize the deformations in the structural connections. Another problem with the structural connections occurred when the spanner nuts that secure the threaded rod to the actuator became loose. Once this problem was recognized, the spanner nuts were tightened periodically.

Challenges were not limited to the LSAT structural frame. Due to irregular behavior of the electronic signals that monitored the displacement and load of both actuators, ground wires were attached from the ground connection of the control system to each actuator and the steel box that housed the data acquisition system. These additional ground wires reduced the

irregularity (noise) of the signals by eliminating potential ground loops, or differences in potential between the controllers, actuators, and data acquisition system.

The analog control system made signal input difficult because the input voltage was read from a digital multi-meter that was accurate within a millivolt (mV). Repeating the input signal was difficult because the signal fluctuated naturally up to a hundredth of a volt (100 mV). Although the input signal with the analog control system was not as precise as a common digital control system, a systematic process was used to increase the repeatability and control of the LSAT. The process consisted of setting the knobs on the analog control system so that the input voltage of the transducer controlling the actuator was set to the nearest millivolt. The variability of the input force and displacement was reduced to less than 10%.

The capacity of the vertical actuator and its load cell was 110 kips. The maximum input load for the deterioration tests in this experiment was 10 kips. Most load cells are only rated to be accurate plus or minus 0.5% of their capacity. Thus, the vertical load could only be controlled and read to an accuracy of plus or minus 500 pounds. For the purposes of this experiment, an actuator with a smaller capacity would have resulted in increased accuracy for vertical load application.

4.3.2 Testing Behavior Challenges

After overcoming several challenges with the test setup, shakedown tests also allowed me to refine the protocol for the deterioration tests. As the duration of the shakedown tests increased, significant challenges became apparent that were not anticipated during the planning and design of the LSAT. One of the first was that the pad material began to deteriorate after only a few hundred loading cycles, and the material degradation increased with loading cycles. The abrasive action of the LSAT resulted in the wear of individual particles and small pieces of the

polymer material such that a progressive decrease in pad thickness was visible. For shakedown tests that lasted from four minutes up to four hours, pad deterioration ranged from scratching and scarring of the pad surface to complete breakdown of pad material. One nylon 6/6 pad was completely worn into small pieces resulting in the loss of the entire ¼-inch exposed portion of the pad.

When each shakedown test ended, the temperature of the contact interface between the pad and concrete was noticeably warmer ambient. As observation of the contact interface progressed, the entire pad did not appear to be bearing on the concrete surface and the increased temperatures were not observed on all portions of the pad. Instead, the increased temperatures appeared to be localized at the primary load bearing contact points on the pad. These localized regions of increased temperatures hot to the touch, and this was where the most severe deterioration, softening, and plastic flow of material was observed. Evidence of the deterioration and softening was documented in the photos in Appendix A: Detailed Results of Deterioration Experiment.

Since the deterioration of the pad exceeded that of the concrete surface, water was used to keep the pad temperature down. In order to provide water to the contact interface, a 3/8-inch diameter hole was drilled into the loading head. A water tank was attached to the test frame, and water was carried to the loading head via a flexible plastic tube. The tube deposited the water into a funnel that fed directly into the hole in the loading head. The hole began near the top of the loading head and carried water to the terminal end of the hole in the center of the cavity that holds the pad. Grooves were cut into the top surface of the cavity to allow water to travel from the center of the pad to each of the four edges of the pad. Consequently, water was deposited at the contact interface from each edge of the pad continuously for the remainder of the

deterioration tests. The water system was successful in slightly reducing the temperature build up and severe deterioration of the pad material. However, the temperature increase and severe pad degradation occurred consistently at the primary load-bearing contact points, regardless of the amount of water that was applied to the contact interface.

One additional problem that stemmed from the design of the loading head and cavity was that removing pads after testing was extremely difficult. This problem was exacerbated by temperature build up and pad degradation because portions of the pad began to adhere to the loading head cavity. First, a hammer and chisel were used to remove pad materials after a completed test. Subsequently, damage to the steel along the edges of the cavity made it nearly impossible to install or remove pads. Therefore, the loading head was removed from the test setup so that the cavity could be restored to its original geometry. A portion of the loading head was cut out and modified so that it could be unbolted for pad removal. This method proved to be effective and repeatable.

4.4 Final Deterioration Test Protocol

The intent of the final protocol for the deterioration tests was to reduce the variability among tests. First, a new concrete specimen was installed by pressing the angles against the specimen (by tightening the threaded rods). Then a new pad was inserted into the cavity of the loading head by tapping it with a hammer. Next, the water drip was started by adjusting the nozzle on the water tank until the drip rate was approximately 1 milliliter per second, which was measured by counting water drops for ten seconds. After the water drip was initiated, 80 grams of sand was placed by hand on the concrete surface and spread evenly over the pad bearing area.

Then, the static normal load was applied with the vertical actuator by turning the set point control of the analog control system until the output voltage of the actuator, measured with a

digital multi-meter, matched the desired force from the load cell calibration curve. After the data collection system was started, the function generator was turned on so that the lateral actuator in displacement control began to cycle through the designated displacement range. Periodically, the nozzle on the water tank was adjusted to maintain the water drip as consistently as possible.

After 3 hours, the cycling lateral load was stopped and the normal force was removed. In order to better understand the heat increase at the contact interface, the temperature of the concrete surface was measured with an infrared thermometer after the test, as soon as a measurement could be recorded safely. The infrared thermometer used in this study was an Extech Instruments IR 250, compact thermometer that had an internal laser for identifying the target area. The entire concrete surface was scanned with the laser to find the maximum temperature.

4.5 Results

After overcoming significant challenges that surfaced during the shakedown tests, the severity of the concrete deterioration was tested and quantified for a total of ten concrete specimens (Table 4.3).

The LSAT consistently caused deterioration of these concrete specimens. The abrasion mechanism caused up to 0.32 inches of concrete loss based on the calculation of maximum wear depth. Including the shakedown tests, concrete deterioration was observed for all specimens, regardless of pad type, normal force, magnitude of displacement, etc. The concrete deterioration initiated near the edges of the pad and propagated inward. The deterioration was typically more severe along the two edges that were perpendicular to the direction of motion (Figure 4.3).

Table 4.3 Summary of deterioration test data

Test No.	Pad Type	Mean Normal Force (Kips)	Max Displacement Range (in)	Load Rate (Hz)	Number of Cycles	Maximum Wear Depth D_{max}	Average Wear Depth D_{avg}
1	Nylon 6/6	3.2	0.10	3	18,900	0.139	0.013
2	Nylon 6/6	3.2	0.05	6	64,800	0.104	0.015
3	Nylon 6/6	3.2	0.05	6	65,520	0.144	0.011
4	Nylon 6/6	3.3	0.14	6	64,800	0.178	0.028
5	Nylon 6/6	1.3	0.13	6	64,800	0.202	0.016
6	Polyurethane	3.3	0.13	6	64,800	0.173	0.012
7	Nylon 6/6	2.5	0.13	3	32,400	0.153	0.021
8	Nylon 6/6	3.3	0.14	3	25,200	0.320	0.062
9	Nylon 6/6	2.9	0.13	3	32,400	0.176	0.040
10	Nylon 6/6	3.0	0.13	3	32,400	0.186	0.020

Figure 4.3 Increased abrasion along pad edges of concrete specimen after deterioration test

Similar to the shakedown tests, the pad materials in the ten deterioration tests exhibited severe deterioration at the primary load bearing contact points where increased temperatures led to softening and plastic flow of the material. The recorded temperature of the concrete was as high as 181° F when it was measured a few seconds after the test ended. Therefore, the pad temperatures were assumed to be above 200° F during the tests. The increased temperature and

pad deterioration, not typically observed in the field, must be acknowledged as a limitation of this test.

The small sample size and experimental variability made finding correlations between the input variables and the response variables difficult. Increasing displacement magnitude and normal force appear to result in increased levels of deterioration. The load rate and number of cycles may be independent of severity of abrasion in this experiment. Based on physical observations, nylon 6/6 pads appeared to cause more deterioration than polyurethane pads. Overall, the sample size was too small to determine the relationships between the variables, and more replicates are needed to increase the understanding of the mechanics of abrasion.

4.6 Conclusions

Abrasion was confirmed as a viable RSD mechanism based on results from numerous shakedown and deterioration tests with the LSAT that caused measurable losses on the concrete surface. This experiment confirmed that a substantial amount of concrete could be worn away from a concrete surface by isolating the abrasion mechanism.

Though the pattern of concrete deterioration resembled that of many cases of RSD in the field, the rapid deterioration and plastic deformation of the pad materials was much more severe than typical pad wear. Consequently, the protocol was too aggressive, resulting in a disproportionate amount of mechanical energy input into the interface between the pad and the concrete.

The limitations of this experiment include the excessive heat that was generated and the small sample size. These factors limited the correlation of the normal force and displacement with the severity of concrete abrasion.

This experiment showed that replicating the mechanics of abrasion, a phenomenon that occurs in the field of railway engineering, directly conflicts with the desire to accelerate progressive deterioration. Future experiments focused on improving the understanding of the abrasion mechanism must balance field representativeness with the pursuit of accelerated results.

Due to the amount of variability in this deterioration experiment, the focus of this project shifted in order to increase the experimental control. Diverging from the initiative to measure the severity of abrasive wear, the frictional forces that resisted the movement of the pad became the focus (Chapter 3). Seeking to reduce the number of variables, a new experiment was developed that enabled the measurement of the frictional forces at the contact interface (Chapter 5).

CHAPTER 5: FRICTION EXPERIMENT

5.1 Motivation

As described in Chapter 3, friction at the rail seat may have an effect on the response and performance of the fastening system. Friction likely affects the movement of the pad relative to the rail seat, the transfer of wheel loads as they move from the top of rail through the fastening system components into the rail seat, and the abrasive wear behavior of both the rail pad assembly and concrete rail seat. Based on observations made during the deterioration experiment described in Chapter 4, the frictional relationships that exist between rail pad materials and mock concrete rail seats appeared to change throughout the tests and vary based on a number of factors (Kernes 2012). In order to examine the frictional relationships, the LSAT setup described in Chapter 4 was used to simulate the demands on the rail pad and concrete rail seat materials when high lateral loads and/or fastener component wear result in cyclic, lateral translation of the pad. In contrast to the deterioration experiment where many thousands of loading cycles were necessary to understand the magnitude of progressive abrasion, observations related to the frictional characteristics were feasible after a smaller number of loading cycles. As a result, the testing procedure was designed to simulate a single train pass. It was hypothesized that the coefficient of friction (COF) would be reduced as (a) the temperature of the contact interface increased, (b) plastic deformation occurred at contact points on the concrete surface after multiple simulated train passes, (c) the stiffness of the pad material was increased, (d) the magnitude of the normal load on the pad was increased, and (e) water and sand were added. Hypotheses (a) and (d) stemmed from observations made during deterioration tests. Hypothesis (e) was based on the results of the fundamental friction test described in Chapter 3. The testing protocol described below was implemented in order to evaluate the validity of these

hypotheses and to investigate the relationship between friction and abrasion of concrete crosstie rail seats.

5.2 Friction Experiment Protocol

5.2.1 Testing Procedure

A testing protocol was devised with the objective of simulating a single pass of a 100-car unit train using the LSAT (Chapter 4). The train was simulated by applying 400 loading cycles to the pad and concrete specimen, representing 100 four-axle rail cars. For each individual pad and concrete specimen, 400 lateral load cycles were applied at a frequency of 3 cycles per second (3 Hz) using the horizontally mounted actuator in displacement control. The magnitude of the displacement of the pad was fixed at 1/8 inch. The vertical actuator in force control applied a specified normal load to the pad that essentially remained static throughout the test. The number of loading cycles and magnitude of displacement were fixed to reduce the number of variables relative to the deterioration experiment.

Throughout each test, a data acquisition system was used to record information from both actuators. The vertical force, P, and vertical displacement were recorded from the vertical actuator's load cell and linear variable differential transformer (LVDT), respectively. Similarly, the acquisition of data from the load cell in the horizontal actuator allowed me to constantly monitor the force, F, required to move the loading head to a specified position. The lateral displacement data were collected from the LVDT in the horizontal actuator. The fundamental relationship for coefficient of friction described in Chapter 3 was used to calculate the coefficient of friction (μ) at five different instances during each test.

$$\mu = |\boldsymbol{F}|/\boldsymbol{P}$$

100-cycle intervals were selected to periodically capture the frictional behavior throughout the test while reducing the amount of data so that it could be analyzed with greater efficiency.

In order to monitor the thermal effects on the friction of the pad materials, the temperature of the pad surface was measured with an infrared thermometer before each test, and again as soon after the 400^{th} cycle that it could be safely recorded. The infrared thermometer used had an internal laser to identify the target area. The entire pad surface was scanned to find the maximum temperature. After the initial temperature, T_i, was measured, the normal load was applied to the pad with the vertical actuator. The position of the lateral actuator was verified so that the midpoint location of each test was consistent. Next, the data acquisition system was initiated and the function generator that controls the horizontal actuator was turned on. The horizontal actuator started at position "0", moved forward 1/16 inch, returned to "0", and moved in the opposite direction for 1/16 inch for a total lateral displacement of 1/8 inch. After approximately 2 minutes and 14 seconds of continuous, cyclic motion, or 400 cycles, the test was stopped. Approximately 7 seconds passed between the last loading cycle and the time of the temperature measurement while the cyclic motion of the lateral actuator was stopped and the loading head lifted to facilitate the temperature measurement. Once I retracted the loading head and the hydraulic system was turned off, I scanned the surface of the pad continuously in the same manner as prior to the test and recorded the maximum detected temperature, T_f. Before the next test was started, the pad was allowed to cool to within one degree of its original starting temperature.

5.2.2 Experimental Design

Three groups of friction tests were performed to evaluate the previously-mentioned hypotheses. The three groups of tests are referred to as the heat/deformation tests, normal load

tests, and rail seat contaminant tests. In each group of tests, nylon 6/6 and polyurethane pads were tested to compare the most common materials that are currently used in rail pad assemblies.

5.2.2.1 Heat/Deformation Tests

The heat/deformation tests were designed to distinguish the effect of the heat buildup from the effect of increasing levels of plastic deformation at contact asperities, relative to the coefficient of friction. In other words, the effect of heat that resulted from multiple load cycles within a single test should be separated from the effects of deterioration that occurred from sequential tests on the same concrete specimen and pad pair. Four 400-cycle tests, denoted by Test R, Test S, Test V, and Test W were performed on each concrete specimen and pad. Allowing the pad to cool between each test helped me understand how heat influenced the coefficient of friction independent of the plastic deformation that was present at the beginning of the second, third, and forth tests on each specimen.

Eleven nylon 6/6 pads and concrete specimen pairs underwent four replicate tests, yielding a total of 44 tests. Eight polyurethane and concrete specimen pairs underwent four replicate tests, yielding a total of 32 tests. A static 5-kip normal load was applied to the pad but no environmental contaminants such as water or sand were added to the contact interface.

5.2.2.2 Normal Load Tests

These tests were conducted to evaluate the effect of increasing normal load on the frictional coefficient between the pad and concrete surface. Normal loads of 3 kips and 10 kips were applied to both pad types. Each pad and concrete specimen pair was tested four times at each load magnitude. Two sets of four tests were performed for nylon 6/6 and polyurethane pads, resulting in a total of sixteen tests of each pad type. Similar to the heat/deformation tests,

no water or sand was added to the contact interface. The results from the normal load tests could be compared to the heat/deformation tests that were performed with a 5-kip normal load.

5.2.2.3 Rail Seat Contaminant Tests

These tests were designed to determine the effect of three common conditions where contaminants from the environment infiltrate the rail seat. Manufactured sand (Ottawa 20-30 gradation) and tap water were used to simulate the effect of moisture and abrasive fines that penetrate into the rail seat interface. The conditions simulated were (i) dry contact interface with no sand, (ii) water but no sand, and (iii) water and sand added. Condition (i) is the control case for these tests. Condition (ii) was created by adding water continuously through the channel in the loading head (Chapter 4). In addition to the water drip, I manually added sand to the contact interface before each test with condition (iii). The condition of sand but no water was eliminated from the experimental design because the pads could not withstand the heat buildup without the water to cool the contact interface. Extreme pad deterioration resulted from a few shakedown tests with sand but no water.

For each concrete specimen and pad pair, four simulated train passes were performed for each condition in sequential order. Thus, after four tests with condition (i) (1,600 total cycles), water was added (condition (ii)) for four tests, or 1,600 additional cycles. Finally, four tests were performed on the same specimen for rail seat contaminant condition (iii). Overall, each specimen underwent 4,800 loading cycles spread over twelve tests, corresponding to four tests for each of the three conditions. Similar to the deterioration experiments, water was applied at the top of the pad and allowed to drip into the contact interface via the pad edges. After the water drip was initiated, 80 grams of sand was placed by hand on the concrete surface and spread

evenly over the pad bearing. The concrete and pad materials were cleaned with compressed air and cooled to their original surface temperature between each 400-cycle test.

5.3 Results and Discussion

The ratio of lateral load to vertical load was plotted at loading cycle 5, 100, 200, 300, and 400. Information from the first few loading cycles was difficult to interpret because these portions of the tests were not as repeatable as the remainder of the tests due to limitations of the testing equipment. The fixed connections on the equipment combined with imperfect test specimens resulted in minor misalignments of the pad relative to the concrete. Typically, the minor misalignments were compensated and the test setup reached equilibrium after the first three loading cycles. Therefore, the first few loading cycles were excluded from this analysis. Nonetheless, when the pad slid relative to the concrete surface, the plot of lateral and vertical load relative to time showed repeatable behavior for the majority of the test duration. Upon plotting the calculated COF, a few general trends in the shape of the graph were observed. Figure 5.1 shows an example plot for three loading cycles that occurred during a friction test.

During the lateral movement phase of each cycle, the COF decreases slightly as the pad slides, where kinetic friction is resisting pad movement. As the movement of the loading head slows to reverse direction, the magnitude of the lateral force drops to zero. At the end of each lateral displacement cycle, static friction resists pad movement and the COF value is at its highest magnitude just as the pad begins sliding in the opposite direction. The COF drops to zero again as the pad changes direction. This pattern is consistent with fundamental tribological principles, where the kinetic COF is expected to be lower than the static COF (Chapter 3). The peak value for COF during the specified loading cycle, between the changes in direction, was selected as the COF value for that loading cycle.

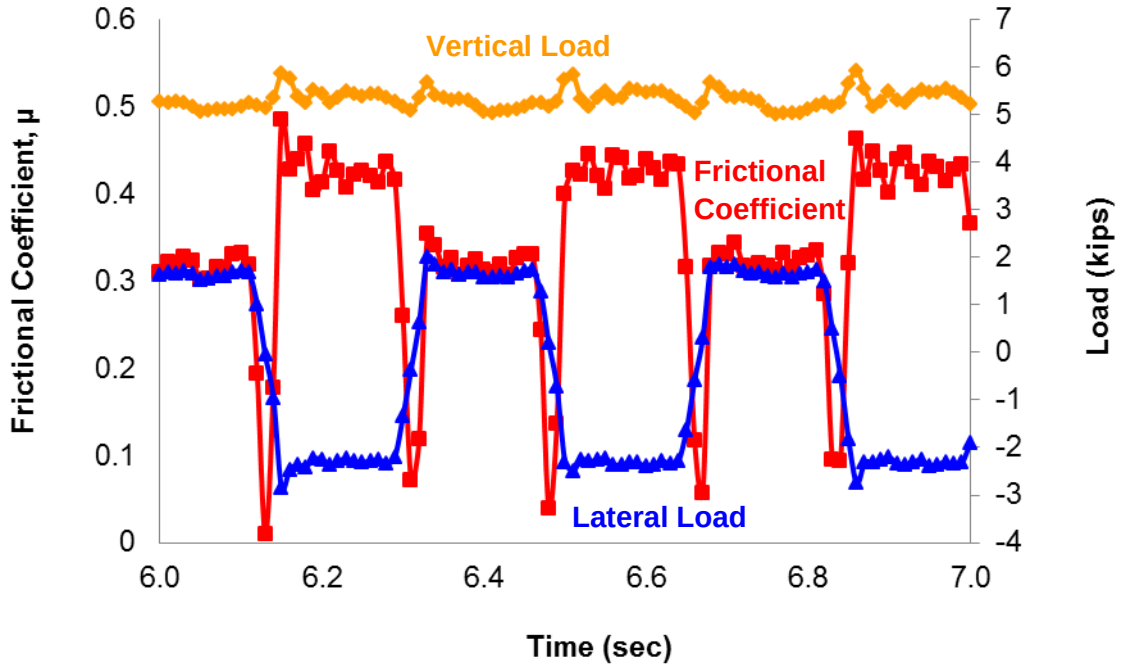

Figure 5.1 Sample frictional coefficient, vertical load, and lateral load during three loading cycles

5.3.1 Heat/Deformation Tests

The mean COF values were plotted at loading cycles 5, 100, 200, 300, and 400 for all tests with nylon 6/6 pads and polyurethane pads (Figure 5.2). Error bars on these graphs (throughout Chapter 5) show two standard errors. The most noticeable trend observed during the heat/deformation tests is that the COF appears to decrease as loading cycles increase. For both pad materials tested, a noticeable decline in the COF was observed from the beginning of each test (loading cycle 5) to the end of each test (load cycle 400). The COF values for each concrete specimen and pad pair for all friction tests are plotted in Appendix B: Detailed Results of Friction Experiment.

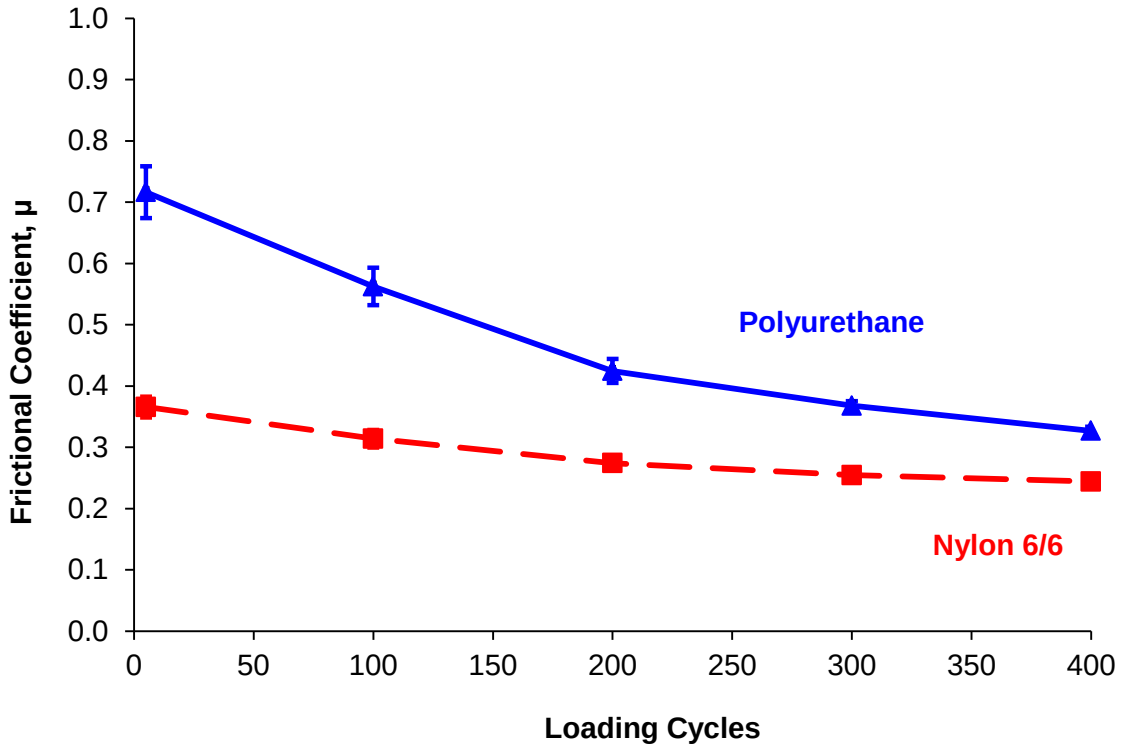

Figure 5.2 Mean coefficients of friction of polyurethane and nylon 6/6 pad materials during heat/deformation tests (mean ± 2SE)

The decline in COF as a function of time during a simulated train pass is most likely due to the buildup of thermal stresses at the contact interface. Increases in the temperature of the pad at the local contact points were observed in all of the friction tests. T_f values as high as 351° Fahrenheit (F) were recorded on the surface of nylon 6/6 pads and 277° F on the surface of polyurethane pads. The temperature build-up appeared to be localized to the primary load-bearing contact points on the pad. On portions of the pad that did not appear to be in direct contact with the concrete, temperatures were measured within 5° of T_i. At these regions of increased temperatures, the material appeared to soften, leading to plastic flow and severe deformation. Evidence of the plastic flow and tearing are presented in Appendix C: Examples of Pad Deterioration from Friction Experiment.

The second conclusion from the mean COF values in Figure 5.2 is that the nylon 6/6 pads appear to have lower COF values than polyurethane pads. The COF values for polyurethane pads were consistently higher than the values for nylon 6/6 pads, including different pads tested on the same concrete specimen. During tests with polyurethane pads, the pad appeared to be absorbing a portion of the shear strain internally (i.e. within its own geometry and thickness), such that gross slip of the pad relative to the concrete was smaller than that of the nylon 6/6 pads.

Third, although there was visible evidence that plastic deformation of the pad and smoothing of the concrete surface occurred during each simulated train pass, there was no conclusive result regarding the effect of subsequent test runs on the frictional characteristics. The COF values were separated by test order (R, S, V, and W) and the mean values were plotted separately for each pad material during the heat/deformation tests (Figures 5.3 and 5.4). The mean COF values remained nearly constant for nylon 6/6 pads with no apparent effect of the previous tests as can be seen in the tight band of curves in Figure 5.3. Alternatively, the first 100 cycles of the polyurethane pads resulted in higher COF values than any other cycles (Figure 5.4).

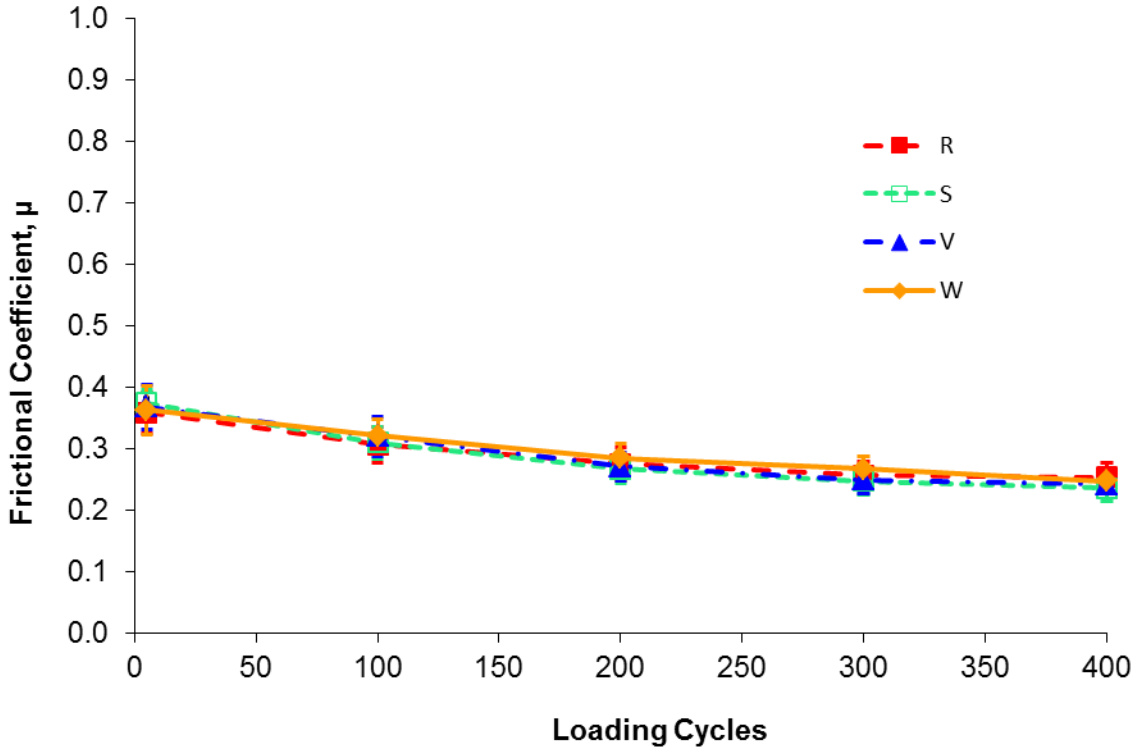

Figure 5.3 Mean coefficients of friction by test order of nylon 6/6 pad materials

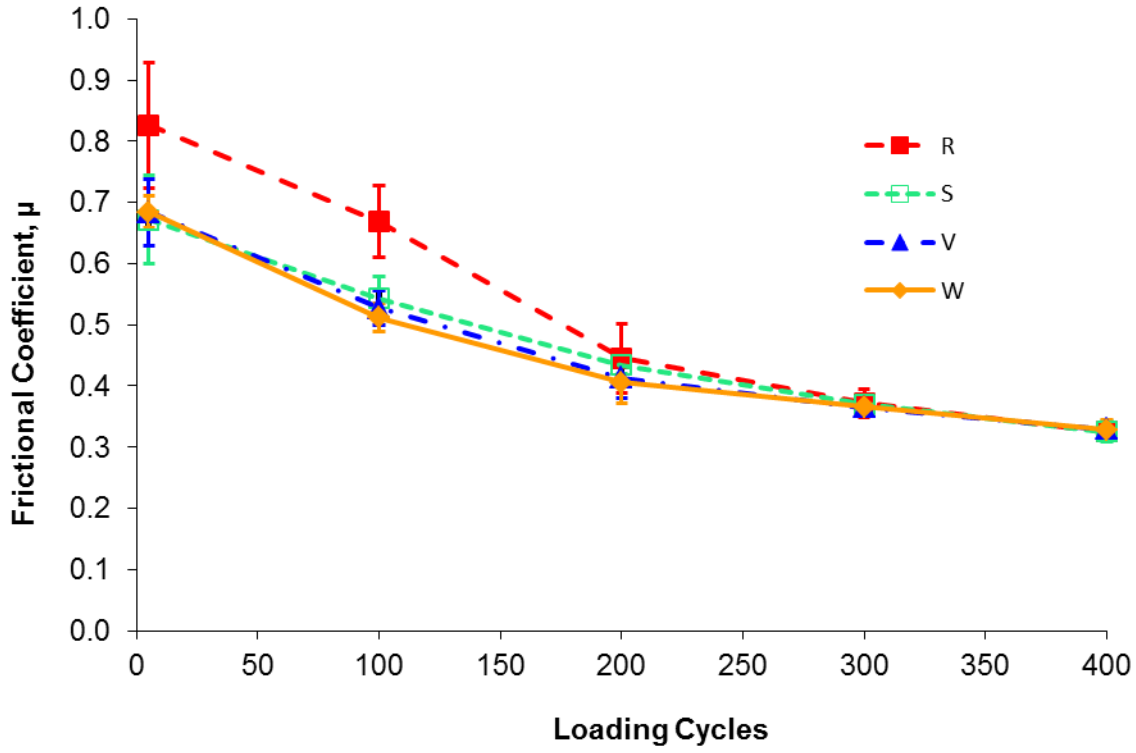

Figure 5.4 Mean coefficients of friction by test order of polyurethane pad materials

5.3.2 Normal Load Tests

Plastic deformation of the pad materials and the concrete surfaces occurred at each load magnitude tested. Based on changes in surface color and reflectivity, the concrete appeared to be polished during tests at 3, 5, and 10 kips. Evidence of measurable abrasion, or noticeable loss of concrete material, was not observed upon completion of the heat/deformation tests and the normal load tests. Second, as the magnitude of the normal force on the pads increased, the COF values generally appeared to decrease. The tests with normal load values of 3 kips and 10 kips were compared to the heat/deformation tests that were executed with a normal load of 5 kips.

The mean COF values for the 5 kip tests are lower than the 3 kip tests and higher than the 10 kip tests for nylon 6/6 pads (Figure 5.5).

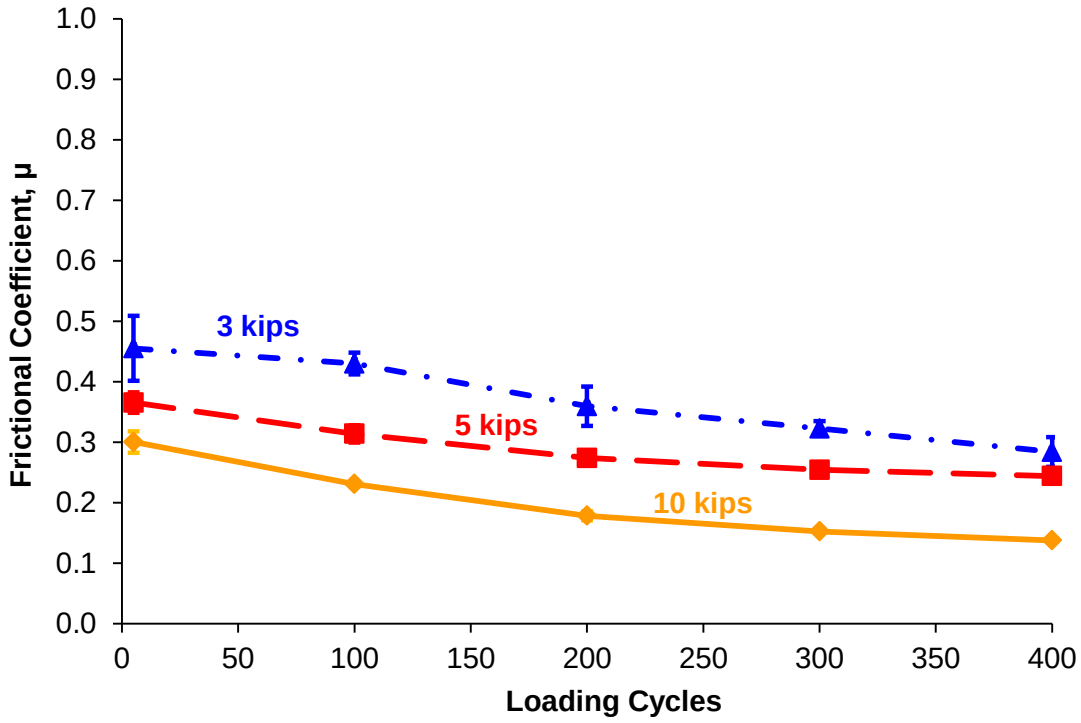

Figure 5.5 Mean COF values of nylon 6/6 pads under 3-kip, 5-kip, and 10-kip normal loads

These data are consistent with the hypothesis that increases in normal load correlate to reductions in COF.

By contrast, the COF data for the polyurethane pads do not show a strong correlation between normal force and COF for tests with loads of 3 kips and 10 kips (Figure 5.6). The COF values at loading cycles 5 and 100 were lower at 10-kip loads than at 3-kip loads, but the COF values were higher at 10-kip loads than 3-kip and 5-kip by the end of the tests. However, the COF values for tests with a 5-kip normal force were consistently lower than the COF values for polyurethane pads loaded to 3 kips.

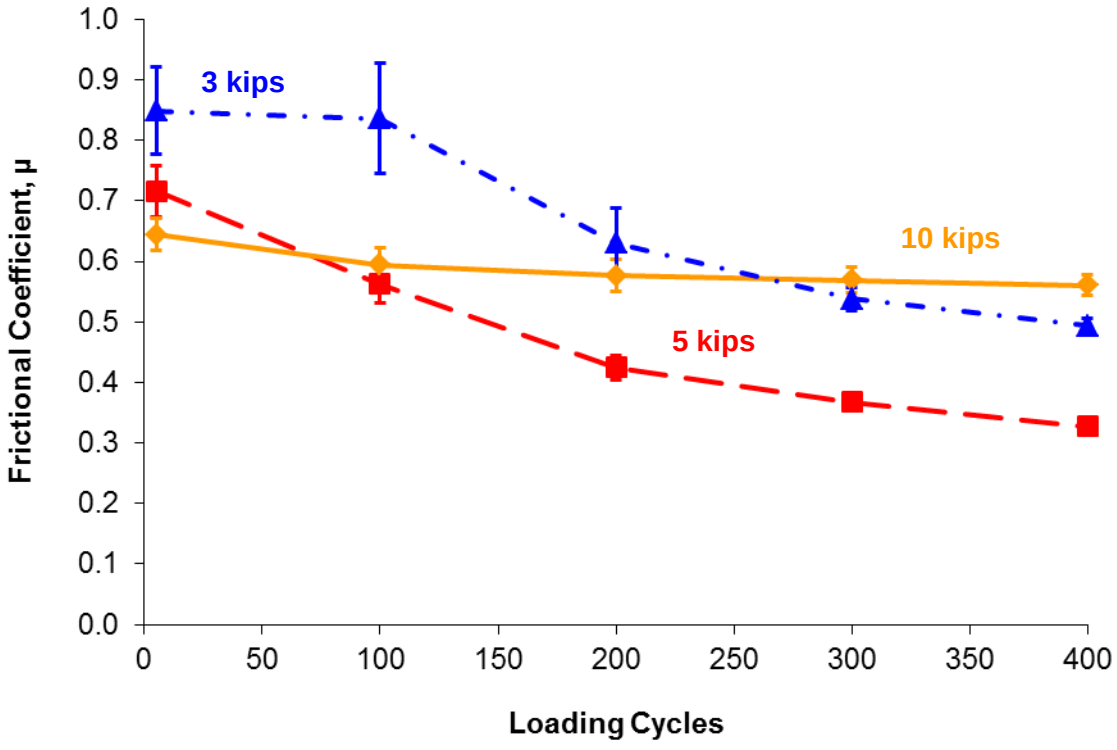

Figure 5.6 Mean COF values of polyurethane pads under 3-kip, 5-kip, and 10-kip normal loads

The nylon 6/6 pads displayed similar sliding behavior at 3 and 10 kips based on visual observations, but the frictional response of the pads under 10-kip normal loads yielded lower

COF values. The COF recorded at 10 kips were consistently lower than those under a 3-kip load, including those recorded from a few trials on the same specimen that were tested in order to ensure that specimen-to-specimen variability was not affecting the perceived relationship between normal load and COF.

During the tests with a normal load of 10 kips, observations of the polyurethane pad under loading revealed minimal sliding of the pad relative to the concrete. Instead, the pad appeared to be absorbing nearly all of the shear strain internally, that is within its own thickness, such that gross slip of the pad relative to the concrete was barely visible. As a result, the increase in temperature of these tests was significantly lower than in tests with 3-kip normal loads. The average temperature of 3-kip tests was 267° F compared to 199° F for 10-kip tests, which is a 25% decrease as a result of a 233% increase in normal load (Table 5.1). Additionally, less plastic deformation was visible on the pad surface after the 10-kip tests where minimal gross sliding was observed during the tests. Due to the combination of less slip, lower temperatures, and less deterioration, the COF values under a 10-kip normal force remained relatively constant. These values are more representative of the internal shear properties of the pad than of the sliding frictional coefficient.

Table 5.1 Mean surface temperatures in degrees Fahrenheit of pads by normal load

Normal Force	Nylon 6/6		Polyurethane	
	T_i	T_f	T_i	T_f
3	75	311	75	267
5	75	305	75	249
10	75	341	76	199

5.3.3 Rail Seat Contaminant Tests

From the mean COF values of all 16 trials on nylon 6/6 pads for each rail seat contaminant condition, the COF values were slightly higher with sand and water added relative to the control (Figure 5.7). As the loading cycles progress, the COF values for each environmental condition trended toward the same value, near 0.3.

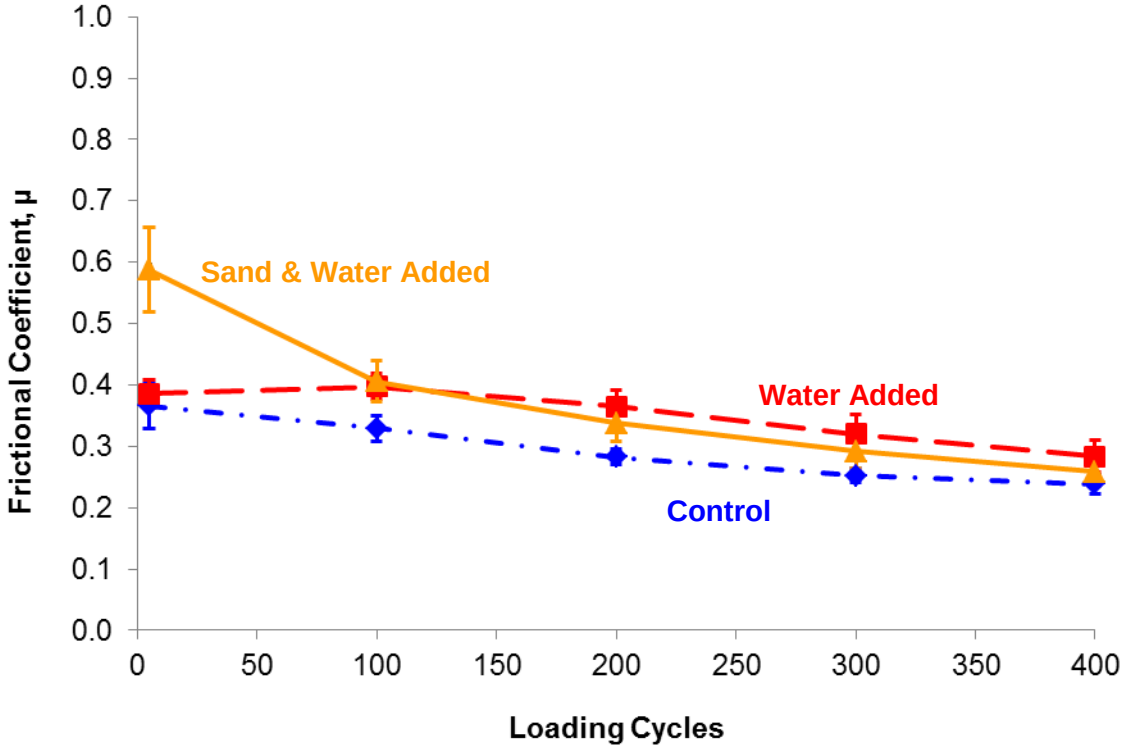

Figure 5.7 Mean COF values of nylon 6/6 pads with 3 rail seat contaminant conditions

In contrast, the COF was slightly lower than the dry condition when water and the combination of sand and water were added to tests with polyurethane pads during the first 200 loading cycles (Figure 5.8).

After loading cycle 200, the polyurethane pads with water added continued to have lower COF values than the control condition. However, polyurethane pads with sand and water appeared to have an average COF that is slightly greater than the control after loading cycle 300.

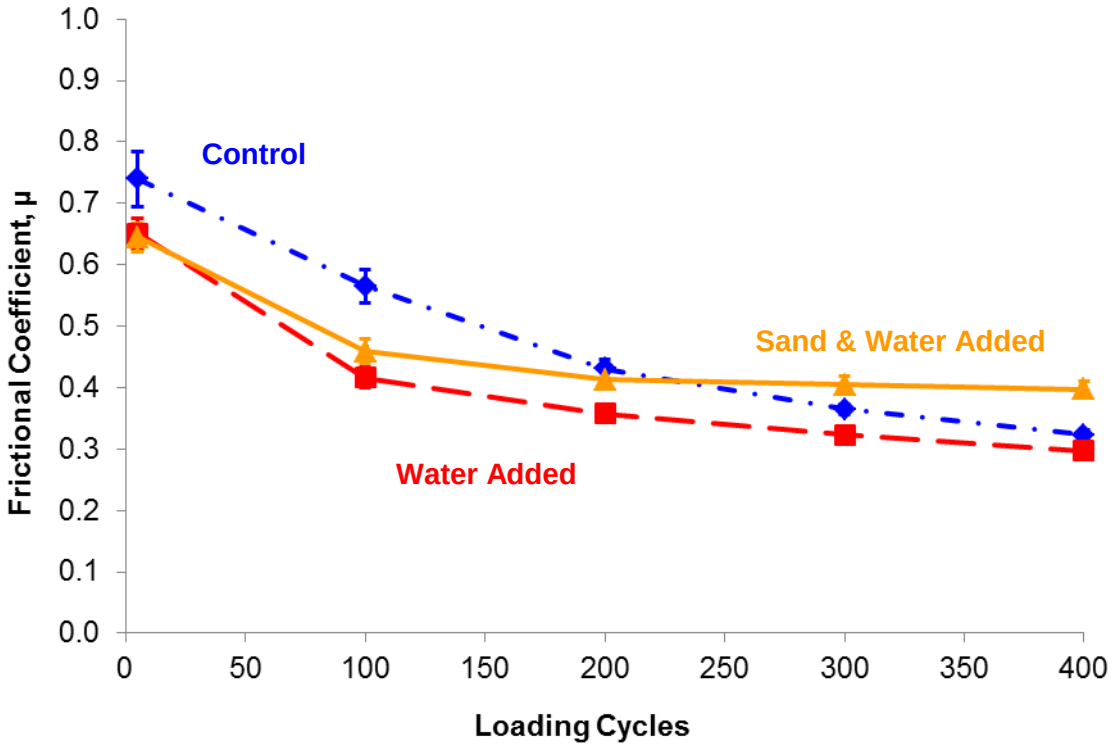

Figure 5.8 Mean COF values of polyurethane pads with 3 environmental conditions

For nylon 6/6 pads, the final temperatures were lower when water was present at the contact interface between the pad and concrete (Table 5.2). The final mean temperature was 27% lower with water added and 12% lower with the combination of sand and water as compared to the condition with no water and no sand. Similarly, the final average temperature of polyurethane pads was reduced by 23% when a constant water drip was added. However, the addition of the abrasive slurry led to an average temperature increase of 3%.

Table 5.2 Mean surface temperatures in degrees Fahrenheit of pads by environmental condition

Contaminant Condition		Nylon 6/6		Polyurethane	
Sand	Water	T_i	T_f	T_i	T_f
No	No	75	305	75	249
No	Yes	75	224	74	192
Yes	Yes	73	267	72	256

The introduction of sand consistently resulted in noticeable abrasion of the mortar paste of the concrete surface in as few as 400 loading cycles. Additionally, the amount of plastic deformation and wear of the pad increased significantly when sand was added to the interface in addition to the water for both pad materials. The nylon 6/6 and polyurethane pads experienced wear at concentrated points of contact where patterns of sand particles were cut into the surface. The sand tended to clump together and the highest surface temperatures and the majority of the pad deterioration were observed in these areas.

5.4 Discussion

5.4.1 Heat/Deformation Tests

Previous research has shown that the COF and wear behavior of polymers depend on the temperature at the contact interface and the material paired with the polymer (Srinivasan 2009; Briscoe 1986). There are two hypotheses to explain the effect of heat on the reduction of COF values at the interface between the bottom of the pad and the concrete rail seat. First, the shear strength of the pad material is likely being reduced at the contact interface as the temperature increases. Once the glass transition temperature of the material is exceeded, shear strength is significantly reduced. The glass transition is that temperature at which the material properties change and softening occurs. When the shear strength of the pad is reduced, plastic deformation and tearing of the material can occur at local contact points, resulting in a reduction of the force required to cause the pad to slip. Since the glass transition temperatures of most relevant nylon 6/6 and polyurethane materials can be estimated at approximately 150° F and -20° F, respectively, we can assume that softening was occurring, and the shear strengths of both materials were reduced during testing.

Alternatively, the increases in temperature at local contact points may have resulted in the local melting of the pad materials that remain in the interface as a transfer film (Badhadur 2000, Srinath and Gnanamoorthy 2005). This transfer film can act as a lubricant, resulting in the reduction of the COF values. The melting point of most nylon 6/6 materials is above 480° F, while polyurethane materials melt above 400° F. Although the temperatures measured in these experiments were lower than the melting temperatures, some heat may have been dissipated in the few seconds that passed after the tests were stopped and before the temperatures were measured. The possibility of localized melting remains based on the visible evidence of plastic material flow. Even if melting is not occurring, the results from this experiment show that the temperature of the pad material increases as it slides on the concrete surface and the COF is reduced.

The differences in COF values between nylon 6/6 and polyurethane can best be explained by the inherent properties of the materials that are a result of the crystalline structure and chemical characteristics. For this study, the most relevant property is shear modulus, which is a measure of the response of a material when a shear force is imposed. The published shear modulus of nylon 6/6, 145 kips per inch^2 (ksi) at 86° F, is approximately 5 times higher than the shear modulus of polyurethane, 7 ksi, at 86° F (BASF 2012). The shear behavior of these materials can be illustrated by Dynamic Mechanical Analysis (DMA) curves for materials similar to those tested (BASF 2012). The DMA graphs illustrate that the shear moduli (both elastic and plastic) decreases as the temperature increases within the range of temperatures measured during the friction tests (75° F to 350° F). Although the polyurethane pads have a lower shear modulus, the COF values that were measured in this experiment were higher than those of nylon 6/6 pads. Therefore, secondary effects, such as the differences in the mechanics

of the motion (e.g. internal shear, sliding), were likely governing the friction response. The mechanics of pad motion are further addressed with the normal load tests in section 5.4.2.

The plastic deformation that occurred at contact points on the concrete surface under a constant normal force after simulated train passes did not appear to have a noticeable effect on the COF values. Any effect that the smoothing of the contact asperities had on the COF values was likely governed by other relationships.

5.4.2 Normal Load Tests

As the normal force on the pad materials increased, the COF values decreased for pads that slid relative to the concrete. For plastic materials, the theoretical value of COF is directly related to the true contact area and shear strength, and is inversely proportional to the normal load (Yamaguchi 1990). Thus, the experimental relationship between load and COF measured in this study is in agreement with the theoretical tribology literature for polymer materials. Since the actual contact area is difficult to measure or estimate, the fundamental relationship of the ratio of lateral force to normal force was selected as the best method to calculate the COF in this study. Other experimental studies that utilized this method of calculating COF reported a similar relationship for COF and normal force (Srinivasan et al. 2009, Yamaguchi 1990, Watanabe 1986).

The higher contact stresses that the pads experienced under increasing normal forces likely caused increased deformation at local contact points, thus changing the geometry of the contact and altering the shear behavior of the material. When the pressure exceeds a critical value based on the strength of a material, the friction and wear behavior of the polymer materials is affected (Anderson 1986). The decreasing COF values with increasing normal load for both

nylon 6/6 and polyurethane pad materials sliding on concrete demonstrate principles from tribology that are typically investigated for mechanical applications such as ball bearings.

Beyond the noticeable sliding of the pads, one of the most interesting observations in this experiment occurred on the softer pad material (polyurethane) under a 10-kip normal load. Nearly all of the deflection of the horizontal actuator (in displacement control) was taken internally, within the thickness of the pad such that the pad did not appear to slide relative to the concrete. As a result, the calculated experimental COF values do not actually describe the frictional relationship. Instead, the internal shear properties of the polyurethane, lateral shear behavior versus normal force, are being described. Thus, the shear properties generally appeared to be constant throughout each of the 16 tests. This distinctly contrasts with the variable frictional relationship that was observed for sliding pads. The fact that a large shear force can be input into the top of the pad material, absorbed within the ¼-inch thickness of polyurethane, with minimal slip on the concrete, may have implications for the shear contact behavior and performance of rail pad assemblies.

5.4.3 Rail Seat Contaminant Tests

The introduction of water and sand into the interface between the pad and concrete surface had a small effect on the frictional relationship. Water had contrasting effects on the COF values for nylon 6/6 and polyurethane. While water successfully reduced the contact temperature of both pad materials, water appeared to act as a lubricant for the polyurethane pad, by slightly reducing the COF values. By contrast, the COF was higher than that of the control condition for polyurethane pads, likely due to the reduction in softening because the temperatures were less than the dry condition.

Although it was hypothesized that the sand particles beneath the pad might act as bearings as the sand particles rolled relative to the concrete, the COF values for the nylon 6/6 pads actually increased for the first few hundred loading cycles. Combined with the patterns of abrasion that were observed with the increased COF values, I concluded that the sand particles slid and cut into the concrete and nylon 6/6 rather than rolling. Alternatively, the softer polyurethane material resulted in a lower COF when sand was introduced with the water drip. The sand particles likely rotated or shifted under the cyclic, translational motion of the pad. The rolling of particles resulted in wear of the concrete, but the wear did not appear to be as severe as the wear on concrete with nylon 6/6 pads.

As loading cycles progressed, the COF trended towards a common value between 0.3 and 0.4 for nylon 6/6 and polyurethane when sand and water were present. Under these extreme loading conditions where heat built up and plastic deformation occurred, the relatively different materials tended to behave similarly.

5.4.4 Sources of Variability

Overall, the variability in the friction tests was minimal compared to the variability of the deterioration tests described in Chapter 4. The difficulty in maintaining a uniform contact angle of the pad relative to the concrete specimen led to some variability in the friction tests. The testing equipment was attached with mostly rigid connections, making it difficult to obtain a perpendicular contact angle of the normal force through the pad onto the concrete. Subsequently, the pressure distribution of the normal force was probably not completely uniform, as the deterioration patterns observed during testing illustrated that portions of the pads were not contacting the concrete surface. Only 15% to 30% of the pad area exhibited signs of plastic deformation or temperature build-up.

In order to improve the repeatability of achieving a certain contact angle, a sulfur capping compound was applied to the underside of the concrete specimens. This method improved the orientation of the concrete specimen and appeared to provide a more uniform pressure distribution.

5.5 Conclusions

The load magnitude and displacement used in the friction tests were the same as the parameters used in the deterioration tests. These parameters represent an aggressive loading condition that, for example, generated greater heat than one might expect in the field. Based on the results, secondary effects that are not typically seen in railway engineering applications of these materials governed the friction and wear relationships in this experiment. In future laboratory tests for rail seat deterioration, careful consideration should be given to achieving a balance between accelerated results and maintaining representative relationships. Nevertheless, the relationships that were observed provide insight into the mechanics of abrasion.

Based on the results of these experiments, the frictional characteristics at the contact interface between a rail pad and concrete rail seat appear to have an impact on the transfer of forces and relative movement, and thus the abrasion mechanism. The properties of rail pads such as the shear modulus, flexural modulus, hardness, and geometry appear to affect frictional behavior. In addition, temperature changes that can occur due to repeating loading cycles, the magnitude of the normal force, and the presence of water and abrasive fines impact the shear contact behavior at the rail seat interface. Increases in temperature can affect the material properties of the pad material. Additionally, water and sand can affect the way the pad slips relative to the concrete while causing significant damage to both the pad and concrete. Finally, increasing pressures due to higher normal forces reduce the COF, and may increase the

propensity of the pad to slip relative to the concrete, thus exacerbating the demands on the rail seat.

CHAPTER 6: CONCLUSIONS AND FUTURE WORK

6.1 Summary

This study has shown that abrasion is a feasible RSD mechanism. Whenever a pad is displaced relative to the concrete, the potential exists for local damage, presence of loose particles, and wear of surfaces. Abrasion has been shown to occur at relatively low contact pressures (400 psi) as well as high contact pressures (1,800 psi). Water and abrasive fines can make the deterioration more severe, but abrasion initiates without their presence. Frictional characteristics at the contact interface between the rail pad assembly and concrete rail seat vary and influence the transfer of forces and relative movement. The modulus, hardness, and geometry of the rail pad assembly affect frictional behavior.

6.2 Criticality of RSD Mechanisms

The factors that control the abrasion mechanism (i.e. relative motion at the rail seat, normal and shear stresses, presence of abrasive fines, and moisture) are frequently encountered on heavy-haul freight corridors in North America. The other four mechanisms – hydraulic pressure cracking, hydro-abrasive erosion, freeze thaw damage, and crushing – also appear to be feasible when a number of critical factors occur simultaneously. High impact loads and a saturated concrete pore structure are necessary for hydraulic pressure cracking or hydro-abrasive erosion to occur. Significant temperature swings and water in the concrete pore structure are necessary for freeze thaw damage at the rail seat. Crushing may occur under high impact loads, extreme L/V ratios, and uneven rail seat pressures. The key factors for each of these four mechanisms are possible, yet the probability that they occur regularly seems less likely than the factors that cause abrasion. As a result, concrete rail seats and pad assemblies should be designed based on the considerations for mitigating the abrasion mechanism.

Significant variability is found regarding the location, severity, and pattern of RSD on heavy-haul freight infrastructure in North America. Crossties in a single curve may have different levels of RSD. Thus, producing one solution that will eliminate RSD is unlikely. The idea that the rail seat interface can be shielded from abrasive fine material and moisture does not seem feasible based on observations in the field. Even in arid climate regions, moisture has been found trapped under the rail seat. The fact that moisture in the air can accumulate at the rail seat is evidence that methods of mitigating the infiltration of moisture and abrasive fines seem unlikely. Additionally, abrasive fines have been observed beneath the rail pad assembly on most rail seats, in a variety of locations and climates. A rail seat that does not contain some type of abrasive fines trapped beneath the rail pad assembly is rare. Many of the solutions designed to keep moisture and fines out of the rail seat may actually be sealing the contaminants in the rail seat. Therefore, more effort should be directed toward reducing relative slip at the rail seat.

6.3 Proposed Methods of Mitigating RSD

Three approaches to reducing the severity of RSD by mitigating the abrasion mechanism are suggested by this study. First, wear can be mitigated by reducing the magnitude of slip relative to the interacting surfaces. Second, the life cycle of the concrete crosstie can be increased by using a more abrasion resistant material at the rail seat. Third, reducing the magnitude of the contact pressure between the two surfaces at local contact points can increase its wear life. Of these three approaches, the most feasible way of mitigating abrasion may be to reduce the amount of slip at the rail seat.

Slip at a particular interface can be reduced in a number of ways. The friction experiment (Chapter 5) showed that polyurethane pads tested with a 10-kip normal force exhibited the least amount of deformation of the pad and concrete because minimal relative slip

occurred. Instead, elastic shear occurred within the pad. Therefore, one method of reducing slip at critical interfaces is redesigning the components to influence the transfer of displacement so that the slip occurs within a component that is capable of accepting elastic shear. In other words, the rail pad should deform such that the shear displacement is absorbed within the pad instead of slip at the rail seat interface (e.g. elastic shear instead of gross slip) (Chapter 3). The pad must be thick enough and have a low enough shear modulus to experience elastic shear under the shear and normal forces that the pad is subjected to.

The onset of abrasion can be mitigated by influencing the load path and location of slip through materials selection and component design. For example, slip at the rail seat can be reduced by increasing the frictional forces at the rail seat interface. The magnitude of the frictional force can be increased by a higher coefficient of friction. Also, the coefficient of friction can be increased by increasing mechanical interlock at a particle level (e.g. surface roughness) and decreasing the hardness of the part. Once the frictional force at the rail seat is increased, the friction between the rail pad and abrasion frame should be reduced so that slip can occur between the two layers of the pad assembly.

For each of these methods of reducing relative slip, the overall stiffness of the fastening system should be maintained. The rail should not move more than current standards allow, but the location of deformation and slip should be a subject of the design process.

The shear contact behavior at each interface, of which friction is an important characteristic, and lateral force transfer should be considered in the design of concrete crossties and fastening systems. Determining the optimal shear contact properties at each interface of multi-layer pad assemblies (top, bottom, and between layers) could reduce the movement and shear stress at the most critical interface, the concrete rail seat. By reducing the movement and

shear stress at the rail seat, better shear designs could delay the onset of abrasive wear. In the future, this methodology may be extended to other fastening system components and effectively increase the service life of concrete crossties and fasteners.

Another method of reducing relative component movement is by increasing the confinement or mechanical interlock between the parts. Increased confinement can be achieved by introducing more normal surfaces to resist relative movement. Additional confinement can be achieved by reducing the tolerances to which the concrete crosstie and fastening system are manufactured.

6.4 Future Work

Understanding the shear behavior of the fastening system is a critical step to mitigating the harmful effects of RSD. The first step in understanding the shear behavior is mapping the transfer of shear forces as a lateral or longitudinal force is imposed on the rail. The stiffness of each component in the shear plane (e.g. load versus displacement characteristics) must be investigated to ensure that fastening system components are able to properly distribute the wheel loads into the crosstie. Therefore, determining the pressure distribution is essential to extending component life. The tendency exists to make components more robust in order to decrease the contact pressure, but uneven pressure distributions may prove that greater elastic deformation is needed instead of a larger surface area. Finite element modeling of the crosstie and fastening system will help determine the effects of interface friction and component stiffness on the shear behavior of the fastening system.

Since abrasion appears to be the most common RSD mechanism, more research must be done to understand the correlation between pad movement, normal force, and the severity of abrasion. To investigate this relationship, a smaller test setup should be used in order to provide

more experimental control than the experiment described in Chapter 4. Also, the magnitude of the relative displacement between the concrete and pad material should be smaller than the displacement used in this study, on the order of 0.05 inches. This kind of basic research is needed so that the results of full-scale abrasion tests on concrete crossties and fastening systems can be understood.

In order to learn more about abrasion at the rail seat of full-scale concrete crossties, AREMA Test 6 could provide an alternative protocol for investigations of the rail seat. A standard fastening system, preferably one that is known to have RSD issues, should be selected and the testing duration extended so that a measurable amount of RSD is achieved after each test. Once measureable wear is accumulated, the parameters affecting the amount of abrasion can be analyzed and alternative rail seat materials can be compared between tests. Improved rail seat surfaces (e.g. more durable concrete mixtures, surface coatings) should be evaluated in order to determine if these solutions are more effective than increasing the size (surface area) of the track components. Abrasion must be investigated more thoroughly as heavy axle loads continue to increase. RSD will remain a significant challenge until a greater effort is made to understand abrasion and the other RSD mechanisms.

REFERENCES CITED

Anderson, J.C. 1986. The wear and friction of commercial polymers. In: K. Friedrich, (Ed) *Friction and Wear of Polymer Composites*, Elsevier, Amsterdam, pp. 329-362.

American Railway Engineering and Maintenance-of-Way Association (AREMA). 2012. *AREMA Manual for Railway Engineering,* American Railway Engineering and Maintenance-of-Way Association, Landover, Maryland, Chapter 30.

Atis, C. D. 2002. High volume fly ash abrasion resistant concrete. *Journal of Materials in Civil Engineering* 14.3: pp. 274-277.

Badhadur, S. 2000.The development of transfer layers and their role in polymer tribology. *Wear* 245: 92-99.

Bakharev, T. 1994. *Microstructural features of railseat deterioration in concrete railroad ties*. MS Thesis. University of Illinois at Urbana-Champaign.

Bakke, K. J. 2006. Abrasion resistance. In: J.F. Lamond and J.H. Pielert, (Eds.) *Significance of Tests and Properties of Concrete and Concrete-Making Materials,* ASTM International, West Conshohocken, PA, pp. 184-193.

BASF Polyurethanes GmbH. 2012. *CAMPUS datasheet Elastollan 1195 A.* Available at: http://www.campusplastics.com/campus/en/datasheet/Elastollan%C2%AE+1195+A/BASF+Polyurethanes+GmbH/59/b5a54956. [Accessed 31 January 2012].

Bayer, R.G. 2004. *Mechanical wear fundamentals and testing*, Marcel Dekker, New York, NY.

Briscoe, B.J. 1986. Interfacial friction of polymer composites. In: K. Frederich and R.B. Pipes, (Eds.) *Friction and Wear of Polymer Composites*, Elsevier, Amsterdam, pp. 44.

Cardarelli, F. 2008. *Materials Handbook: A Concise Desktop Reference*, Springer, London, England: pp. 19-20.

Choros, J., B. Marquis and M. Coltman. 2007. Prevention of Derailments Due to Concrete Tie Rail Seat Deterioration. In: *Proceedings of the ASME/IEEE Joint Rail Conference and the ASME Internal Combustion Engine Division, Spring Technical Conference*, Pueblo, CO, March 2007, pp. 173-181.

The Concrete Society. 2000. Diagnosis of Deterioration in Concrete Structures, *Technical Report No. 54, Section 3.4.6.* The Concrete Society, London, England.

Cong, D.X., M.H. Reed, L.J. Powers, B.L. Shotwell and B.D. Brown. 2006. Relationship between indentation hardness and water to cement ratio of hardened mortar and concrete. *Journal of ASTM International* 3 (2).

Czichos, H. 1986. Introduction to friction and wear. In: K. Frederich and R.B. Pipes, (Eds.) *Friction and Wear of Polymer Composites*, Elsevier, Amsterdam, pp. 1-21.

Daphalapurkar, N.P., F. Wang, B. Fu, H. Lu and R. Komanduri. 2011. Determination of mechanical properties of sand grains by nanoindentation. *Experimental Mechanics* 51: 719-728.

Dhir, R.K., M.R. Jones, E.A. Byars, and I.G. Shaaban. 1994. Predicting concrete durability from its absorption. *Durability of Concrete – Proceedings Third CANMET – ACI International Conference, American Concrete Institute Special Publication* 145 (64): 1177-1194.

Edwards, J.R., M.S. Dersch and R.G. Kernes. 2013. *UIUC FRA Concrete Tie and Fastener BAA International Survey*, Federal Railroad Administration. Washington, DC.

Fwa, T.F. and E.W. Low. 1990. Laboratory evaluation of wet and dry abrasion resistance of cement mortar. *Cement, Concrete, and Aggregates, CCAGDP* 12 (2): 101-106.

Gallagher Corporation. 2012. Polyurethane coefficient of friction. Available at: http://www.gallaghercorp.com/design_guide-coefficient_of_friction.html#photo. [Accessed 23 April 2013].

Gao, J., W.D. Luedtke, D. Gourdon, M. Ruths, J.N. Israelachvili and U. Landman. 2004. Frictional forces and Amontons' Law: from the molecular to the macroscopic scale. *Journal of Physical Chemistry B* 108: 3410-3425.

Ghafoori, N. and M. W. Tays. 2010. Resistance to wear of fast-track Portland cement concrete. *Construction and Building Materials* 24: 1424-1431.

Ghafoori, N. and H. Diawara. 2007. Strength and wear resistance of sand-replaced silica fume concrete. *American Concrete Institute Materials Journal* 104 (2): 206-214.

Godet, M. 198. The third-body approach: a mechanical view of wear. *Wear* 100: 437-452.

Granta Design. 2013. Hardness conversion charts. Available at: http://www.grantadesign.com/resources/materials/hardnesscharts.htm. [Accessed 6 May 2013].

Gunaratne, M., N. Bandara, J. Medzorian, M. Chawla and P. Ulrich. 2000. Correlation of tire wear and friction texture of concrete pavements. *Journal of Materials in Civil Engineering* 12(1): 46-54.

Gutierrez, M.J., J.R. Edwards, D.A. Lange and C.P.L. Barkan. 2011. Design and Performance of Elastic Fastening System Assemblies and Measurement of Rail Seat Pressure Distribution for Concrete Sleepers for Heavy-Haul Service. In: *Proceedings of the 9th World Congress on Railway Research*, Lille, France, May 2011.

Halling, J. 1978. *Principles of Tribology*, Macmillan Education, Houndsmills, Great Britain.

Hokkirigawa, K. and K. Kato. 1988. An experimental and theoretical investigation of ploughing, cutting and wedge formation during abrasive wear. *Tribology International* 21 (1): 51-57.

Johns, T. 2011. Discussion on rail seat deterioration testing. [email] (Personal communication, 23 March 2011). Tim Johns was the Manager of Rail Products for Exova Canada, Inc. when this research was conducted.

Kaltzakorta, O., R. Wasche, M. Hartelt, A. Aginagalde and W. Tato. 2012. Influence of polymer filler on tribological properties of thermoplastic polyurethane under oscillating sliding conditions against cast iron. *Tribology Letters* 48: 209-216.

Kernes, R.G., J.R. Edwards, M.S. Dersch, D.A. Lange and C.P.L. Barkan. 2011. Investigation of the Impact of Abrasion as a Concrete Crosstie Rail Seat Deterioration (RSD) Mechanism. In: *Proceedings: American Railway Engineering and Maintenance-of-Way Association Annual Conference*, Minneapolis, MN, September 2011.

Kernes, R.G., J.R. Edwards, M.S. Dersch, D.A. Lange and C.P.L. Barkan. 2012. Investigation of the Dynamic Frictional Properties of a Concrete Crosstie Rail Seat and Pad and Its Effect on Rail Seat Deterioration (RSD). In: *Proceedings of the Transportation Research Board 91st Annual Meeting*, Washington, DC, January 2012.

Kerr, A.D. 2003. *Fundamentals of Railway Track Engineering*, Simmons-Boardman Books, Omaha, NE.

Kettle, R.J. and M. Sadegzadeh. 1987. Influence of Construction Procedures on Abrasion Resistance. In: *Concrete Durability: Proceedings of Katharine and Bryant Mather International Symposium*, *American Concrete Institute Special Publication* 100 (71): 1385-1410.

Mindess, S., J.F. Young and D. Darwin, 2003. *Concrete*, 2nd ed., Pearson Education Inc., Upper Saddle River, New Jersey.

Naik, T.R., S.S. Singh and B. Ramme. 1997. Effect of Source and Amount of Fly Ash on Mechanical and Durability Properties of Concrete. In: *Fourth CANMET/ACI International Conference on Durability of Concrete*, *American Concrete Institute Special Publication* 170(8): 157-188.

Naik, T.R., S.S. Singh and M.M. Hossain. 1995. Abrasion resistance of high-strength concrete made with class c fly ash. *American Concrete Institute Materials Journal* 92 (6): 649-659.

Nanni, A. 1989. Abrasion resistance of roller compacted concrete. *American Concrete Institute Materials Journal* 86 (6): 559-565.

Pointer, P., A. Joerg and J. Jaiswal. 2006. *Definitive Guidelines on the Use of Different Rail Grades, Innotrack Report D4.1.5GL*. International Union of Railways (UIC), Paris, France.

Popovics, S. 1992. Concrete Materials: Properties, Specifications, and Testing, 2nd ed., Noyes Publications, Park Ridge, NJ.

Rapp, C.T. M.S. Dersch, J.R. Edwards, D.A. Lange and C.P.L. Barkan. 2013. Field instrumentation of concrete crossties for investigating rail seat pressure distribution. *Accepted, Transportation Research Record - Journal of the Transportation Research Board.*

Rhodes, D. and S.J. Cox. 2013. Rail Fastenings for Heavy Haul and Extreme Longitudinal Forces. In: *Proccedings: 10th International Heavy Haul Association Conference*, New Delhi, India, February 2013, pp. 122-126.

Rhodes, D. 1988. How resilient pads protect concrete sleepers. *Railway Gazette International*, February. pp. 85-87.

Siddique, R. and J.M. Khatib. 2010. Abrasion resistance and mechanical properties of high-volume fly ash concrete. *Materials and Structures* 43: 709-718.

Shin, M.W., S.S. Kim and H. Jang. 2011. Friction and wear of polyamide 66 with different weigth average molar mass. *Tribology Letters* 44: 151-158.

Shurpali, A. A. R.G. Kernes, J.R. Edwards, M.S. Dersch, D.A. and C. P. L. Barkan. 2013. Investigation of the Mechanics of Rail Seat Deterioration (RSD) and Methods to Improve Rail Seat Abrasion Resistance in Concrete Sleepers. In: *Proccedings: 10th International Heavy Haul Association Conference*, New Delhi, Indai, February 2013, pp. 127-133.

Smith, F.L. 1958. Effect of aggregate quality on resistance of concrete to abrasion. *ASTM International* STP205-EB: 91-106.

Sonebi, M. and K.H. Khayat. 2001. Testing abrasion resistance of high strength concrete. *Cement, Concrete, and Aggregates, CCAGDP* 23(1): 34-43.

Srinath, G. and R. Gnanamoorthy. 2005. Effect of short fibre reinforcement on the friction and wear behaviour of nylon 66. *Applied Composite Materials* 12: 369-383.

Srinivasan, V.. B. Asaithambi, G. Ganesan, K. Karthikeyan and K. Palanikumar. 2009. Mechanism of glass fiber reinforced epoxy composites under dry sliding using fuzzy clustering technique. *Journal of Reinforced Plastics and Composites* 28: 1349-1358.

Thorpe, J.M. 1986. Tribological properties of selected polymeric matrix composites against steel surfaces. In: K. Friedrich, (Ed) *Friction and Wear of Polymer Composites*, Elsevier, Amsterdam, pp. 89-134.

Tripple, S. 2011. Discussion on common rail pad assembly materials and properties. [Telephone] (Personal communication, 23 June 2011). Scott Tripple was the Manager, Track Products for Pandrol North America when this research was conducted.

Turk, K. and M. Karatas. 2011. Abrasion resistance and mechanical properties of self-compacting concrete with different dosages of fly ash/silica fume. *Indian Journal of Engineering and Materials Sciences* 18: 49-60.

Wantanabe, M. and H. Yamaguchi. 1986. The friction and wear properties of nylon. *Wear* 110: 379-388.

Wang, Y. and D.D.L. Chung. 1998. Spatial distribution of mechanical and electrical properties of cement mortar prior to loading. *Cement and Concrete Research* 28(10): 1373-1378.

Williams, J.A. 2005. *Engineering Tribology,* Cambridge University Press, New York, NY.

Williams, J.A. 1997. The laboratory simulation of abrasive wear. Tribotest journal 3(3): 267-306.

Yamaguchi, Y. 1990. *Tribology of plastic materials.* Elsevier, Amsterdam.

Yazici, S., and G. Inan. 1995. An investigation on the wear resistance of high strength concretes. *Wear* 260: 615-618.

Yunfeng, L., L. Yang, D. Rongqiang and K. Fanying. 2009. Effect of steel slag powder on the durability of high performance concrete. *Advanced Materials Research* 79(82): 175-178.

Zeman, J.C., J.R. Edwards, D.A. Lange and C.P.L. Barkan. 2010a, Investigation of Potential Concrete Tie Rail Seat Deterioration Mechanisms: Cavitation Erosion and Hydraulic Pressure Cracking. In: *Proceedings of the Transportation Research Board 89th Annual Meeting*, Washington, DC, January 2010.

Zeman, J.C. 2010b. *Hydraulic mechanisms of concrete-tie rail seat deterioration*, MS Thesis. University of Illinois at Urbana-Champaign.

Zeman, J.C., J.R. Edwards, D.A. Lange and C.P.L. Barkan. 2010c. Sealing Characteristics of Tie Pads on Concrete Crossties. In: *Proceedings: American Railway Engineering and Maintenance-of-Way Association Annual Conference*, Orlando, FL, August 2010.

APPENDIX A: DETAILED RESULTS OF DETERIORATION EXPERIMENT

Table A.1

Test 1

Specimen	G6
Pad	N13
Magnitude of Load	3 kips
Displacement (Range)	1/8”
Displacement (Rate)	3 Hz
Moisture Condition	Constant Drip
Abrasive Fines	Yes, initial Ottawa
Start Date	11/1/2011 (3:10 PM)
End Date	11/1/2011 (4:55 PM)
Maximum Abrasion Depth	0.139
Average Abrasion Depth	0.013

Table A.2

Test 2

Specimen	G2
Pad	N14
Magnitude of Load	3 kips
Displacement (Range)	1/16”
Displacement (Rate)	6 Hz
Moisture Condition	Constant Drip
Abrasive Fines	Yes, initial Ottawa
Start Date	11/7/2011 (9:13 AM)
End Date	11/7/2011 (12:13 PM)
Maximum Abrasion Depth	0.104
Average Abrasion Depth	0.015

Table A.3

Test 3

Picture Unavailable

Specimen	E20
Pad	N15
Magnitude of Load	3 kips
Displacement (Range)	1/16”
Displacement (Rate)	6 Hz
Moisture Condition	Constant Drip
Abrasive Fines	Yes, initial Ottawa
Start Date	11/9/2011 (10:38 AM)
End Date	11/9/2011 (1:40 PM)
Maximum Abrasion Depth	0.144
Average Abrasion Depth	0.011

Table A.4

Test 4

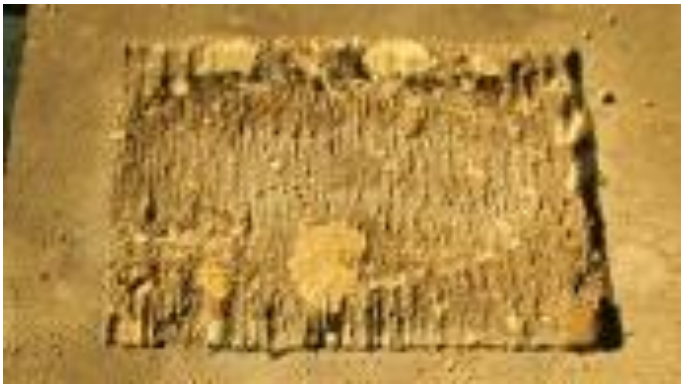

Specimen	G12
Pad	N17
Magnitude of Load	3 kips
Displacement (Range)	1/8”
Displacement (Rate)	6 Hz
Moisture Condition	Constant Drip
Abrasive Fines	Yes, initial Ottawa
Start Date	11/11/2011 (1:58 PM)
End Date	11/11/2011 (4:58 PM)
Maximum Abrasion Depth	0.178
Average Abrasion Depth	0.028

Table A.5

Test 5

Picture Unavailable

Specimen	G3
Pad	N18
Magnitude of Load	1 kip
Displacement (Range)	1/8”
Displacement (Rate)	6 Hz
Moisture Condition	Constant Drip
Abrasive Fines	Yes, initial Ottawa
Start Date	11/14/2011 (1:27 PM)
End Date	11/14/2011 (4:27 PM)
Maximum Abrasion Depth	0.202
Average Abrasion Depth	0.016

Table A.6

Test 6

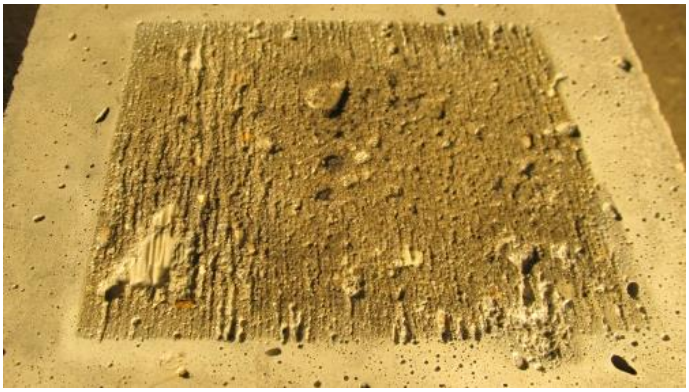

Specimen	F2
Pad	P7
Magnitude of Load	1 kip
Displacement (Range)	1/8”
Displacement (Rate)	6 Hz
Moisture Condition	Constant Drip
Abrasive Fines	Yes, initial Ottawa
Start Date	11/17/2011 (10:00 AM)
End Date	11/17/2011 (1:00 PM)
Maximum Abrasion Depth	0.173
Average Abrasion Depth	0.012

Table A.7

Test 7

Picture Unavailable

Specimen	F4
Pad	N16
Magnitude of Load	3 kips
Displacement (Range)	1/8”
Displacement (Rate)	3 Hz
Moisture Condition	Constant Drip
Abrasive Fines	Yes, initial Ottawa
Start Date	11/23/2011 (10:07 AM)
End Date	11/23/2011 (1:07 PM)
Maximum Abrasion Depth	0.153
Average Abrasion Depth	0.021

Table A.8

Test 8

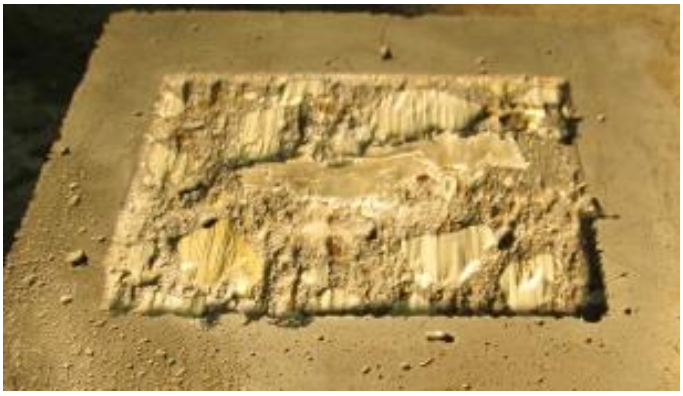

Specimen	F18
Pad	N19
Magnitude of Load	3 kips
Displacement (Range)	1/8”
Displacement (Rate)	3 Hz
Moisture Condition	Constant Drip
Abrasive Fines	Yes, initial Ottawa
Start Date	11/28/2011 (11:25 AM)
End Date	11/28/2011 (1:45 PM)
Maximum Abrasion Depth	0.320
Average Abrasion Depth	0.062

Table A.9

Test 9

Picture Unavailable

Specimen	G14
Pad	N23
Magnitude of Load	3 kips
Displacement (Range)	1/8”
Displacement (Rate)	3 Hz
Moisture Condition	3 drops per second
Abrasive Fines	Yes, initial Ottawa
Start Date	1/19/2012 (2:48 PM)
End Date	1/19/2012 (5:48 PM)
Maximum Abrasion Depth	0.176
Average Abrasion Depth	0.040

Table A.10

Test 10

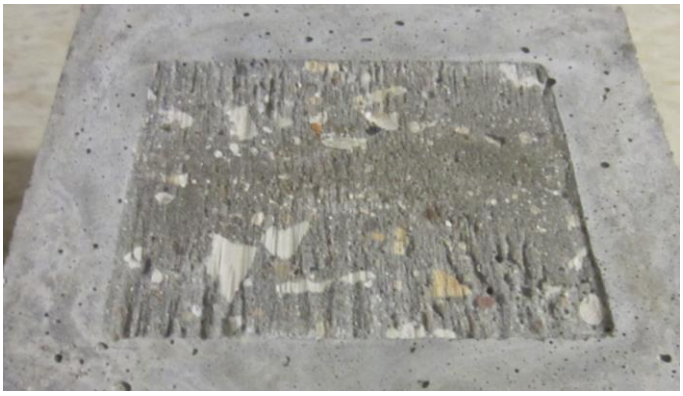

Specimen	I8
Pad	N24
Magnitude of Load	3 kips
Displacement (Range)	1/8”
Displacement (Rate)	3 Hz
Moisture Condition	3 drops per second
Abrasive Fines	Yes, initial Ottawa
Start Date	1/20/2012 (6:30 AM)
End Date	1/20/2012 (9:30 AM)
Maximum Abrasion Depth	0.186
Average Abrasion Depth	0.020

APPENDIX B: DETAILED RESULTS OF FRICTION EXPERIMENT

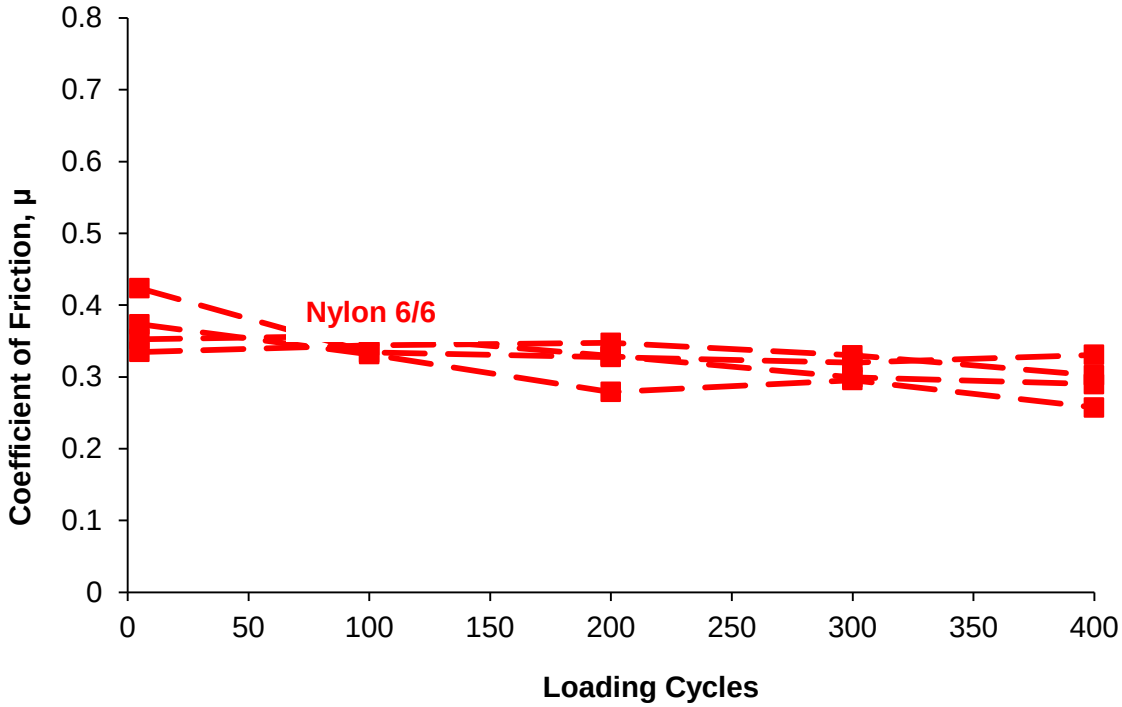

Figure B.1 COF values for nylon 6/6 pad materials during heat/deformation test

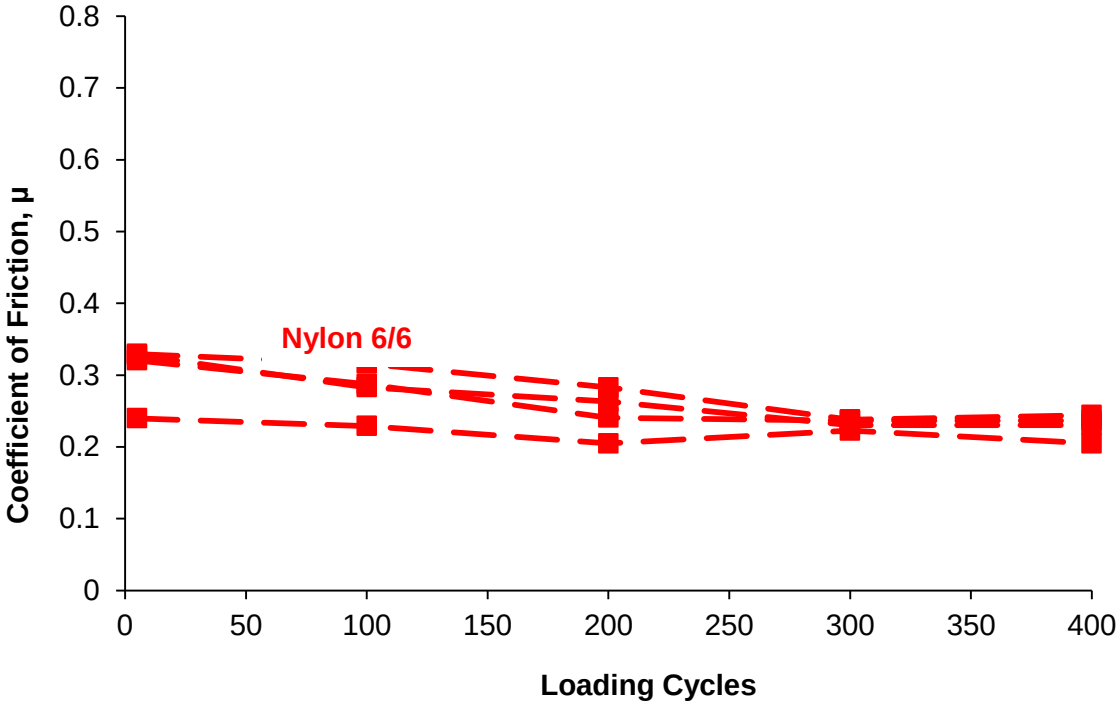

Figure B.2 COF values for nylon 6/6 pad materials during heat/deformation test

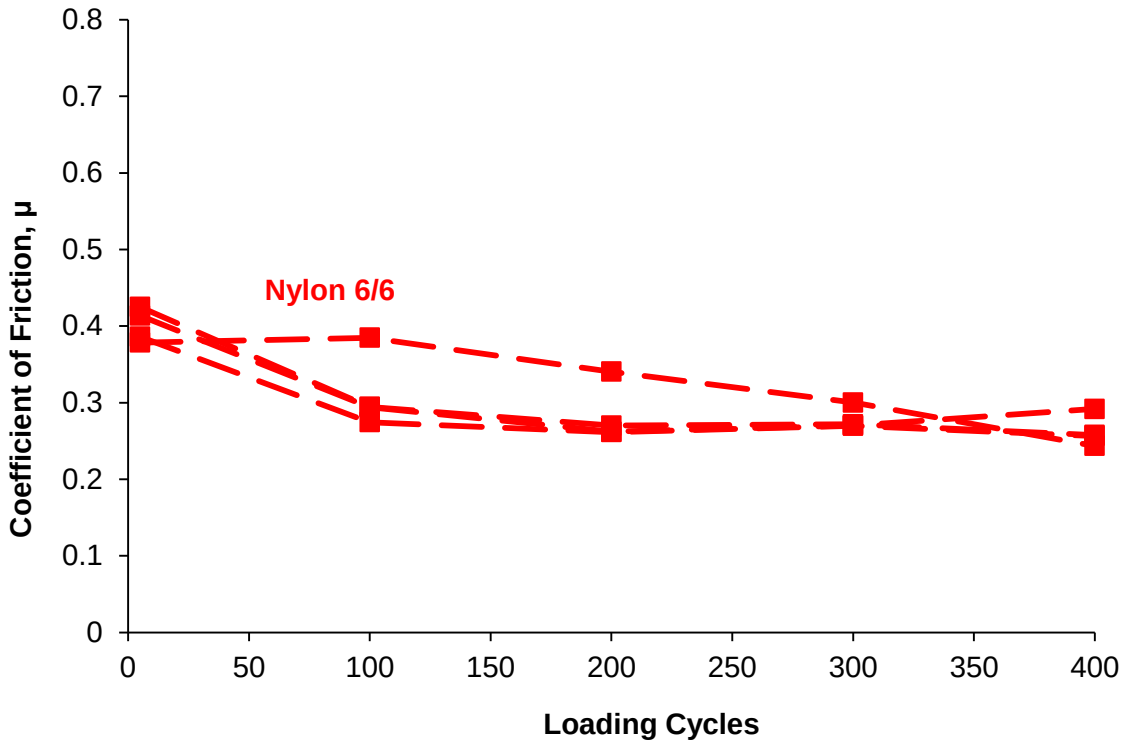

Figure B.3 COF values for nylon 6/6 pad materials during heat/deformation test

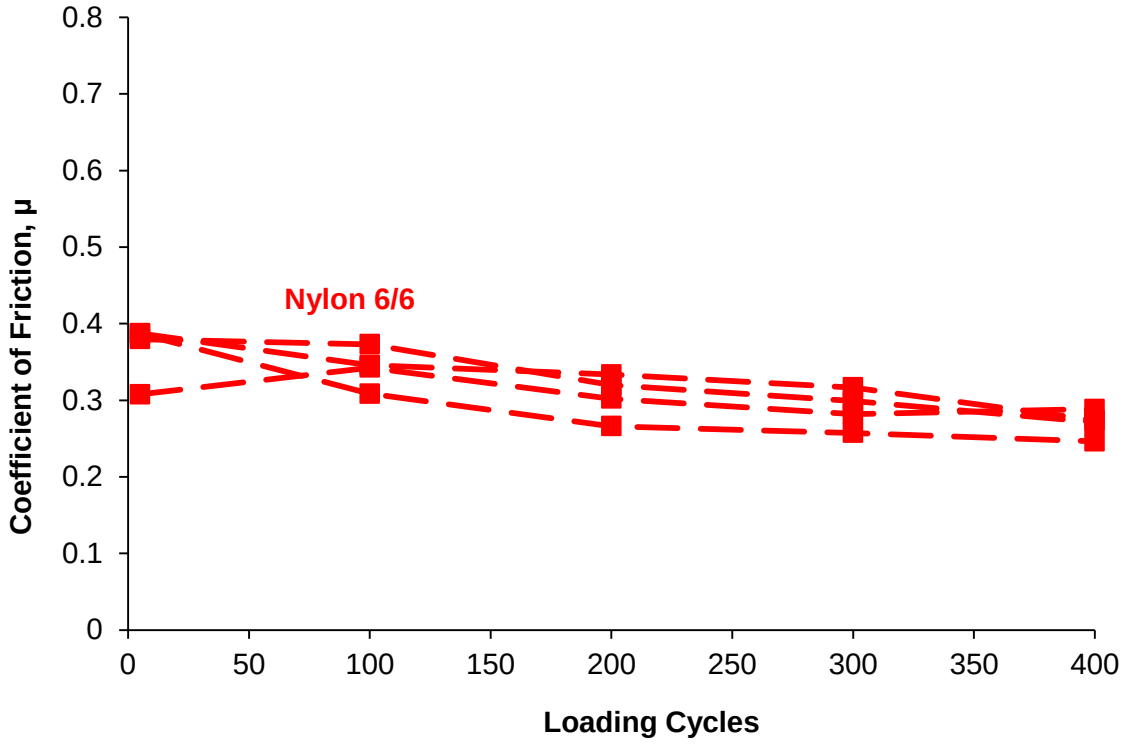

Figure B.4 COF values for nylon 6/6 pad materials during heat/deformation test

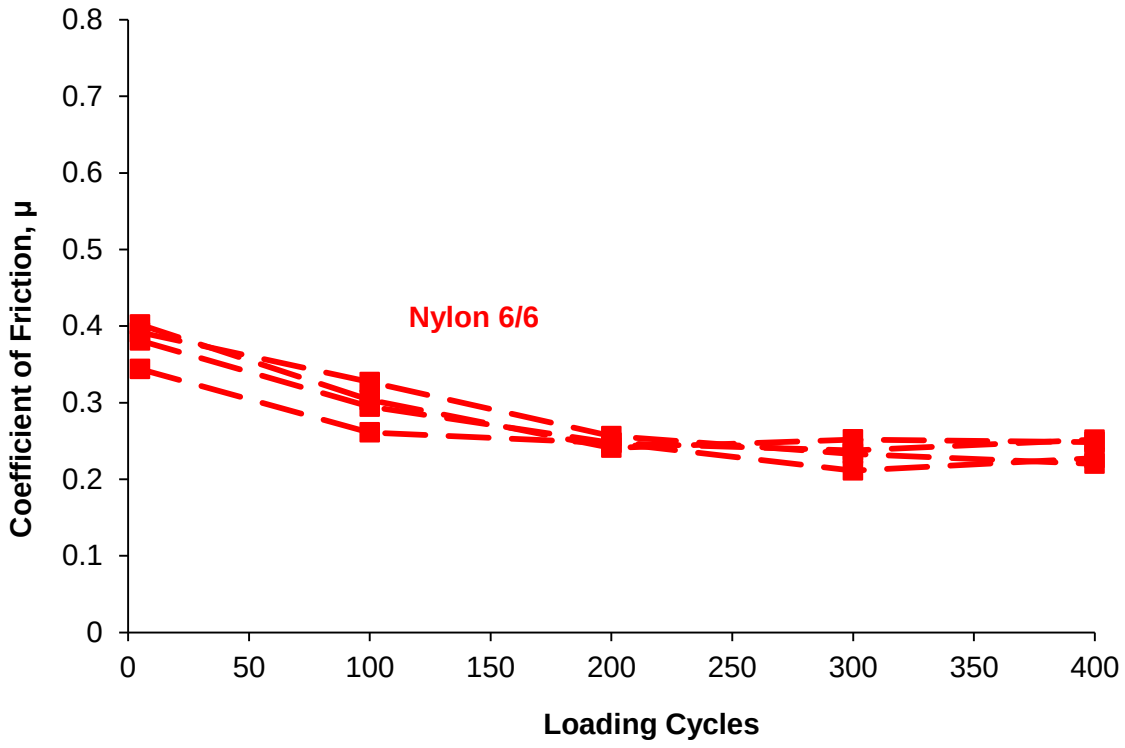

Figure B.5 COF values for nylon 6/6 pad materials during heat/deformation test

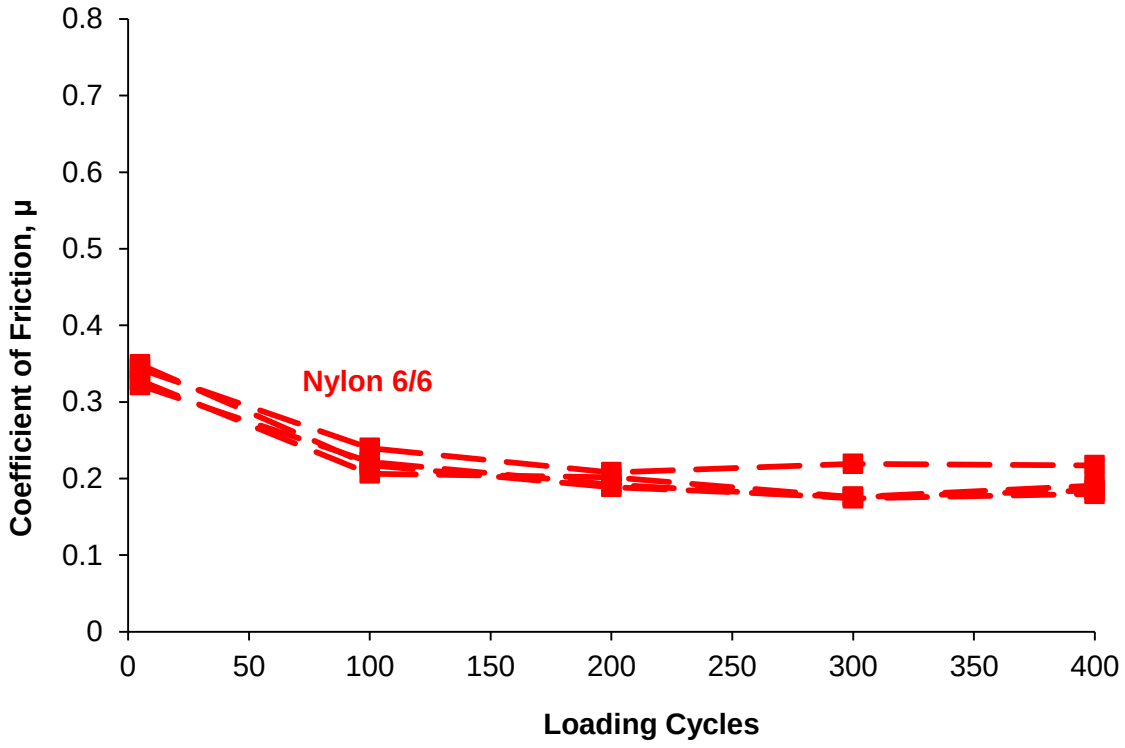

Figure B.6 COF values for nylon 6/6 pad materials during heat/deformation test

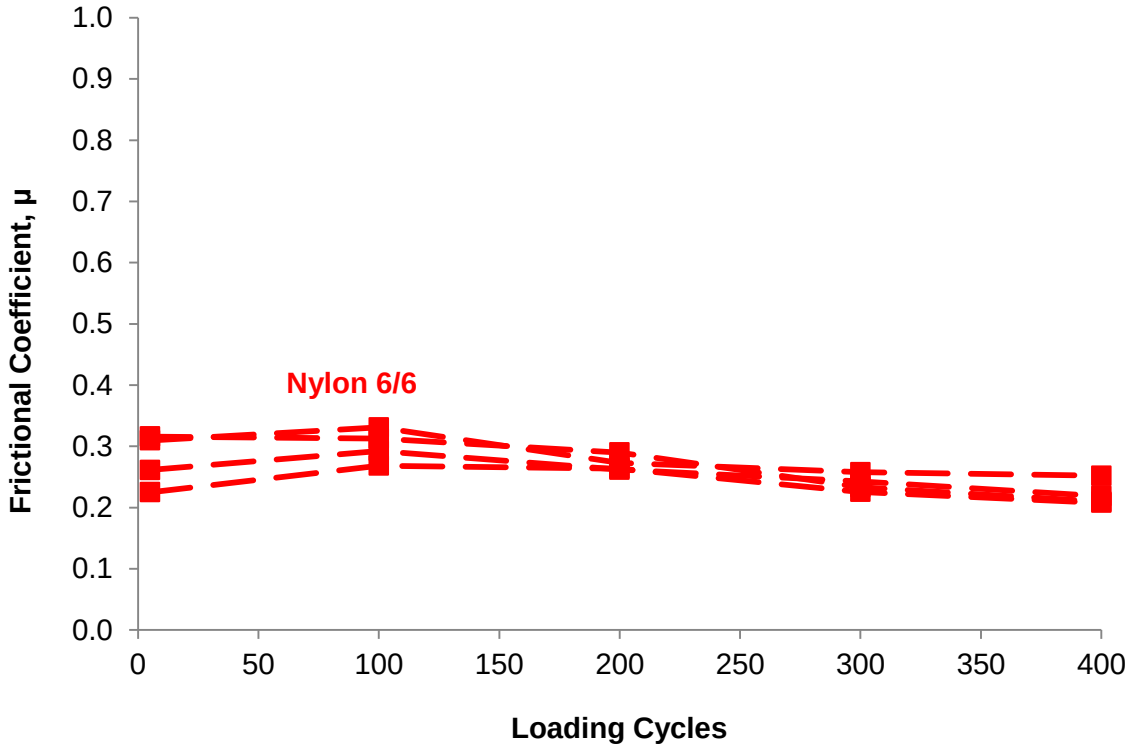

Figure B.7 COF values for nylon 6/6 pad materials during heat/deformation test

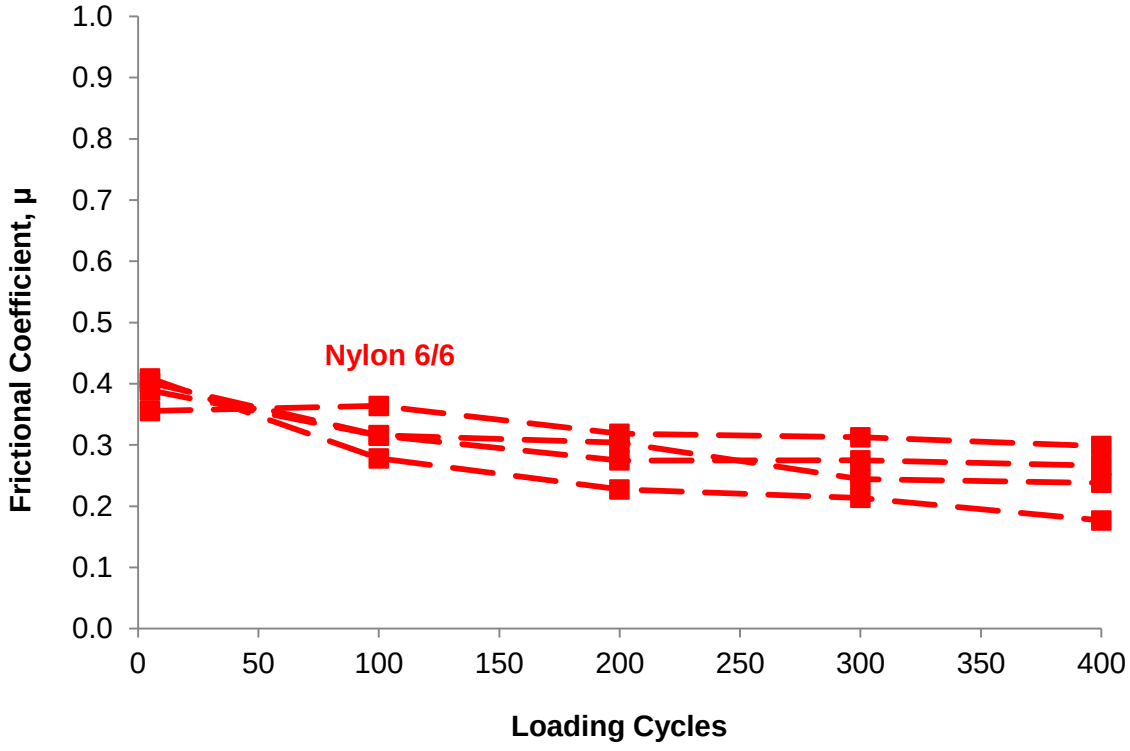

Figure B.8 COF values for nylon 6/6 pad materials during heat/deformation test

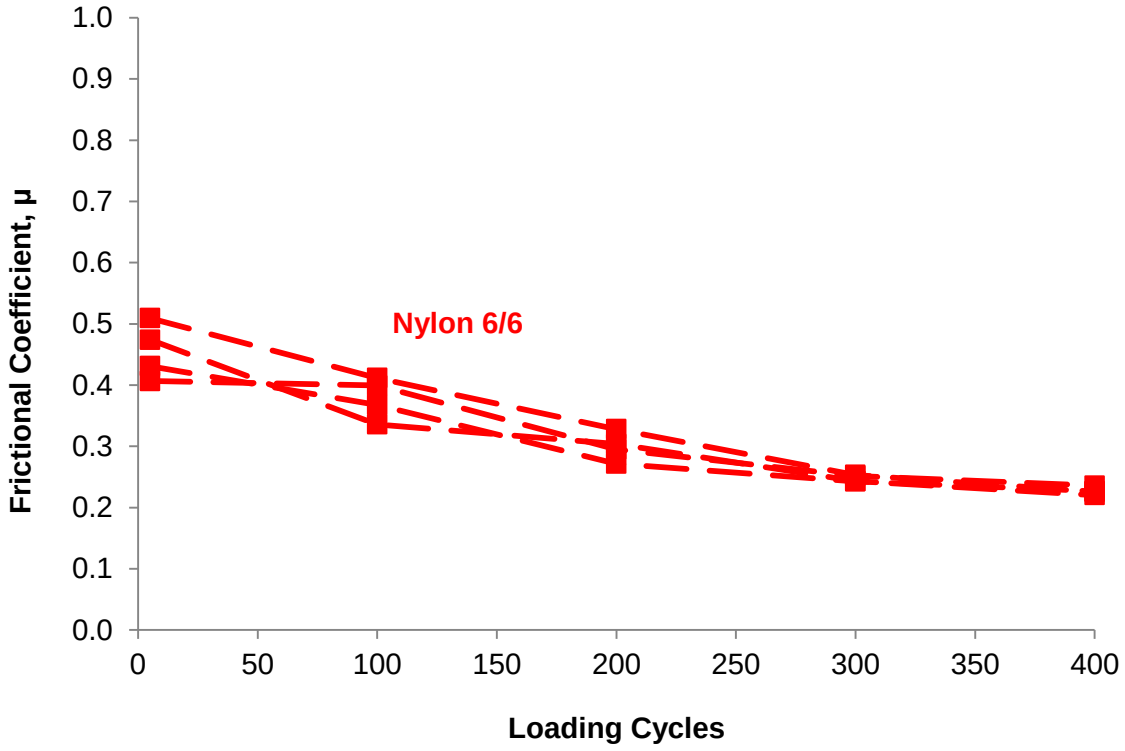

Figure B.9 COF values for nylon 6/6 pad materials during heat/deformation test

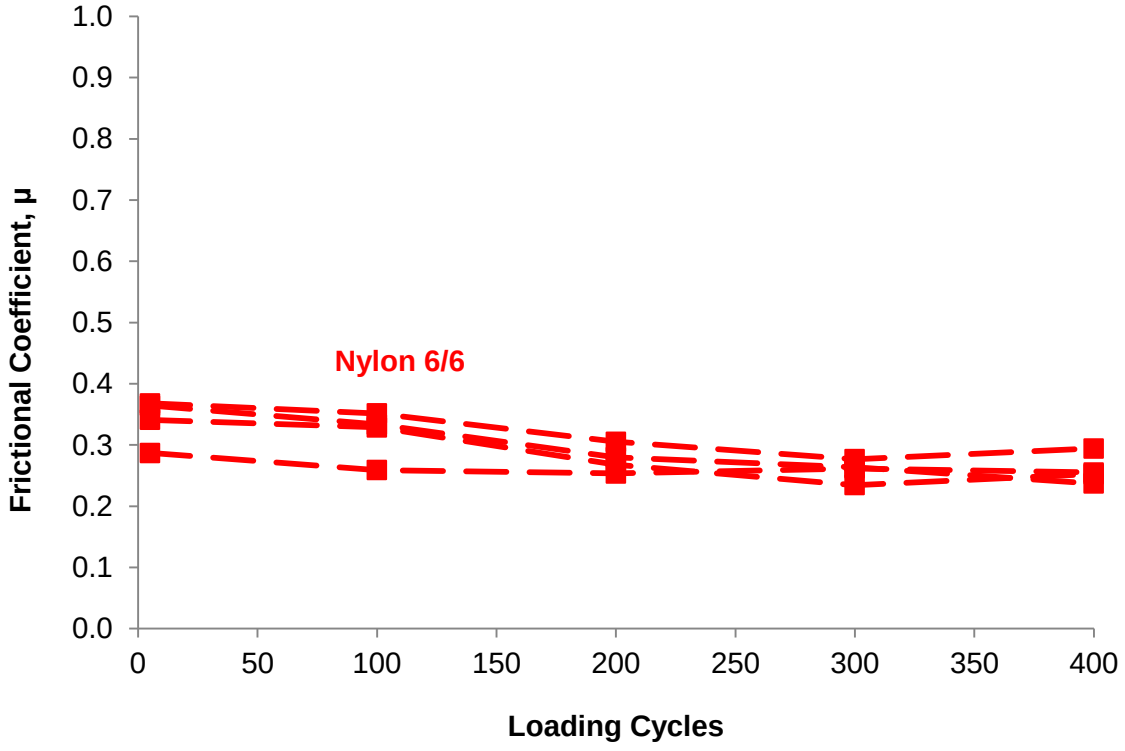

Figure B.10 COF values for nylon 6/6 pad materials during heat/deformation test

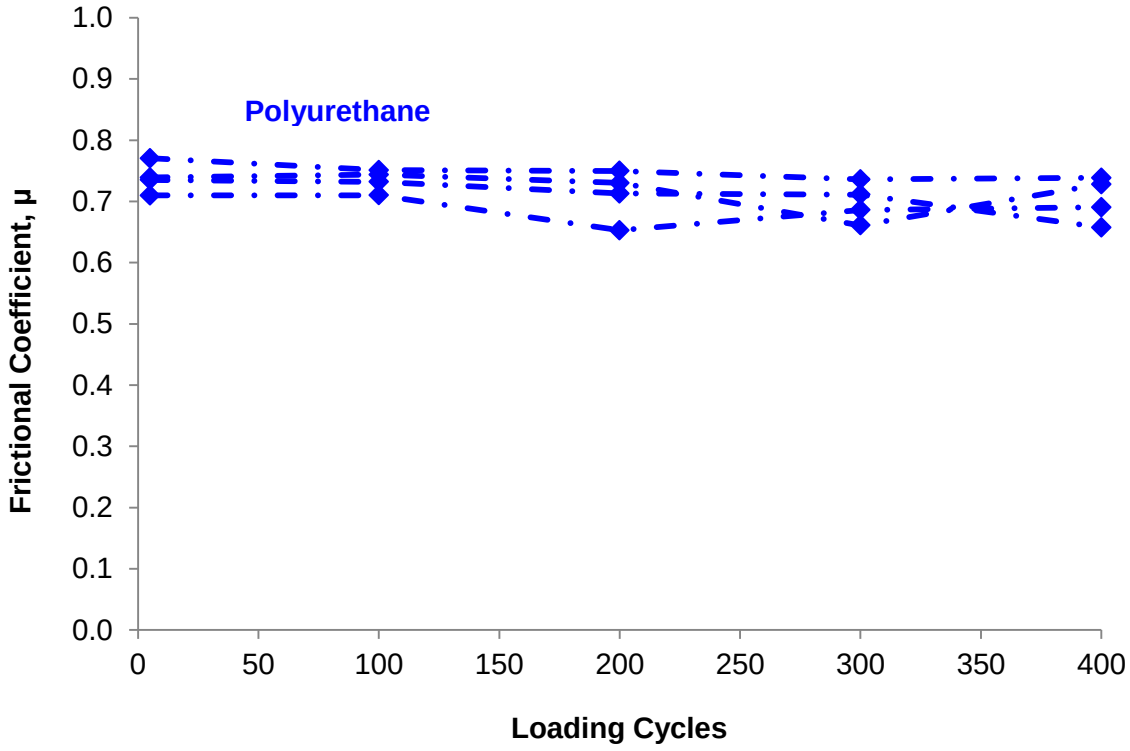

Figure B.11 COF values for polyurethane pad materials during heat/deformation test

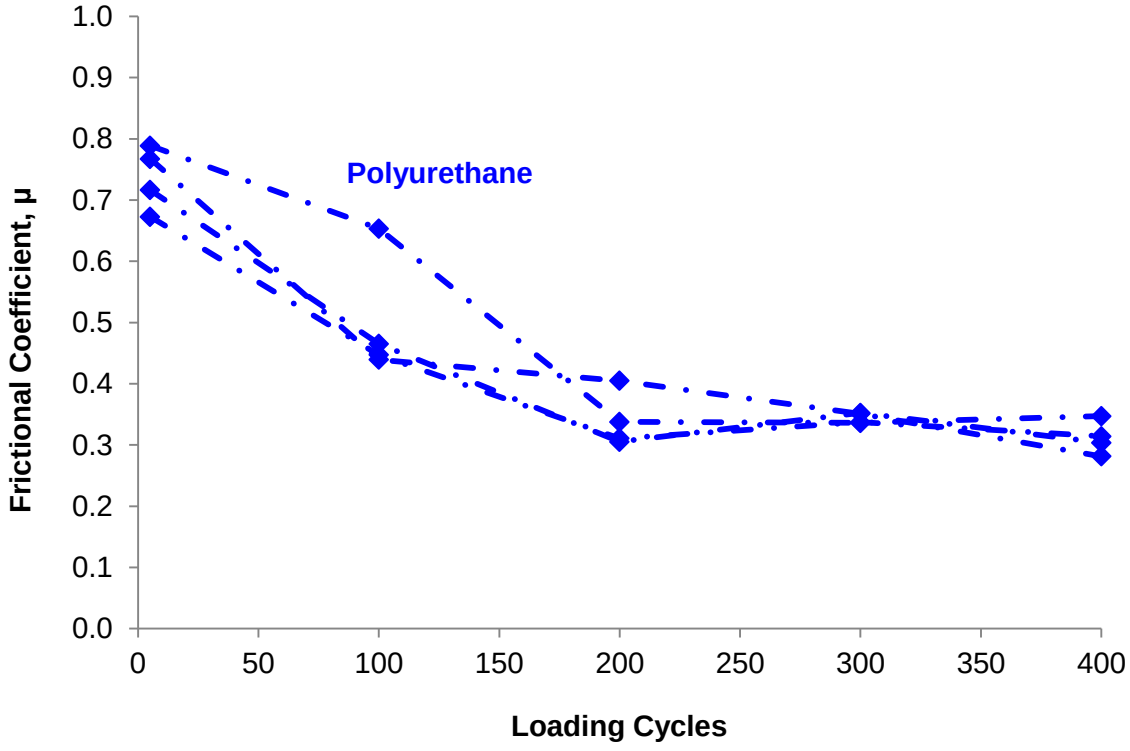

Figure B.12 COF values for polyurethane pad materials during heat/deformation test

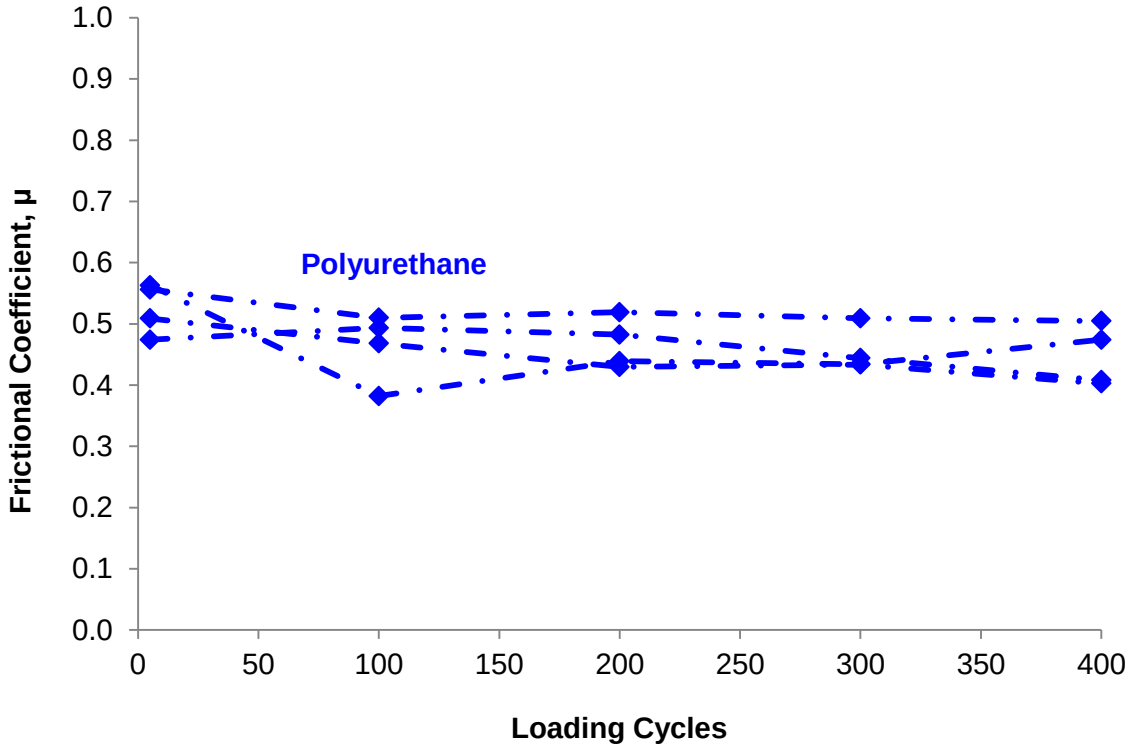

Figure B.13 COF values for polyurethane pad materials during heat/deformation test

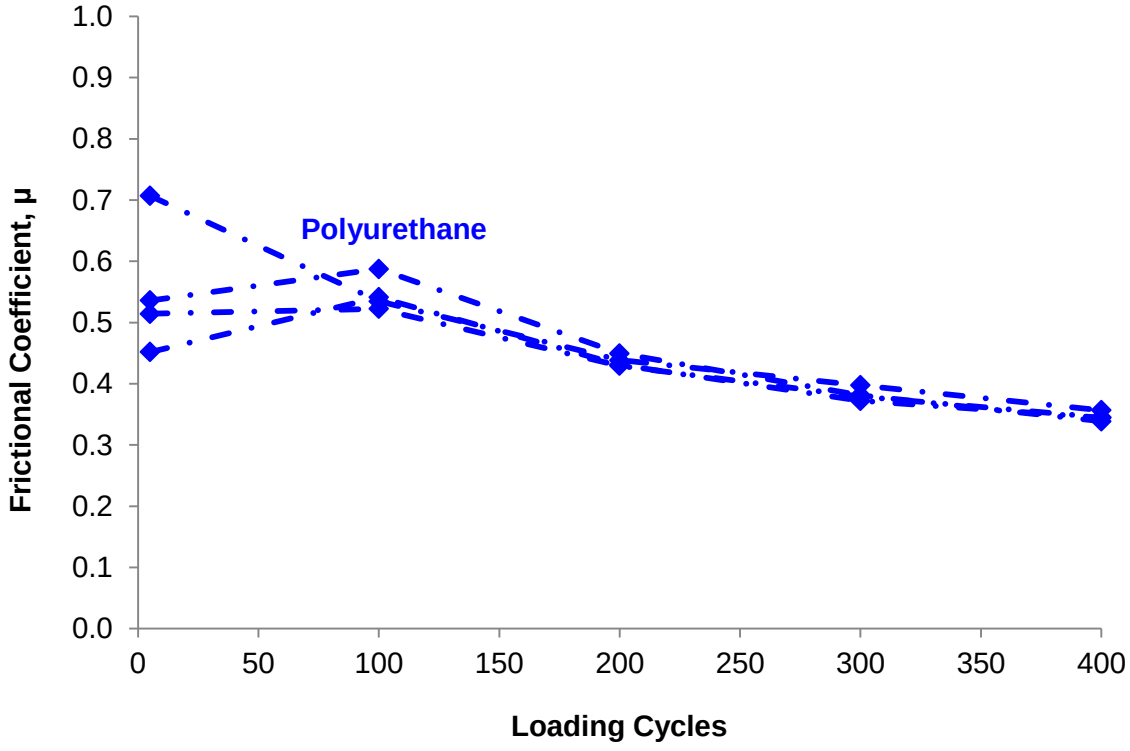

Figure B.14 COF values for polyurethane pad materials during heat/deformation test

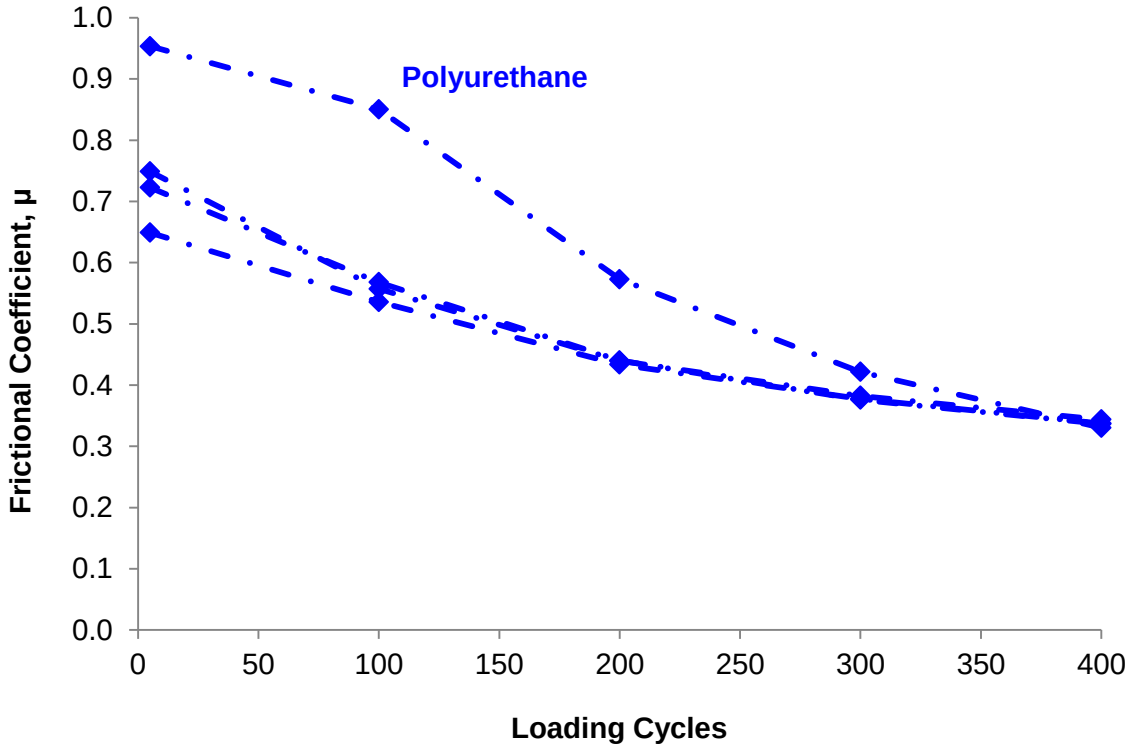

Figure B.15 COF values for polyurethane pad materials during heat/deformation test

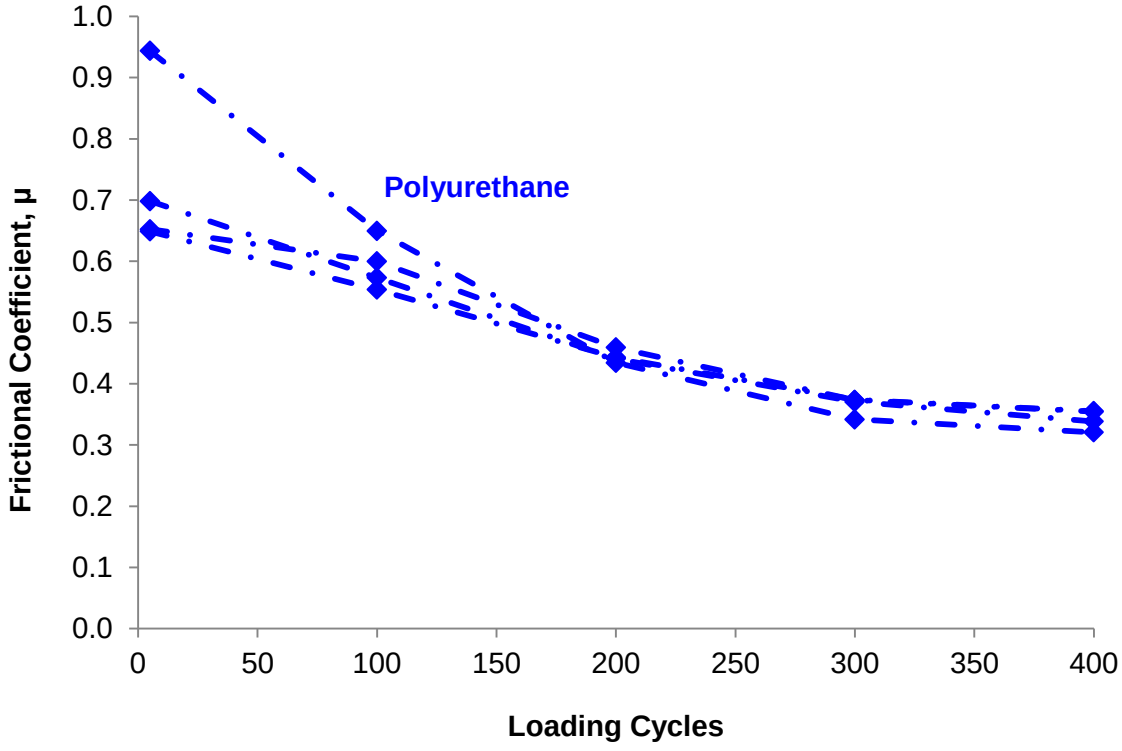

Figure B.16 COF values for polyurethane pad materials during heat/deformation test

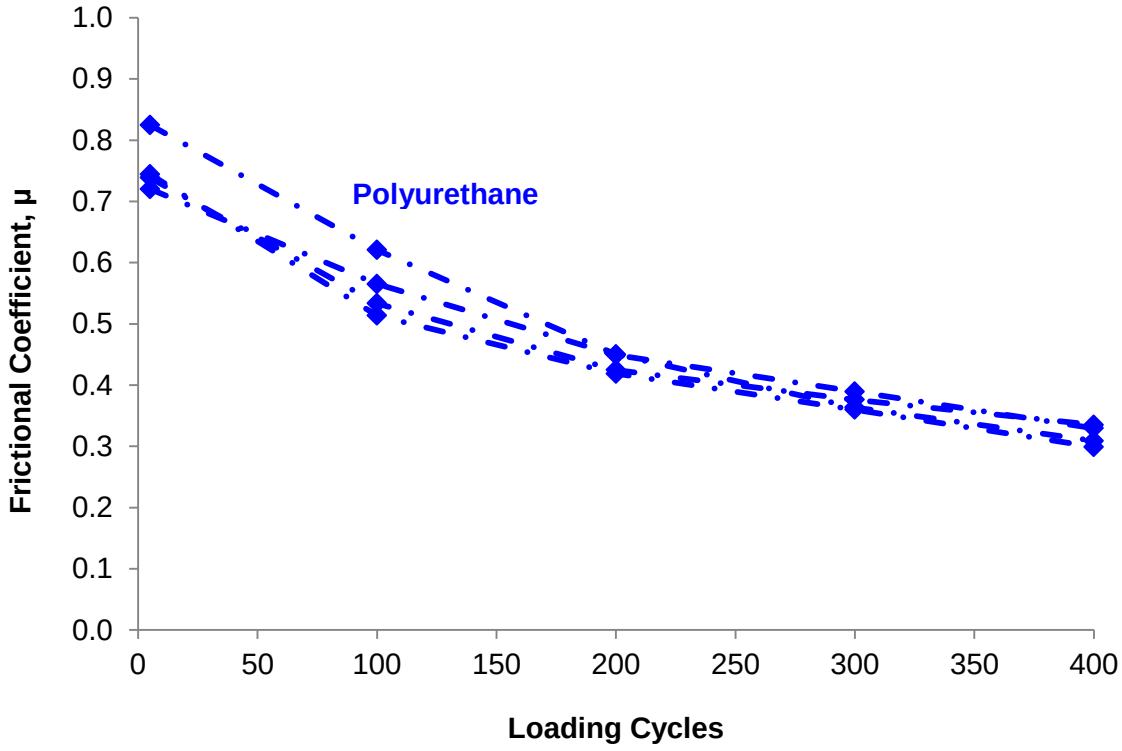

Figure B.17 COF values for polyurethane pad materials during heat/deformation test

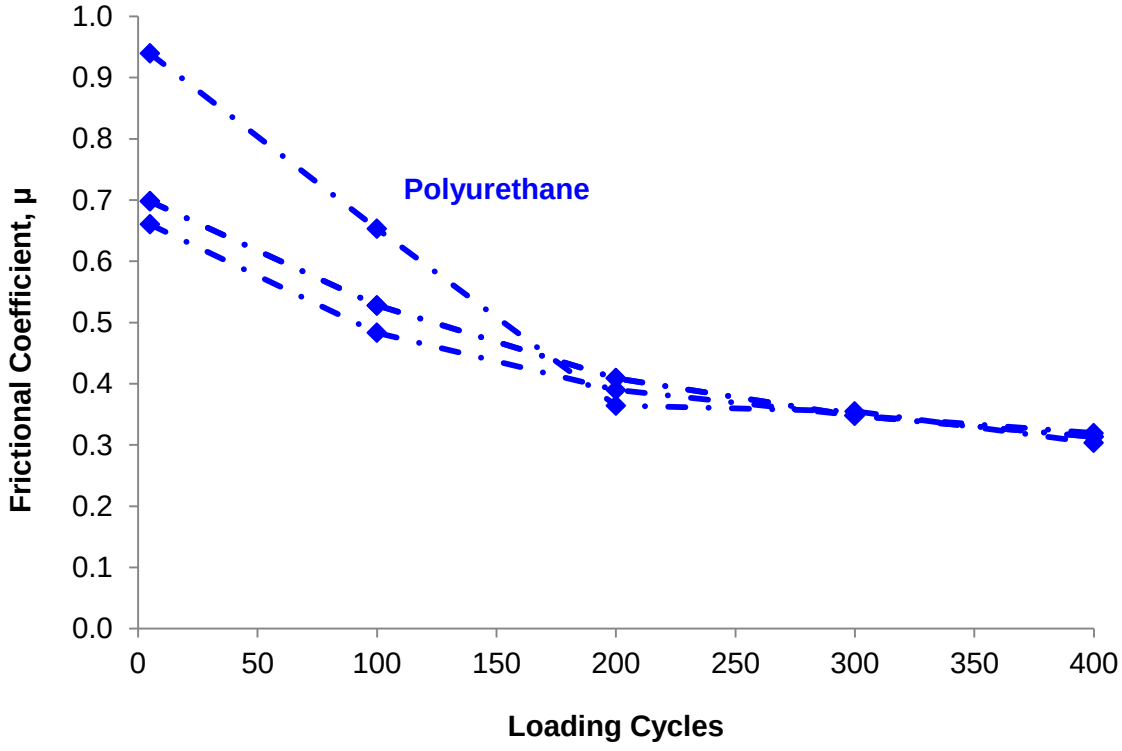

Figure B.18 COF values for polyurethane pad materials during heat/deformation test

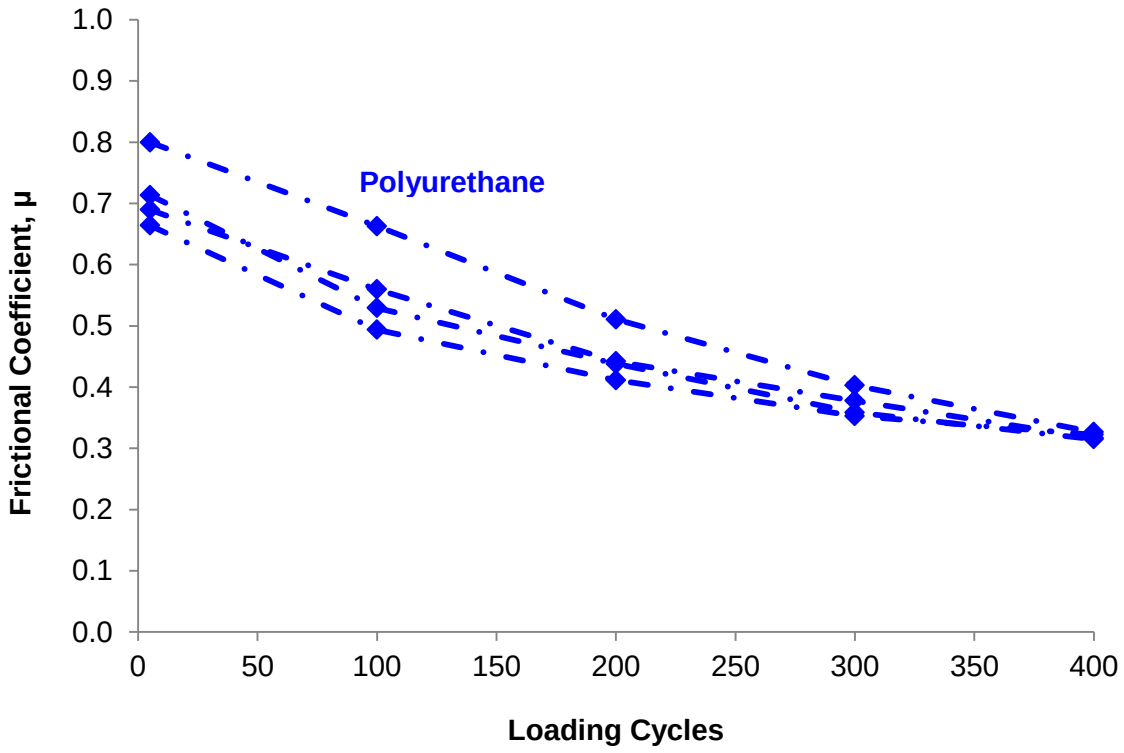

Figure B.19 COF values for polyurethane pad materials during heat/deformation test

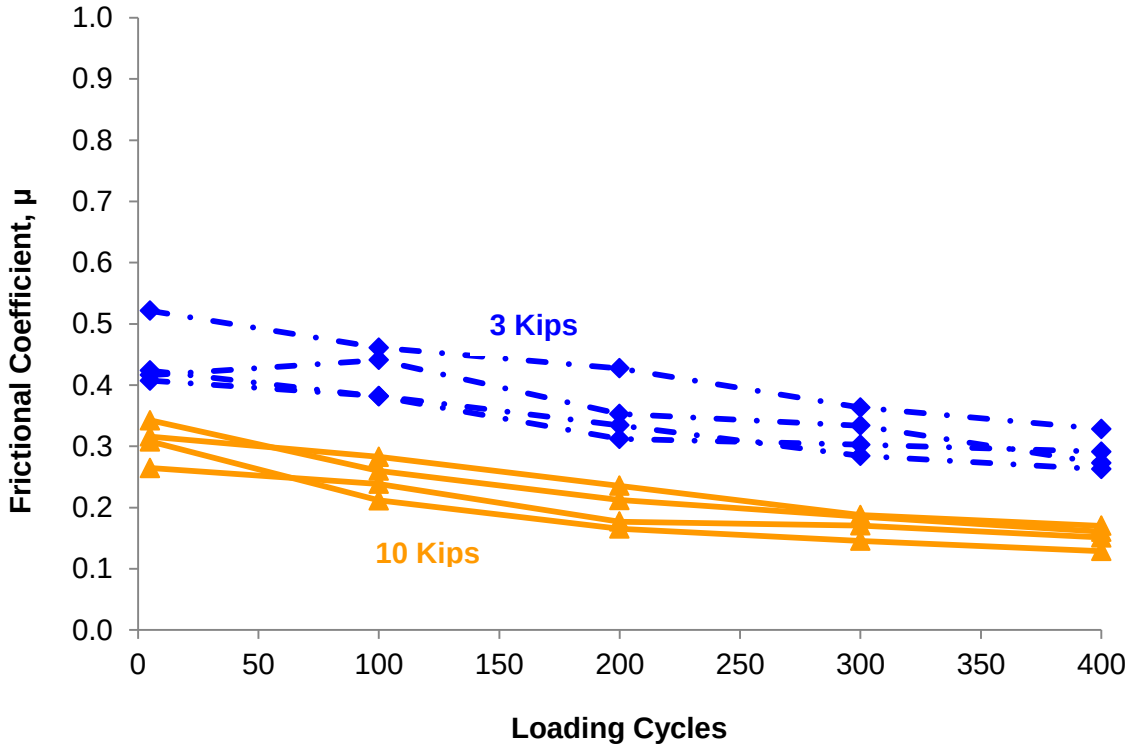

Figure B.20 COF values for nylon 6/6 pad materials during normal load test

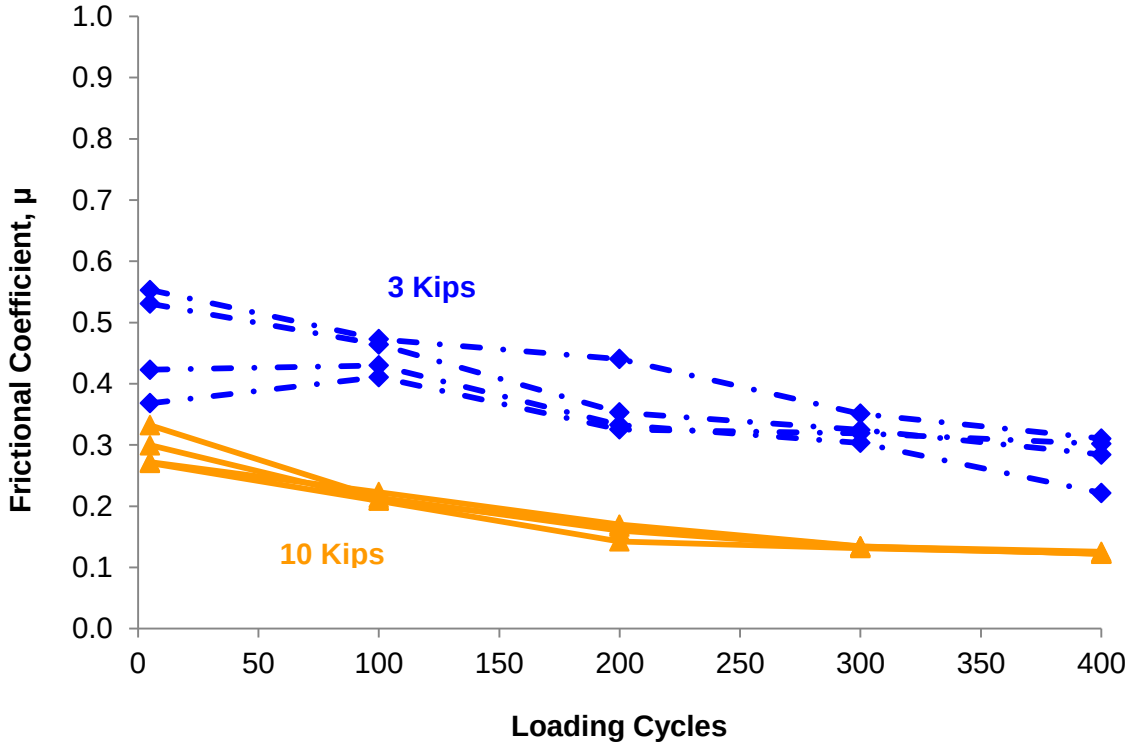

Figure B.21 COF values for nylon 6/6 pad materials during normal load test

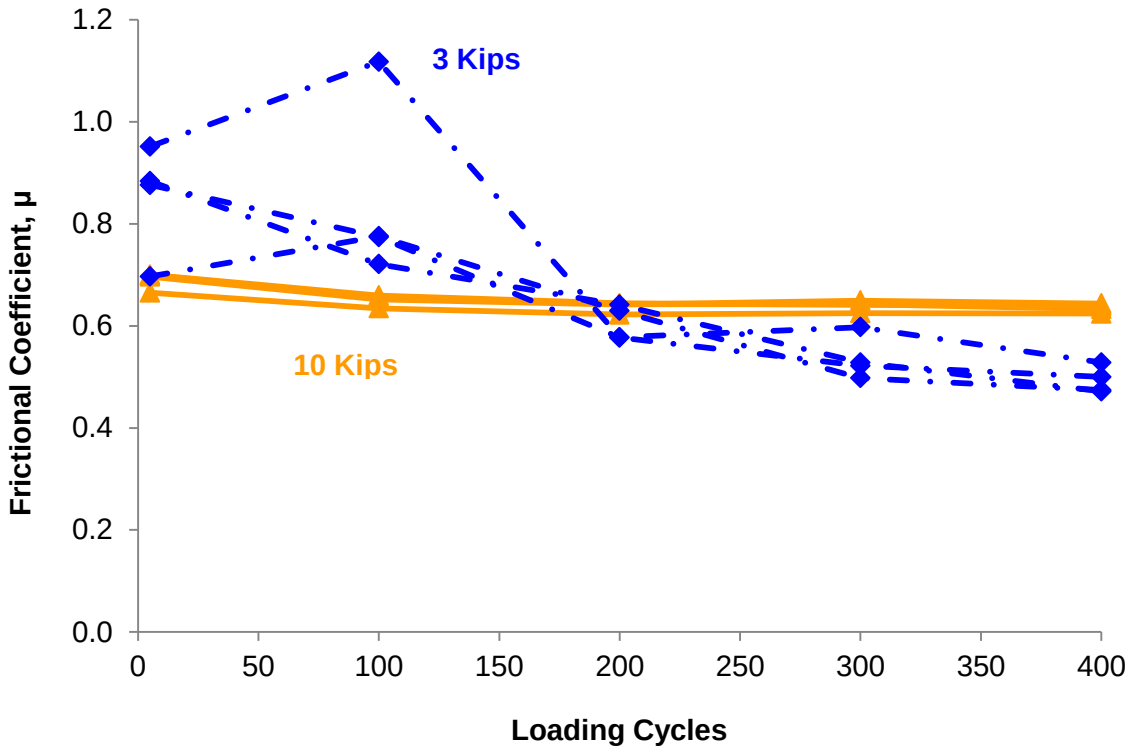

Figure B.22 COF values for polyurethane pad materials during normal load test

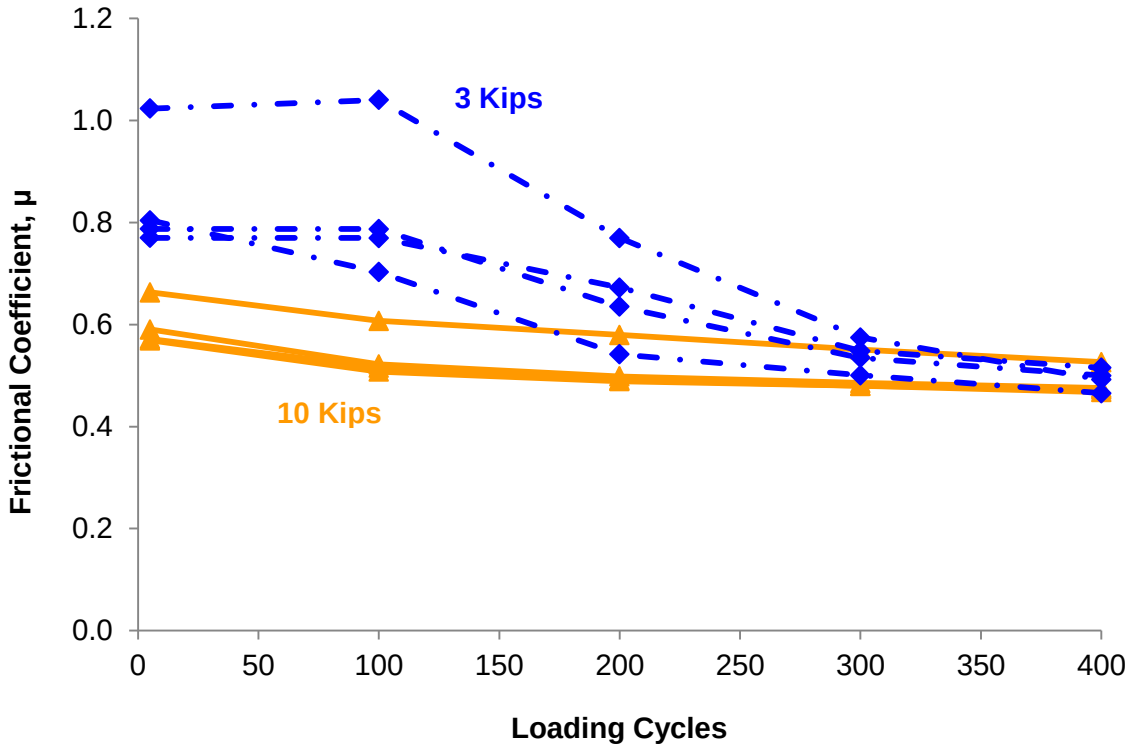

Figure B.23 COF values for polyurethane pad materials during normal load test

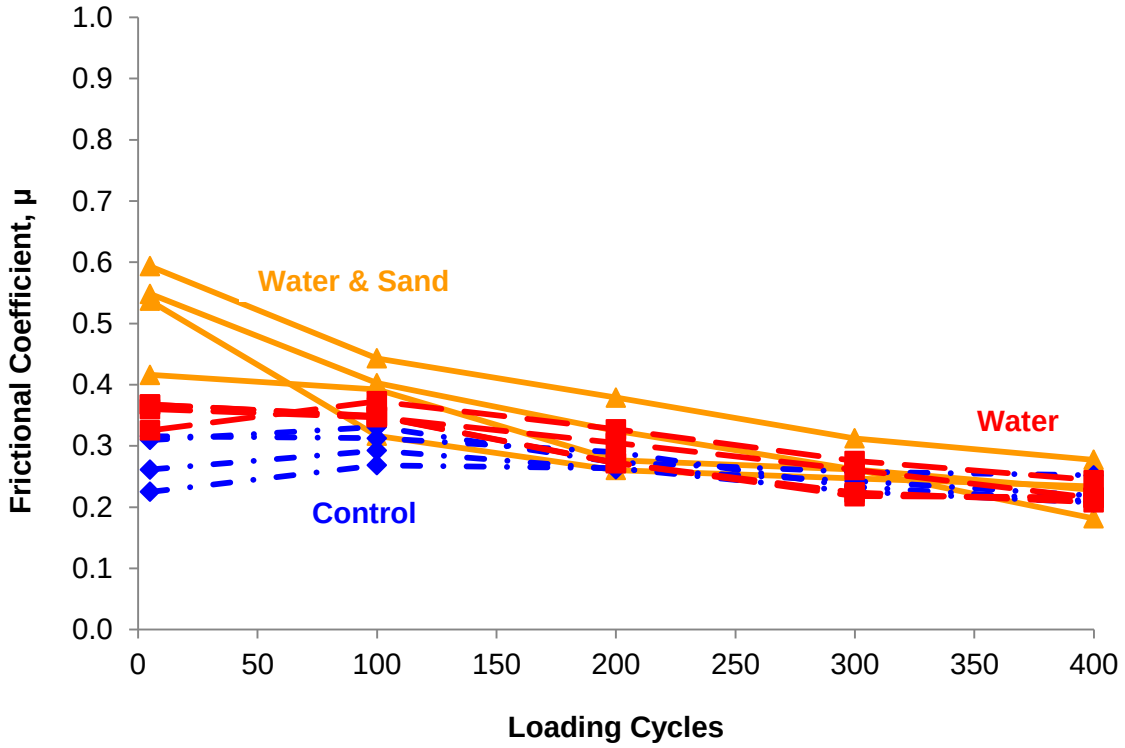

Figure B.24 COF values for nylon 6/6 pad materials during rail seat contaminant test

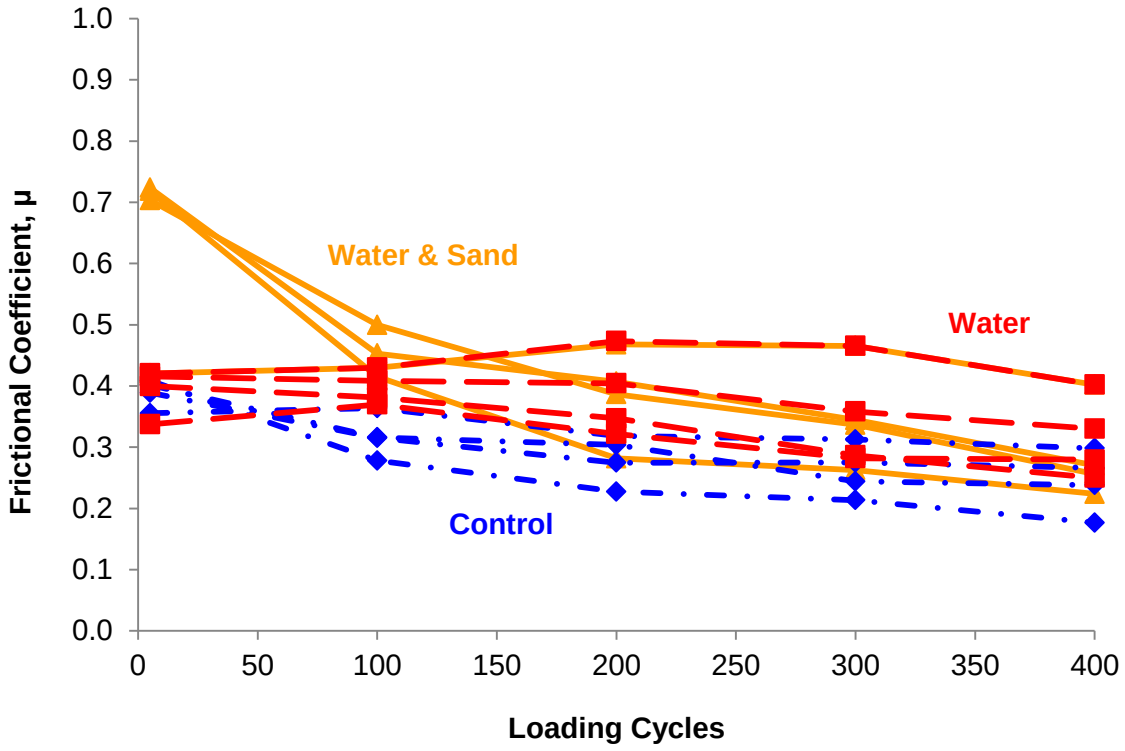

Figure B.25 COF values for nylon 6/6 pad materials during rail seat contaminant test

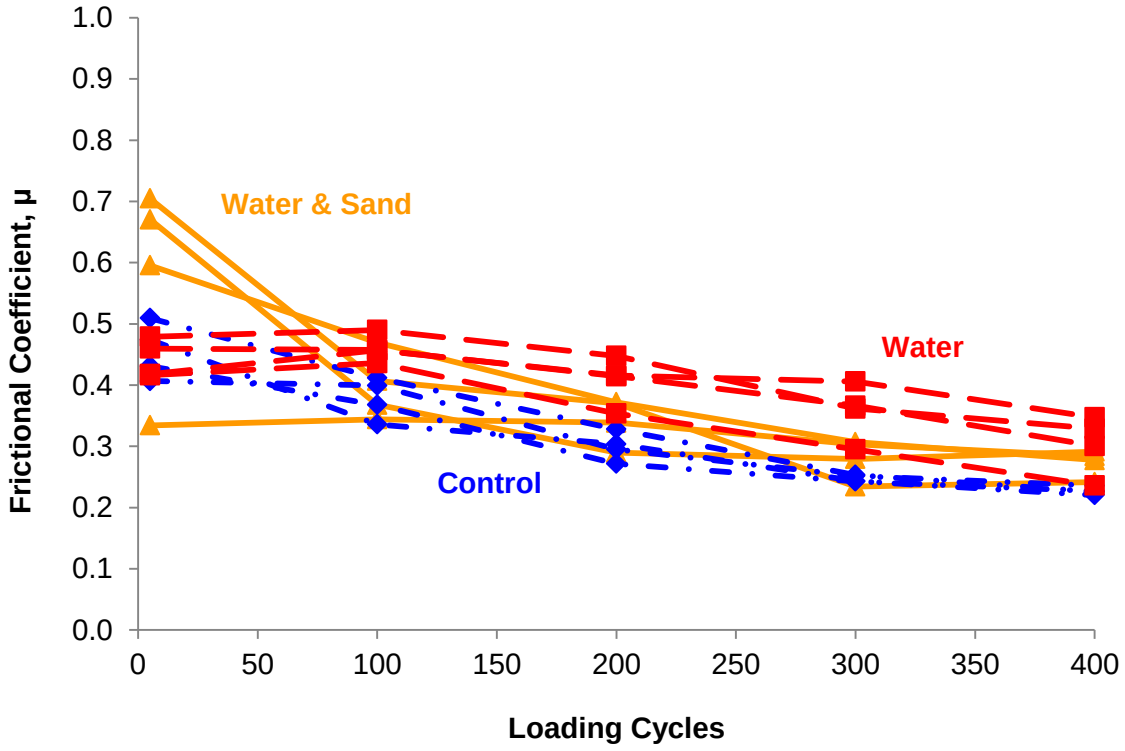

Figure B.26 COF values for nylon 6/6 pad materials during rail seat contaminant test

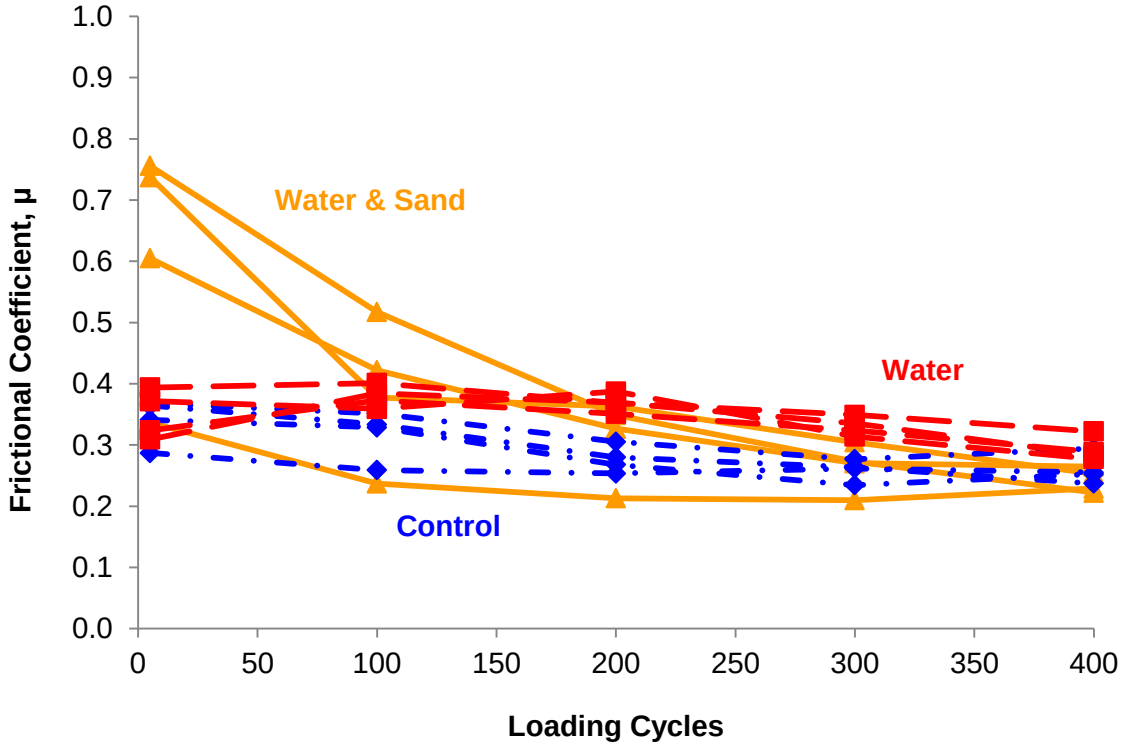

Figure B.27 COF values for nylon 6/6 pad materials during rail seat contaminant test

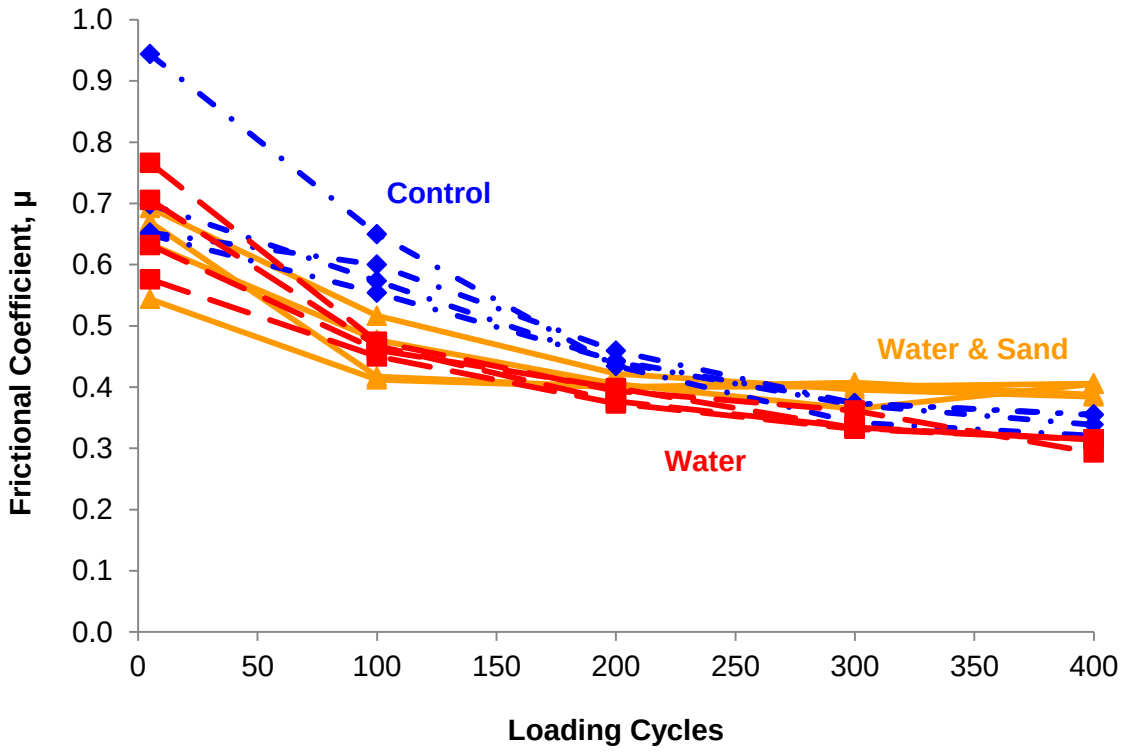

Figure B.28 COF values for polyurethane pad materials during rail seat contaminant test

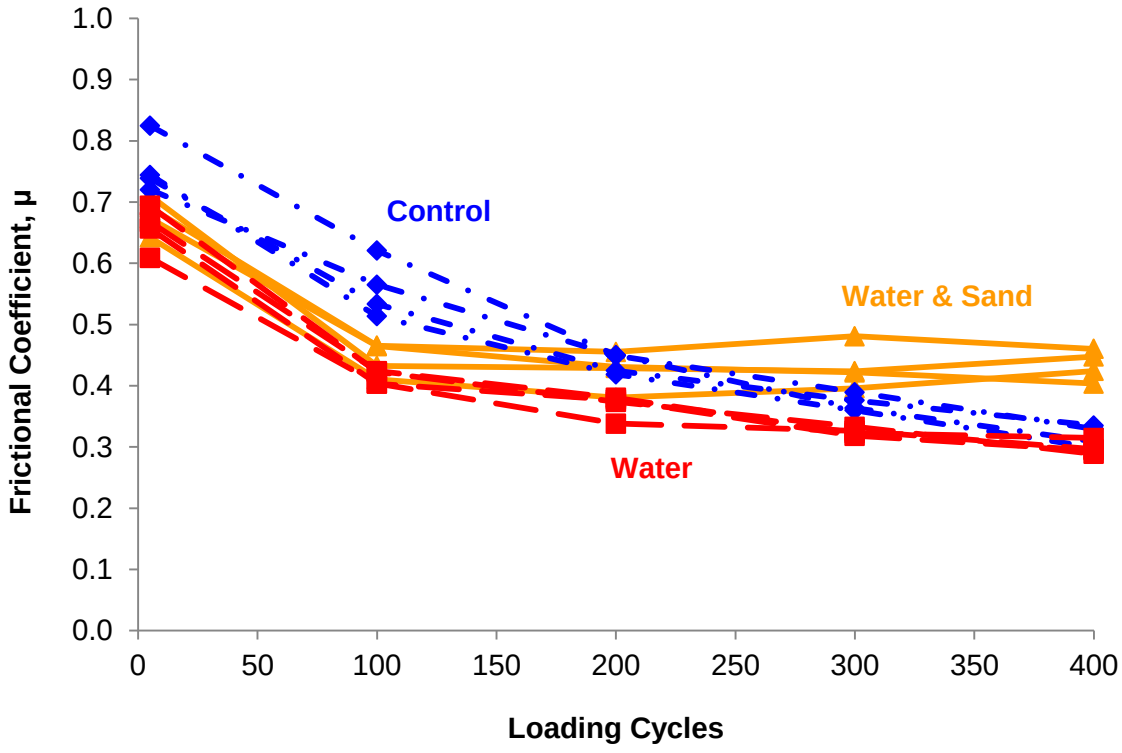

Figure B.29 COF values for polyurethane pad materials during rail seat contaminant test

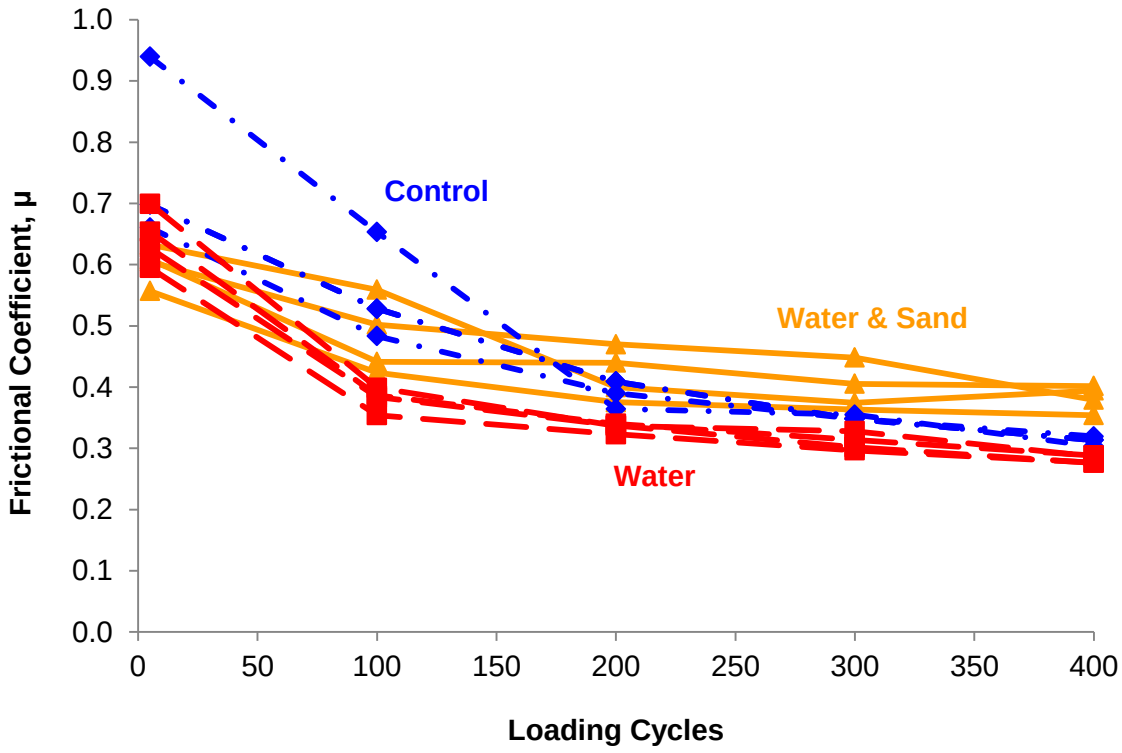

Figure B.30 COF values for polyurethane pad materials during rail seat contaminant test

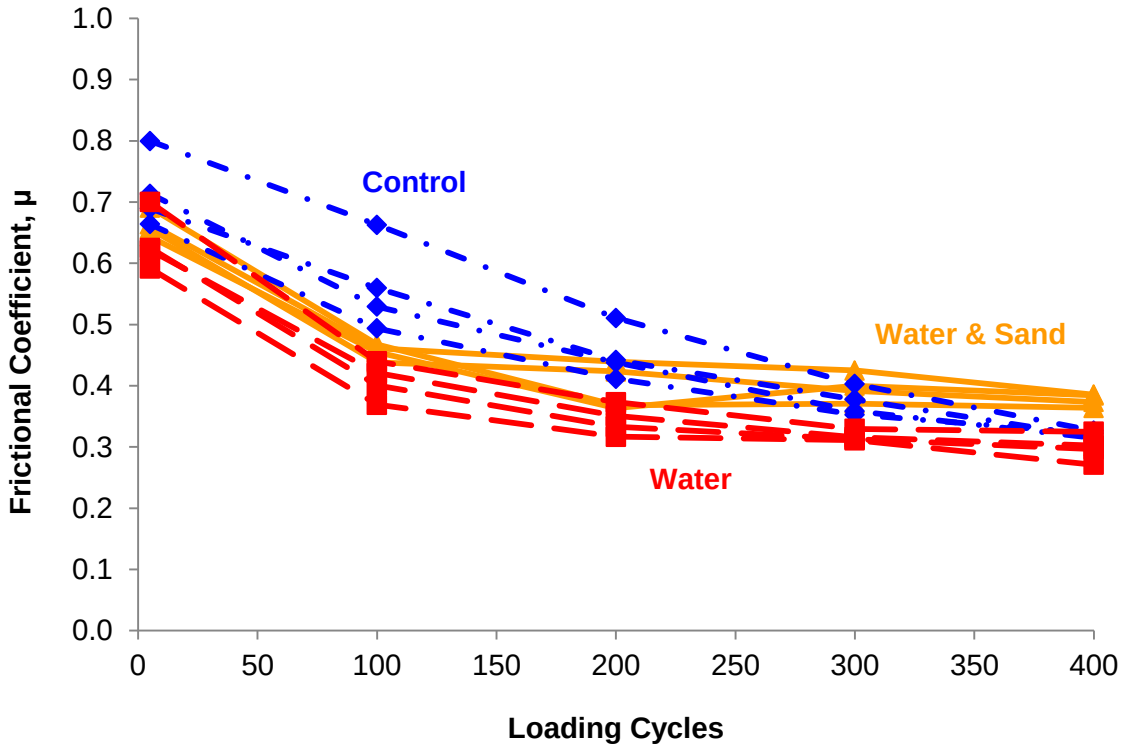

Figure B.31 COF values for polyurethane pad materials during rail seat contaminant test

APPENDIX C: EXAMPLES OF PAD DETERIORATION FROM FRICTION EXPERIMENT

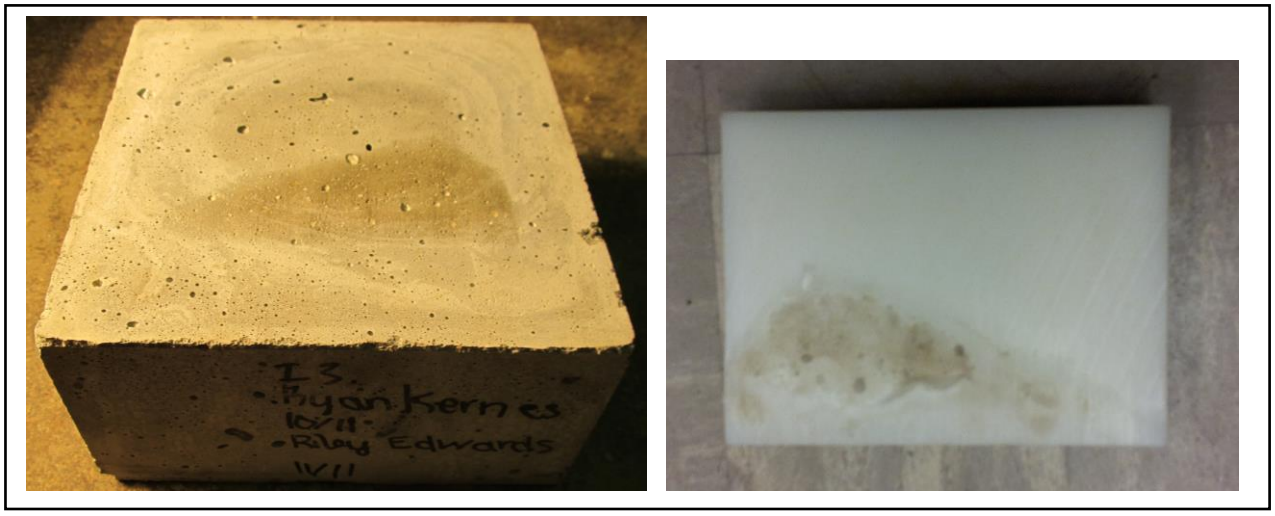

Figure C.1 Heat/Deformation Test 1.1 Nylon 6/6 Pad

Figure C.2 Heat/Deformation Test 1.2 Nylon 6/6 Pad

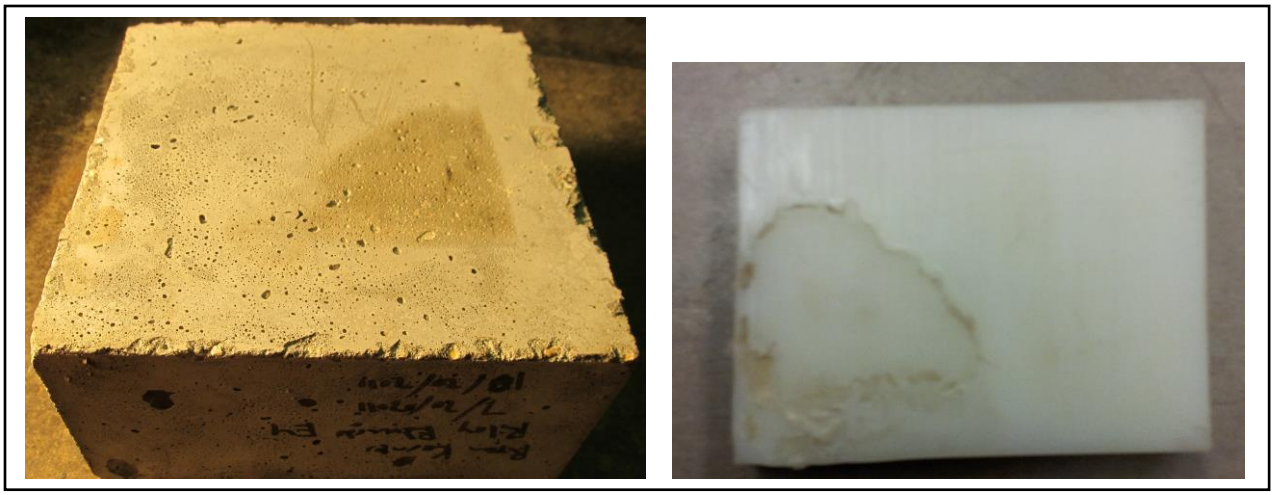

Figure C.3 Heat/Deformation Test 1.3 Nylon 6/6 Pad

Figure C.4 Heat/Deformation Test 1.7 Polyurethane Pad

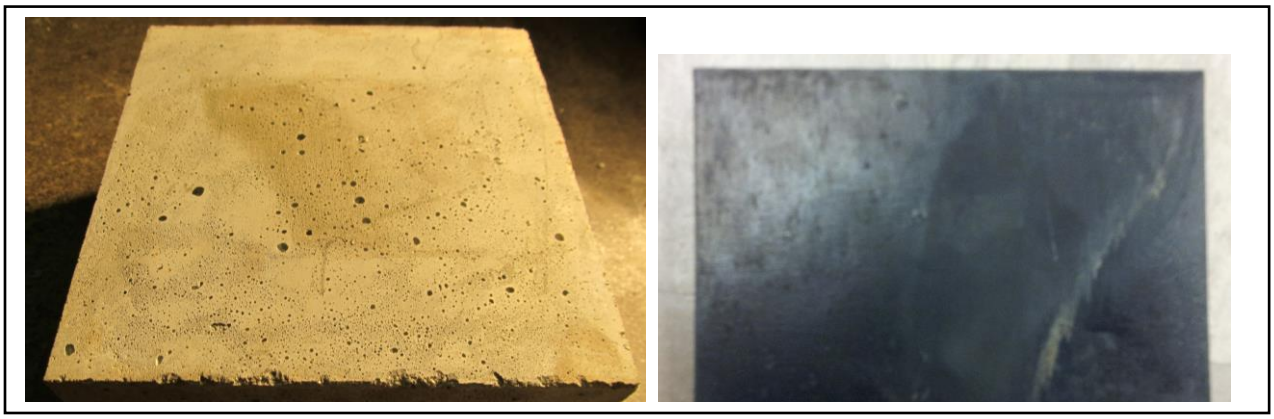

Figure C.5 Heat/Deformation Test 1.8 Polyurethane Pad